Unidirectional Sensing via Dual-Sensitivity Bi-Axial Flexible Sensors

Based on Electrically Aligned Carbon Nanotube Nanocomposites

Tim de Rijk

Unidirectional Sensing via Dual-Sensitivity Bi-Axial Flexible Sensors

Based on Electrically Aligned Carbon Nanotube Nanocomposites

Unidirectional Sensing via Dual-Sensitivity Bi-Axial Flexible Sensors

Based on Electrically Aligned Carbon Nanotube Nanocomposites

Dissertation

for the purpose of obtaining the degree of doctor
at the IMSAS University Bremen
to be defended publicly on Friday 12 of January, 2024 at 11:00.

by

Tim Mike de Rijk

Master of Science in Electrical Engineering
Master of Science in Biomedical Engineering
IMSAS University Bremen, Germany

First Reviewer:	Prof. Dr.-Ing Walter Lang
Second Reviewer:	Prof. Dr.-Ing Steffen Paul
Date of submission:	25^{th} of October, 2023
Date of colloquium:	12^{th} of January, 2024

This dissertation has been approved by the promotor

Composition of the doctoral committee:

Prof. Dr. -Ing Walter Lang:	Institut für Mikrosensoren -aktoren und -systeme (IMSAS) University Bremen
Prof. Dr. -Ing Steffen Paul:	Institut für Theoretische Elektrotechnik und Mikroelektronik University Bremen
Independent members:	
Prof. Dr. Ulrich Giese:	Deutsches Institut für Kautschuktechnologie (DIK), Hannover
Prof. Dr. -Ing Björn Lüssem:	Institut für Mikrosensoren -aktoren und -systeme (IMSAS) University Bremen

This work was supported by the AiF as part of the program for the promotion of industrial community research (IGF) project 20986N of the research association DFMRS e.V.

Gefördert durch:

Bundesministerium für Wirtschaft und Klimaschutz

aufgrund eines Beschlusses des Deutschen Bundestages

Forschungsnetzwerk Mittelstand

Cover & Inside Design by: Wendz ID || www.wenzid.nl
Title pages by: ProefschriftMaken || www.proefschriftmaken.nl
Printed by: ProefschriftMaken || www.proefschriftmaken.nl

DOI: 10.26092/elib/2741
Orchid ID: 0000-0003-2737-3774

An electronic version of this dissertation is available at https://www.suub.uni-bremen.de accident

Abstract

Imagine a regular flexible pressure sensor that can be integrated inside a host material, e.g. an industrial sealing, to measure the applied pressure. With pressure, the sensor changes its vertical dimensions and changing its intrinsic resistance. However, aside from the vertical change, the pressure also causes lateral strain in the sensor, changing its outer dimensions and affecting the measurement value of the sensor. A possibility to minimize this cross-sensitivity is by creating unidirectional sensitive sensors. A sensor that only response to a force from a single direction, and is insensitive to all other.

This research presents the fabrication and characterization of flexible polymer-based sensors that can measure externally applied pressures and forces. A polymer substrate is implemented as a substrate to ensure its flexibility. Carbon nanotubes (CNTs) are integrated in the polymer to achieve a piezoresistive polymer. The working principle follows the fact that with an externally applied pressure, the polymer volume decreases, effectively decreasing the distance between individual CNTs. This in turn increases the composites conductivity, which can be measured. This work is divided into two major parts: flexible sensors with integrated carbon nanotubes that are either randomly dispersed within the polymer or aligned by means of an electrical field. The dissertation goes through all fabrication steps of dispersing the carbon nanotubes in the polymer, and the different available methods. Afterwards, the first strain and pressure results are shown with the two chosen polymers: Polydimethylsiloxane (PDMS) and Polyimide (PI). The advantages of both polymers and sensor types are discussed, followed by the introduction of the possibility to decrease the cross-sensitivity of the sensors by aligning the carbon nanotubes in the polymer before it is cured.

The principle of the induced dipole moment within the CNT, causing the rotation in the presence of an electric field is highlighted. Numerical and analytical models are included to support the experimental results found in this research. The possibility of creating highly sensitive piezoresistive sensors based on aligned carbon nanotubes is attributed due to the electron tunneling effect. Electrons in CNTs that are within a few nanometer can 'tunnel', jumping over a short distance of non-conductive material. The resistance of such connections increases exponentially with distance, giving rise to highly sensitive sensors with Gauge factors up to 10^3 found in this research. The aligned PDMS-based sensors show a high degree of alignment, which can be even improved further by utilizing functionalized carbon nanotubes. Experiential results show a greater strain region for the sensor, and more controllable and connected carbon nanotube alignment.

Finally, the randomly CNT-oriented and stable polyimide pressure sensors are integrated into rubber sealings in order to monitor the condition and applied pressure on the sealings.

Kurzfassung

Bei einem regulären flexiblen Drucksensor, der in ein Trägermaterial (z. B. eine industrielle Dichtung) integriert ist und einen anliegenden Druck misst, ändern sich durch den Druck die vertikalen Abmessungen des Sensors selbst und damit auch dessen Eigenwiderstand. Neben der vertikalen Änderung verursacht der Druck jedoch auch eine laterale Dehnung des Sensors, wodurch sich seine Außenabmessungen ändern und der Messwert negativ beeinflusst wird. Eine Möglichkeit, diese Querempfindlichkeit zu minimieren besteht darin, unidirektional empfindliche Sensoren zu entwickeln, die nur auf Kräfte aus einer Richtung reagieren und für alle anderen unempfindlich sind.

Die vorliegende Dissertation befasst sich mit der Herstellung und Charakterisierung flexibler Sensoren auf Polymerbasis, die von außen angelegte Drücke und Kräfte messen können. Um die Flexibilität zu gewährleisten wird dazu ein Polymersubstrat als Trägermaterial eingesetzt. Dem Polymer werden Kohlenstoff-Nanoröhrchen (CNTs) zugesetzt, um dem Material piezoresistive Eigenschaften zu verleihen. Das Funktionsprinzip beruht auf der Tatsache, dass sich das Polymervolumen bei einem von außen ausgeübten Druck verringert, wodurch sich der Abstand zwischen den einzelnen CNTs effektiv reduziert. Hierdurch erhöht sich die Leitfähigkeit des Verbundwerkstoffs, die gemessen werden kann. Diese Arbeit gliedert sich in zwei Hauptteile: Flexible Sensoren mit integrierten Kohlenstoff-Nanoröhren, die entweder zufällig im Polymer dispergiert sind oder aber durch ein elektrisches Feld ausgerichtet werden. In der Dissertation werden alle Herstellungsschritte zur Dispersion der Kohlenstoffnanoröhren im Polymer erläutert und die verschiedenen existierenden Verfahren vorgestellt. Darauf werden erste Dehnungs- und Druckergebnisse mit den beiden ausgewählten Polymeren Polydimethylsiloxan (PDMS) und Polyimid (PI) dargestellt. Die Vorteile beider Polymere und Sensortypen werden erörtert. Es folgt die Einführung der Möglichkeit, die Querempfindlichkeit der Sensoren zu verringern, indem die Kohlenstoffnanoröhrchen vor der Aushärtung des Polymers ausgerichtet werden.

Das Prinzip des induzierten Dipolmoments innerhalb der CNT, das die Rotation in einem elektrischen Feld verursacht, wird erörtert. Dabei werden numerische und analytische Modelle zur Unterstützung der experimentellen Ergebnisse herangezogen. Die Möglichkeit, hochempfindliche piezoresistive Sensoren auf der Grundlage von ausgerichteten Kohlenstoff-Nanoröhren zu schaffen, wird auf den Tunneleffekt zurückgeführt. Der Widerstand solcher Verbindungen nimmt mit dem Abstand exponentiell zu, was zu hochempfindlichen Sensoren mit Gauge-Faktoren von bis zu 10^3 führt, die im Rahmen dieser Arbeit gefunden wurden.

Schließlich werden die Drucksensoren mit zufällig angeordneten CNTs in Gummidichtungen integriert, um deren Zustand und den auf sie ausgeübten Druck zu überwachen.

Contents

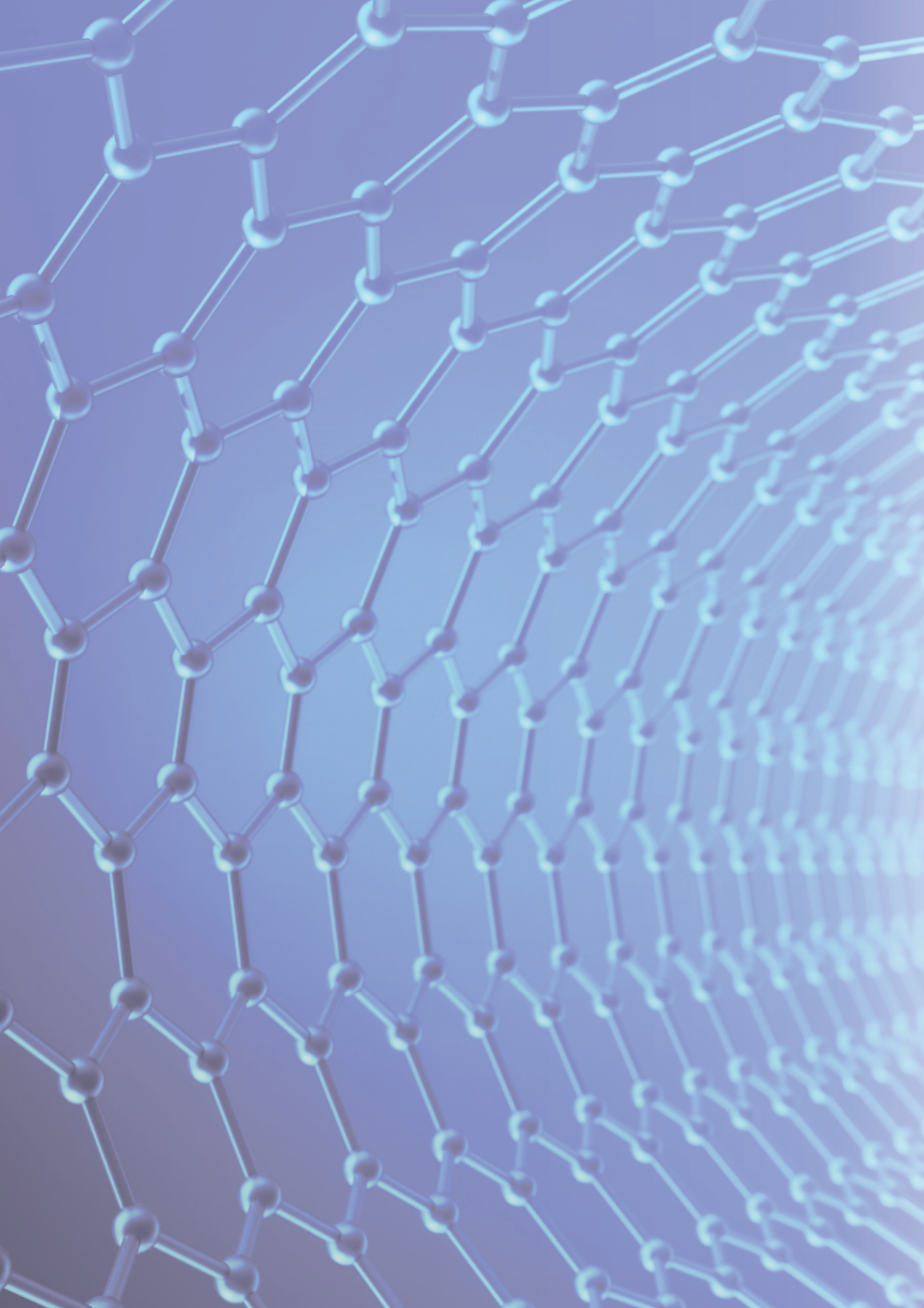

CHAPTER I

Introduction

Abstract

This Chapter starts by briefly discussing the main material of this research: Carbon Nanotubes-based sensors. These high aspect ratio conductive nanotubes are key in fabricating highly sensitive piezoresistive polymers. After this brief introduction, a few state of the art examples are highlighted, giving the reader a first impression of flexible sensors with integrated carbon nanotubes. A quick overview of the structure of this dissertation is given, after which the research topics and goals are stated that will be answered throughout this work and summarised in the final Chapter.

The words Carbon Nanotubes, CNTs, nanotubes and Multi-walled carbon nanotubes (MWCNTs) are arbitrarily mentioned in this dissertation. Unless specifically mentioned, all carbon nanotubes were Multiwalled CNTs (MWCNTs). Therefore, it is implied that when spoken off CNTs, actual Multi-walled CNTs are meant, unless specifically single-walled CNTs are written.

I.1 The History of Carbon Nanotubes

Carbon nanotubes were discovery by Iijima and Ichihashi in 1991 [4]. They synthesised the first reported single-wall carbon nanotube with a diameter of 1 nm [6] [7]. The world quickly realised the great potential of this newly found single-layer rolled graphene layer. Exceptional tensile strength, thermal and electrical conductivity and promising electrochemical properties are several properties of CNTs that would revolutionise numerous fields.

Several years later, in the year 2018, the first CNT reinforced composites were manufactured which showed to strengthen the materials up to 30% [3]. It started with bike components and worked their way up to wind turbines [10], and into the biomedical field. Especially the latter gave rise to a near infinite possibilities due to the ability to use carbon nanotubes as scaffolds for bone growth in tissue engineering [15]. New arising trends show the possibility of repairing neurons, which could open a whole new world of possibilities regarding neurological diseases [4] [11].

The trend of creating nanoparticle polymer composites is shown in Figure I.1. It is clear that CNTs are a highly researched field, with a ongoing growing interest in creating reinforced composites or polymers. Implementing carbon nanotubes in polymer layers opens the field for creating thin, but still conductive sensors that can be wrapped, rolled, and twisted without having the risk of damage. The shift from stiff silicon-based electronics to flexible electronics is still ongoing. The interests of aligning CNTs can be found as early as the year 2005 [9]. In this case, growing vertically the CNTs directly, is not meant. In this research, alignment of CNTs, is by applying an external force like an applied electric field to rotate and align the carbon nanotubes.

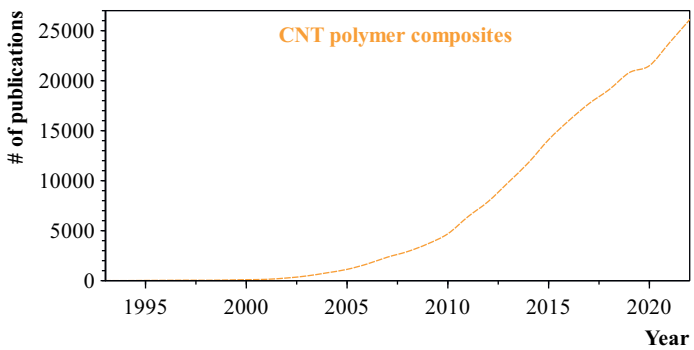

Figure I.1: Number of published papers related to CNT polymer composites [13].

The creation of aligned carbon nanotubes for creating uni-directional conductive (heat or electrical) is still in its infancy and features a high potential in creating sensors sensitive to a single direction, high heat conductive sensors, and optical transparent sensors [1] [14] [12].

This research presents sensors based on the piezoresistive property, produced by mixing carbon nanotubes into polymers. Applying pressure reduces the gaps between them, resulting in a change in the material's conductivity. Various mixing and manufacturing methods are presented, and their (dis)advantages are discussed. The integration of the sensors is also addressed, and the results of the sensor behaviour are presented. The experimental findings are supported by numerical and analytical models that illustrate the sensor's effect.

I.2 State of the Art

As mentioned above, the alignment of carbon nanotubes in compounds has been researched and modelled for multiple years now. However, clear fully working flexible (and possibly optically transparent) uni-directional sensitive sensors are not common. Several small-scale studies and working proof-of-concepts and prototypes have been presented and published, but the possible prospect and impact is still great. It is thought that a sensor with a pre-defined conductivity is only sensitive to a geometrical change in a given direction. This would allow the sensor to be less vulnerable to cross-sensitivities. A clear example is that a parallel plate capacitor can measure the pressure when vertically pressed together, but it also changes its value due to lateral strain (changing the area of the sensor). Theoretically, an aligned sensor would be able to ignore the lateral strain and only 'feel' the pressure change from above. Several current literature examples of aligned carbon nanotube compounds are given below to give the reader a first impression of the current research state.

Most commonly, the carbon nanotubes are mixed into the polymer directly or with additional solvents to lower the viscosity. The research of I. Akhtar et al. [1] shows various CNT concentrations (0.01 to 0.1 weight percentages, wt%) mixed directly into PDMS by diluting the mixture with de-ionised water. The carbon nanotubes are functionalised before integration in order to minimise the contamination and amorphous impurities that occur during fabrication. Additionally, this functionalised helps with better alignment into polymers. An AC 300kHz voltage of 50kV/m was applied between two copper electrodes and the suspension showed an alignment already after several seconds. The alignment was stopped after 3 minutes. After the removal of water, the samples are dried and cured in an oven at 60 °C for 8 hours. Results of the piezoresistive layer show a large difference in measurable resistance in the parallel and perpendicular direction. Difference in measured resistance up to a factor of 10 show that the sensing layer indeed features an aligned conductive network in a single direction. Cross-connection do enable the ability to also measure a conductivity in the direction perpendicular to the alignment. The

measured Gauge factors are greatly increased due to the alignment and are presented up to an order of 218.

Another research manufacturing similarly aligned carbon nanotube - PDMS layers presents differences in sensitivity for the perpendicular and parallel directions [12]. The sensing layers are pulled apart up to 16% and the change in resistance is shown in Figure I.2. It can be seen that the sensing layers show a slight drift after repeated cyclic loading but the general trend remains the same. The sensors are highly sensitive in the parallel direction (Gauge factor of 59) and show hardly any change (Gauge factor of 1) in the perpendicular direction.

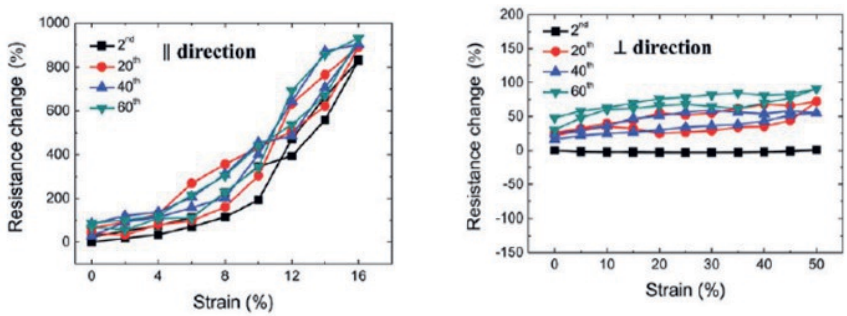

Figure I.2: Relationship of electrical resistance and strain along two orthogonal directions and cyclic loading [12].

The ability to increase the Gauge factor even further by creating a piezotronic tunneling junction was shown by Q. Yu et al. [2] in 2022. They found, for small strain regions up to 0.10%, high Gauge factors up to $4.8x10^5$. The results are compared to conventional Schottky-barrier based strain sensors and presented in Figure I.3. It can be seen that a small region of non-linearity is present in the tunneling junction by means of a jump in conductivity. The presented Gauge factors are several order of magnitude higher than their regular counterparts. It must be mentioned that these sensors were not created using carbon nanotubes, but the principle of increasing the sensitivity of sensors by ensuring the main piezoresistive property is based on electron tunneling is shown in this research.

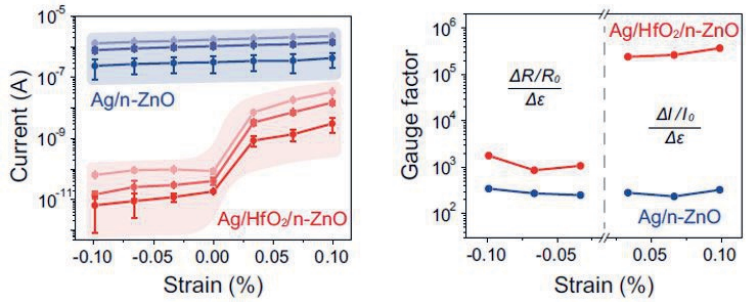

Figure I.3: High Gauge factors of electron tunneling junctions compared to conventional Schottky-barrier based strain sensors ($Ag/n-ZnO$) [2].

The difference in alignment for regular pristine CNTs and oxidised CNTs was quantified by [8] in 2008. It is thought that the functionalisation causes additional repulsive interaction between the -OH and -COOH groups, improving the dispersement and alignment of carbon nanotubes. This is clearly observed in Figure I.4. It is also visible that oxidised carbon nanotube create less agglomerated and bundled conductive pathways, when compared to regular carbon nanotubes.

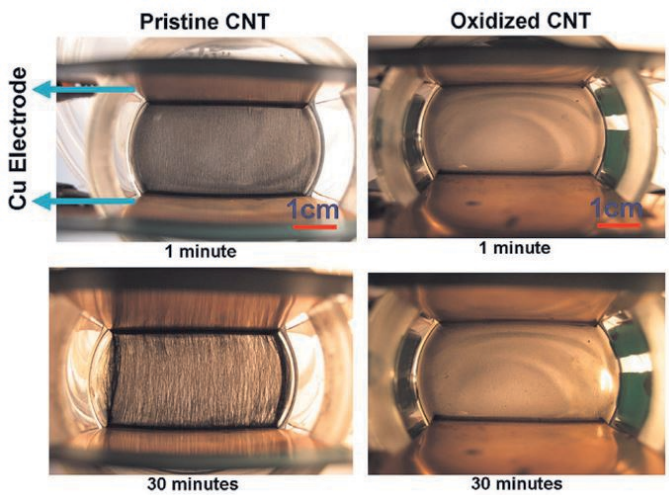

Figure I.4: Comparing the alignment behaviour of pristine and oxidised CNTs [8]. Left: course and agglomerated bundles of CNTs. Right: fine and thin aligned CNT connections.

Finally, different parameters like host polymer material, curing time and temperature, mixing time and speed all effect the final dispersion and hence the sensitivity of the sensor. This effect was shown in [5] and Figure I.5, where the influence was quantified by varying the above-mentioned parameters. For non-aligned carbon nanotubes, the Gauge factor increased with lower weight contents. Increasing the mixing speed or time yielded in more homogeneous mixtures and more sensitive sensing layers. However, as will be mentioned in this work, there is an apparent maximum of mixing time after which the CNTs start to agglomerate again and sensitivity drops.

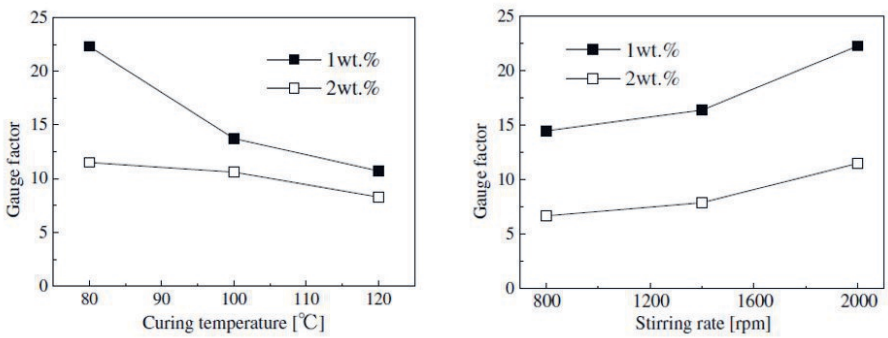

Figure I.5: Effect of curing temperature and mixing speed on the Gauge factor [5].

I.3 Dissertation Structure

This work is divided into three main categories: piezoresistive polymers, polymer layers with and without aligned carbon nanotubes. The first Chapter addresses the fabrication of the piezoresistive layers. The concept of percolation threshold and the dispersement of carbon nanotubes into polymers is discussed. Additionally, the mechanical and electrical influences of nanotubes in the polymers are discussed.

Once the basic concept of the piezoresistive polymer layers is explained, Chapter III introduces the first polymer pressure sensors with randomly dispersed carbon nanotubes. Two polymer types are analysed with corresponding numerical simulations, performed with COMSOL Multiphysics.

Chapter IV introduces the concept of aligning carbon nanotubes by means of an externally applied electric field. This principle is divided into three approaches: numerical, analytical and experimental. The final results show a working strain sensor based on electron tunneling piezoresistivity, resulting in high Gauge factors. The Chapter concludes with the investigation of the alignment quality regarding functionalised carbon nanotubes.

Chapter V shows the integration of the sensors in rubber sealings. The manufacturing of the sealings, the integration parameters and the final integrated sensor and corresponding measurements are presented.

This dissertation ends with an overview of the research topics and the corresponding findings and future outlook.

I.4 Research Topics and Goals

The focus of this project and research questions can be subdivided into several key parts which are summarised below. It was chosen to develop the sensors using a non-conductive polymer and integrating conductive particles (CNTs) into this polymer to create a piezoresistive polymer. The main focus is on the manufacturing of the piezoresistive layers and less on the actual sensor characterisation. Hence, the research questions and goals were chosen with a large focus on the manufacturing of such polymer mixtures and sensor layers.

1. Determination of suitable materials that can be used for flexible pressure sensors and their corresponding (dis)advantages in terms of manufacturing processes and sensitivity.

2. Investigating sensor geometries in term of sensitivity and stability.

3. Manufacturing aligned carbon nanotube networks to minimise the cross-sensitivity of the sensors.

4. Integration of flexible piezoresistive sensors in (industrial) sealings to measure pressure changes over time.

Several additional research goals were set regarding the numerical and analytical part of this thesis:

8. Creation of a numerical model that features the basic principle of a piezoresistive pressure sensor with carbon nanotubes.

9. Creation of a numerical model that can investigate whether a change in CNT orientation (due to alignment) could indeed change the sensors sensitivity for certain directions.

10. Analytical investigation regarding the effect of the electron-tunneling based piezoresistivity and what the corresponding expected sensitivities.

11. Determination of the alignment parameters of carbon nanotubes in polymer liquids; such as field strength, distance, materials and geometries.

I.5 Principle of Unidirectional Sensitivity

The reasoning for aligning the carbon nanotubes in the polymer is graphically depicted in Figure I.6. High amounts of dispersed carbon nanotubes create a sort of web in all directions. The resistivity is low as the nanotubes are well connected and the electron tunneling effect is minimal. If a pressure or strain is applied to the polymer, the material deforms. The high stiffness keeps the nanotubes outer dimensions the same, only possibly changing the orientation and location. Due to the non-changing geometry and the very well connected mesh-like structure of dispersed nanotubes, low Gauge factors are expected. The main effect for a conductivity change is attributed to 'loss of connections' due to the applied strain. The higher the nanotube concentration, the more connections are possible and the change of a disconnecting path due to applied strain is lower. This train of thought is visualised more clearly in the top right side of Figure I.6. When applying a strain this network, keeping in mind that the dimensions of the individual nanotubes do not change, the network behaves like a harmonica. Additionally, the sensitivity in both directions (ϵ_1) and (ϵ_2) is expected to be similar.

Therefore, to increase the sensitivity of the sensing network based on carbon nanotubes, it is theorised to lower the concentration. This in turn increases the the possibility of 'loss of connections' with applied tensile strain, increasing the sensitivity.

With aligned carbon nanotubes, long connections are formed that are either well connected or within very small range of each-other. An applied strain in the direction of ϵ_4 clearly has no effect. Applying a strain in the aligned direction (ϵ_3) could potentially cause major changes in the materials conductivity due to the disconnection of conductive pathways and possible even due to electron tunneling effects. This principle is the basis of this dissertation and will be investigated in the upcoming chapters.

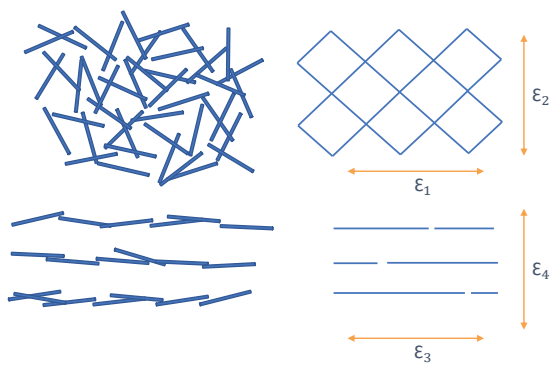

Figure I.6: Influence on carbon nanotube alignment orientation. Randomly oriented well-connected networks are expected to have a low Gauge factor response due to a harmonic compression of CNT networks. Electric field aligned carbon nanotube networks are expected to have a dominating factor of electron tunneling and increased sensitivity.

References

[1] Imtisal Akhtar and Seung-Hwan Chang. "Highly aligned carbon nanotubes and their sensor applications". In: Nanoscale 12.41 (2020), pp. 21447–21458.

[2] Alamusi et al. "Piezoresistive strain sensors made from carbon nanotubes based polymer nanocomposites". In: Sensors 11.11 (2011), pp. 10691–10723.

[3] Devashree Atre and Shashank Pant. "Charged Carbon Nanotubes". In: Carbon Nanotubes: Recent Progress (2018), p. 109.

[4] Junqi Chen, Shiqin Wei, and Haoyan Xie. "A brief introduction of carbon nanotubes: history, synthesis, and properties". In: Journal of Physics: Conference Series. Vol. 1948. 1. IOP Publishing. 2021, p. 012184.

[5] Ning Hu et al. "Investigation on sensitivity of a polymer/carbon nanotube composite strain sensor". In: Carbon 48.3 (2010), pp. 680–687.

[6] Sumio Iijima. "Helical microtubules of graphitic carbon". In: nature 354.6348 (1991), pp. 56–58.

[7] Sumio Iijima and Toshinari Ichihashi. "Single-shell carbon nanotubes of 1-nm diameter". In: nature 363.6430 (1993), pp. 603–605.

[8] Chen Ma et al. "Alignment and dispersion of functionalized carbon nanotubes in polymer composites induced by an electric field". In: Carbon 46.4 (2008), pp. 706–710.

[9] CA Martin et al. "Electric field-induced aligned multi-wall carbon nanotube networks in epoxy composites". In: Polymer 46.3 (2005), pp. 877–886.

[10] Leon Mishnaevsky Jr et al. "Materials for wind turbine blades: An overview". In: Materials 10.11 (2017), p. 1285.

[11] Carlos Redondo-Gomez et al. "Recent advances in carbon nanotubes for nervous tissue regeneration". In: Advances in Polymer Technology 2020 (2020), pp. 1–16.

[12] Chao Sui et al. "Directional sensing based on flexible aligned carbon nanotube film nanocomposites". In: Nanoscale 10.31 (2018), pp. 14938–14946.

[13] Summery of Searching results. URL: `https://scholar.google.com` (visited on 05/18/2022).

[14] Yang Yu et al. "Flexible and transparent strain sensors based on super-aligned carbon nanotube films". In: Nanoscale 9.20 (2017), pp. 6716–6723.

[15] Laura P Zanello et al. "Bone cell proliferation on carbon nanotubes". In: Nano letters 6.3 (2006), pp. 562–567.

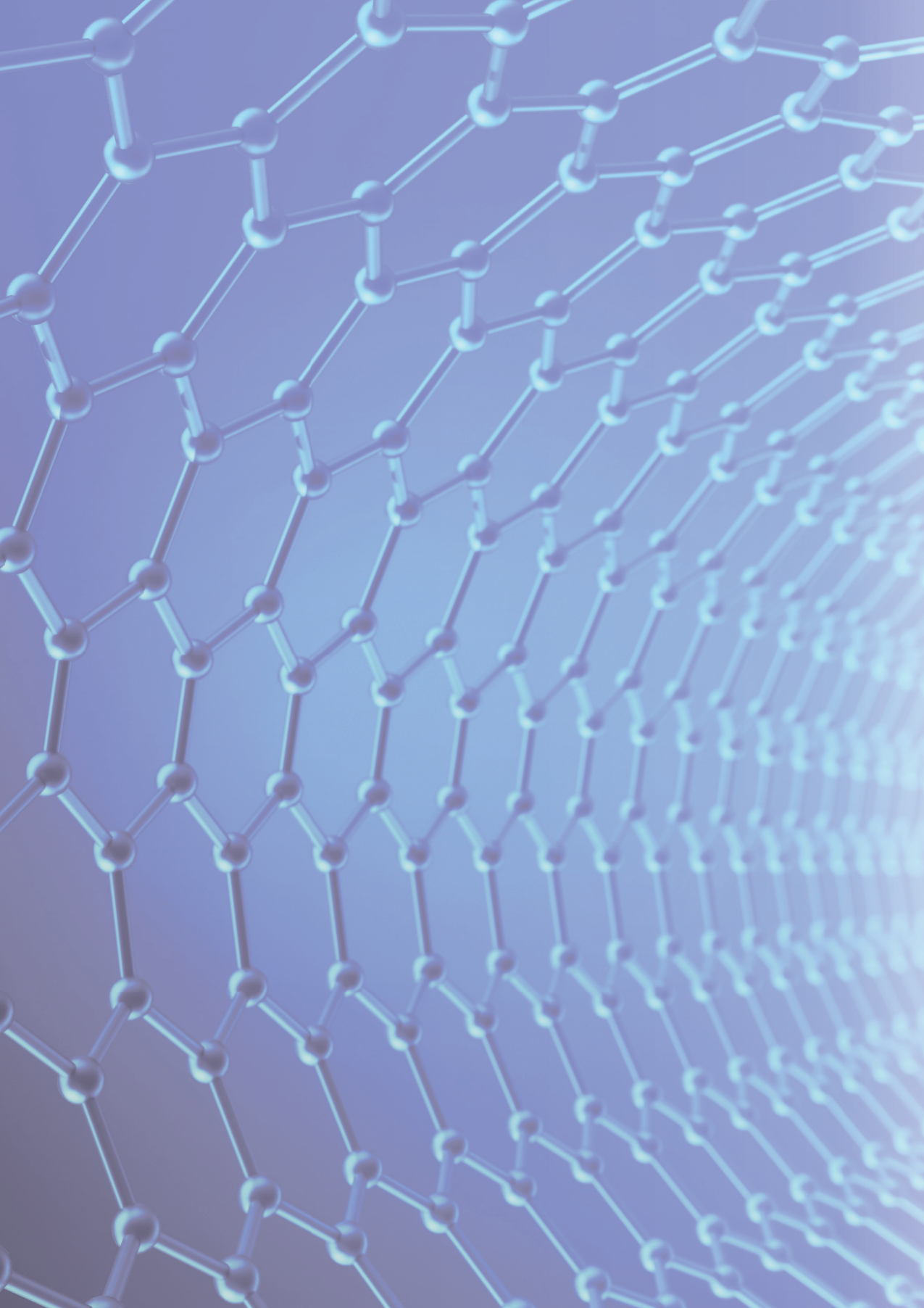

CHAPTER II

Fabrication of Piezoresistive Polymers

Parts of this chapter have been published in:
de Rijk, T. M., & Lang, W. (2021). Low-cost and highly sensitive pressure sensor with mold-printed multi-walled carbon nanotubes dispersed in polydimethylsiloxane. Sensors, 21(15), 5069.

Cen-Puc, M., de Rijk, T.M, Gleason, M. V.,& Lang, W. (2021, October). Carbon Nanotubes/ Polymer Films for Microsensors Applications.
In 2021 IEEE Sensors (pp. 1-4). IEEE.

Abstract

Adding certain amount of conductive particles in a polymer can turn the insulator into a conductor. This specific change in material property is called the percolation threshold. This Chapter will go in depth into the implemented materials and fabrication of such materials.

First, the properties of the carbon nanotubes and chosen polymers polydimethylsiloxane and polyimide are discussed, after which the dispersion methods are shown. The most common method, implementing the addition of solvents and via ultrasonic mixing, is compared to the newly introduced direct mixing method (developed by colleague M. Cen-Puc). The main advantage is the fact that this method does not need solvents to dilute the mixtures and yields faster and more dispersed carbon nanotube - polymer layers.

The second part of this Chapter gives the reader an inside in the difficulties of creating metallic connections on the PDMS layer. Mainly this is due to the extremely hydrophobic nature and the high temperature expansion coefficient. Possibilities into diverting or solving these difficulties are mentioned, as well as finished sensors that are isolated from the wafer via dry etching.

II.1 Piezoresistive Property

The piezoresistive property refers to the phenomenon where the electrical resistance of a material changes in response to applied mechanical strain or pressure. This property allows the material to act as a sensor, converting mechanical stimuli into electrical signals.

The principle behind the piezoresistive effect lies in the alteration of the atomic arrangement and the resulting changes in the flow of electrons within a material when it is mechanically deformed. When a stress or strain is applied to a piezoresistive material, the arrangement of its atoms is distorted, leading to changes in the material's conductivity or resistivity. On top of this, the changing geometry also effects the resistivity of the material. These changes can be measured as a change in the electrical resistance of the material, which is directly proportional to the applied mechanical force or pressure.

Flexible sensors based on the piezoresistive property are particularly interesting due to several reasons:

- Flexibility: Piezoresistive materials based on polymers can be incorporated into flexible substrates, enabling the development of sensors that can conform to curved surfaces, irregular shapes [43], or even be integrated into textiles [11] [18] [56]. This flexibility allows for the creation of wearable devices [51], electronic skins [2] [8] [17], and other applications that require conformable and unobtrusive sensing.
- Sensitivity: Piezoresistive sensors can exhibit high sensitivity to small changes in pressure or strain [43] [54] [19], making them suitable for detecting subtle forces or variations.
- Cost-effectiveness: Piezoresistive sensors can be manufactured using relatively simple and cost-effective techniques, such as thin-film deposition [21] [34] [33] or screen printing [16] [17]. This makes them attractive for large-scale production and integration into a wide range of consumer products and industrial applications.
- Versatility: Piezoresistive materials can be tailored to different requirements by selecting appropriate compositions and structures. This allows for customisation of the sensors' properties, such as sensitivity, linearity, and temperature stability, to suit specific applications.

II.2 Percolation Threshold of Conductive Polymers

Increasing the concentration of conductive fillers in an initially non-conductive polymer leads to a rise in conductivity. Eventually, the non-conductive material reaches a critical point known as the percolation threshold, at which it becomes conductive. At this stage, the resistivity of the material experiences a sudden drop, resulting in a conductive polymer. This change in material property is graphically shown in Figure II.1.

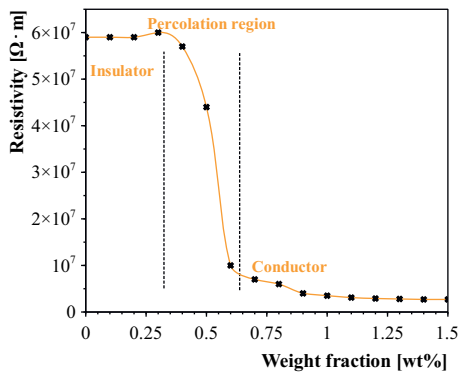

Figure II.1: Material change from insulator to conductor. Values are fictive numbers and serve only for illustration purposes.

Even a slight change in pressure, which corresponds to a small change in the material's dimensions, can result in a significant variation in its inherent resistance. Developing materials that are positioned right at the edge of this threshold could yield highly sensitive sensors.

The percolation threshold can vary widely, ranging from 0.035% to 60%, depending on the dimensions of the filler and it's dispersion [37]. Large metallic powders require as much as 60% concentration to achieve percolation [20], which is generally impractical for most applications due to its substantial impact on mechanical properties. However, reducing the particle size, for example, by employing carbon black micro-particles, can lower the percolation threshold to a range of 3% to 15% [20] [50]. Previous research at IMSAS University Bremen has successfully demonstrated the creation of piezoresistive layers using a mixture of carbon black and polymer through screen-printing these layers onto silver electrodes [12].

By further reducing the particle size to a significantly smaller scale, and employing high aspect ratio (AR) carbon nanotubes, the percolation threshold is shifted even more towards lower concentrations. This is due to the fact that the percolation threshold is highly dependent on the aspect ratio of the fillers, as demonstrated by Chen et al. in their research on determining the theoretical estimation of the percolation threshold for polymer matrix composites [9]. The correlation between the percolation threshold and the fillers' aspect ratio is mathematically represented by Equation II.1 [9].

$$\Phi_{pc} = \frac{(3+\delta_d^2)}{6AR} \tag{II.1}$$

In this context, the dimensionless range of diameter, denoted as δ_d, is defined as $\delta_d = (d_2 - d_1)/(d_2 + d_1)$, assuming a normalised distribution of carbon nanotube (CNT) diameters. A study by Li et al. [20] suggests that the relation of high aspect ratio multi-walled carbon nanotubes between volume and weight percentage can be established at $vol\%$= 2 wt%.

However, it is crucial to acknowledge that this relation holds true only when the carbon nanotubes are perfectly distributed within the polymer matrix. The presence of agglomerations lead to an upward shift in the percolation threshold. This phenomenon was also explored by Li and Jing [20], where it was discovered that an agglomerated volume fraction of 5% can already shift the percolation threshold one order of magnitude.

The wide range of percolation thresholds observed in CNT-polymer layers (ranging from 0.035 wt% to 2.4 wt% [5]) can be attributed to the diversity in CNT dimensions, mixing techniques, and choices of polymer/solvent combinations. A comprehensive discussion on this topic can be found in the upcoming sections.

The impact of the aspect ratio on the percolation threshold is visually depicted in Figure II.2. The graph clearly illustrates that higher aspect ratios allow for lower concentrations of conductive fillers, which brings various advantages. For example, the mechanical properties are less affected and the potential to develop optically transparent conductive polymers remains feasible. For instance, thin layers of CNT-polymer composites containing as little as 0.5 wt% of CNTs can still maintain a high degree of transparency.

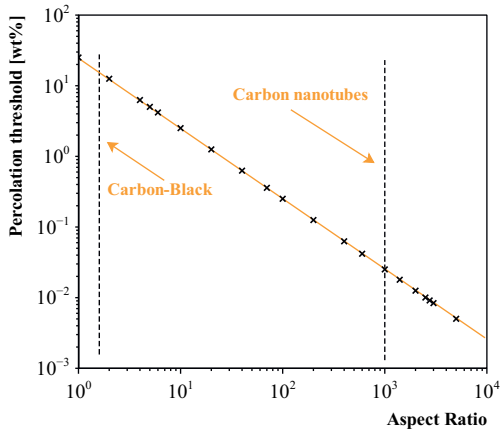

Figure II.2: Relation between CNT aspect ratio and percolation threshold. High aspect ratio carbon nanotube have a lower theoretical percolation threshold.

II.3 Material Selection

II.3.1 Carbon Nanotubes

A carbon nanotube is a one-dimensional carbon material with remarkable aspect ratios that can reach up to 1000 [25]. Conceptually, CNTs can be visualised as rolled-up graphite sheets, forming long rods in the micrometer range with nanometer-scale thickness. There are two main types of CNTs: single-walled carbon nanotubes (SWCNTs) and multi-walled carbon nanotubes (MWCNTs). The name itself provides a concise description of their dissimilarity. SWCNTs consist of a single cylindrical shell, while MWCNTs consist of multiple concentric layers, making them relatively thicker.

Another significant distinction lies in the crystal orientation of CNTs. There are three primary crystal orientations: armchair, zig-zag, and chiral. The chiral vector, determined by different techniques used in wrapping the graphite sheet, plays a crucial role in defining whether the CNTs possesses metallic or semiconducting properties. This chiral vector uniquely characterises the geometry of the carbon nanotube and can be denoted by Equation II.2, where a pair of indices (n, m) represents the connection between two crystallographically equivalent sites on the graphene sheet [48]. These vectors run along the two directions in the honeycomb crystal lattice.

$$\vec{C} = n\vec{a} + m\vec{b} \tag{II.2}$$

With this information, carbon nanotubes (CNTs) can be classified into three distinct types based on their chiral indices (n, m):

- Ziz-zag when m or n = 0
- Armchair when m = n
- Chiral when all other cases and m ≠ n

A graphical representation of the different chiral structures is shown in Figure II.3. Controlling the chirality of single-walled carbon nanotubes (SWCNTs) is difficult [48]. Consequently, a significant portion of SWCNTs are non-metallic in nature. It is estimated that only around one-third of SWCNTs exhibit metallic properties [48]. Therefore, to ensure conductive characteristics, the majority of carbon nanotube structures consist of multi-walled carbon nanotubes (MWCNTs). In MWCNTs, current can flow between the layers, increasing the likelihood of achieving conductivity.

In terms of chiral types, armchair CNTs possess metallic properties due to the absence of a bandgap between the valence band and the conduction band. On the other hand, zigzag CNTs have a small bandgap between the bands, making them semiconducting in nature [15].

The research presented in this work featured multi-walled carbon nanotubes (from Sigma Aldrich Chemie GmbH) with an outer diameter of 50-90 nm and an aspect ratio of >100.

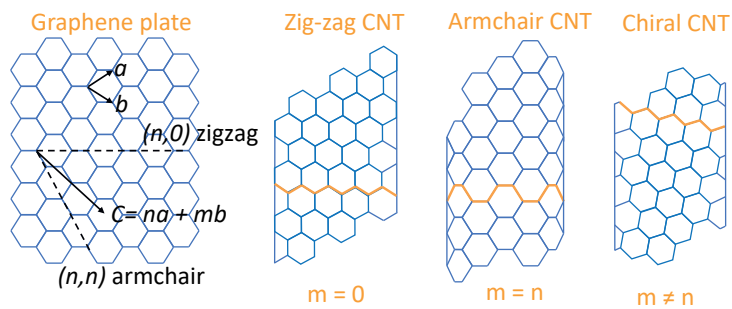

Figure II.3: Crystal orientation of CNTs. The Armchair crystal orientation possesses metallic properties. However, with Multi-walled carbon nanotubes, conductive properties are always present.

II.3.2 Polymer Selection

The sensors rely on a flexible conductive polymer as their key component. Two polymers have been investigated for this purpose, and they are outlined below.

- Polydimethylsiloxane (PDMS) Slygard 184 from Dow Corning.
- Polyimide (PI) precursor U-varnish-S with 20 wt% polyamic acid content from UBE Europe GmbH.

In order to manufacture fully functional sensors, it is necessary to include a metal layer on top of the pressure/strain-sensitive polymer. This metal layer serves as connections to measure the changes in sensor response. Subsequently, the individual sensors, still interconnected on the silicon wafer, need to be isolated by means of dry etching. The specific processes involved in these steps vary for each polymer and will be elaborated upon in the subsequent sections.

Polydimethylsiloxane

PDMS, commonly referred to as silicone elastomer, is a transparent material with a wide range of applications. The chemical structures is shown in Figure II.4. The long and loose PDMS polymer chain structure cause the polymer to remain highly flexible.

It finds use in various fields such as MEMS sensors, micro-fluidic devices [1], flexible electrodes [26] [23], high voltage resistor packs, adhesive and encapsulation for solar cells, and LED lighting encapsulation [42].

PDMS offers several advantages, including its complete transparency and high flexibility. The material is composed of two parts: a base part and a curing agent. The key properties of PDMS relevant to this research are summarised in Table II.1.

Table II.1: PDMS parameters [42] [52].

Property	Unit	Result
Colour		Colourless
Viscosity (base)	Pa-sec	5.1
Viscosity (mixed)	Pa-sec	3.5
Curing time at 25°C	hours	1.5
Curing time at 100°C	minutes	35
Volume resistivity	ohm*cm	2.9E+14
Thermal expansion coefficient	$\mu m\ m^{-1}\ ^{\circ}C^{-1}$	310
Temperature stable below	$^{\circ}C$	150
Tensile strength	MPa	6.7

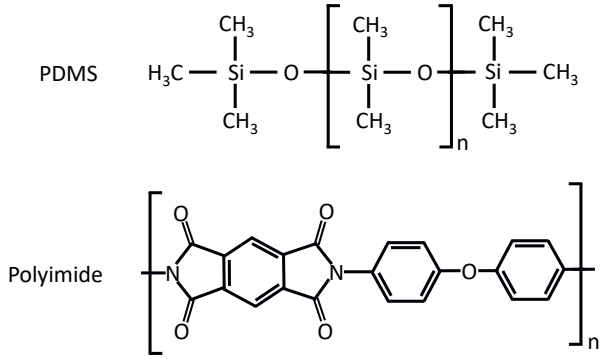

Figure II.4: Chemical structures of PDMS and polyimide [10] [13] [53]. PDMS: other connections are possible at the Methyl-group locations, depending on the specific product. PI: This is an example of a specific polyimide. In general it is classified as the typical imide monomer.

Polyimide

The chemical structure of the more densely (and less flexible) cross-connected thermoset polyimide is depicted in Figure II.4. This thermosetting polymer features for example applications in the automotive industry for plastic car parts [38], re-enforcement for wind-turbines [28] and medical devices [39].

Polyimide belongs to the family of aromatic polyimides. The chemical structure features repeating imide monomers which contain two acyl groups (C=O) bonded to nitrogen [31]. It is well known for its high temperature stability (400-500 °C) and chemical resistance. Polyimide is often used as a substrate material and electrical insulator [39]. The polymer used in this work is polyimide precursor U-varnish-S with 20 wt% polyamic acid content (UBE Europe GmbH). The initial mixture reacts to heat and forms the final polyimide product. The key difference between PDMS and polyimide (except from their chemical structure) is the elastic modulus of both materials once cured. For PDMS the elastic modulus is between 1.4-3 MPa [4], far lower than for polyimide (2.34 GPa) [55] [41].

II.4 Dispersion of Carbon Nanotubes

The dispersion quality is of high importance in order to maximise the potential of carbon nanotube-polymer mixtures. The CNTs tend to agglomerate and form clusters due to the van der Waals forces [24].

A commonly employed technique for incorporating electrically conductive particles into polymers is through the dispersion of particles using ultrasonic waves [29], [46], [35]. In this method, carbon nanotubes are mixed with the polymer and then subjected

to an ultrasonic bath. However, this approach may not always be suitable for more viscous materials. To overcome this limitation, it is often necessary to combine this method with the addition of a significant amount of solvents. This helps reduce the viscosity of the solution and facilitates the dispersion of CNTs through ultrasonication.

One clear disadvantage of this approach is that, prior to the final application of the layer, the solvents used in the process needs to be extracted again. This solvent extraction step can potentially impact the dispersion of CNTs once again, leading to changes in their distribution within the polymer matrix.

II.4.1 Effect of Functionalised Carbon Nanotubes

Regular CNTs are inert and can only interact with the surrounding polymer matrix through van der Waals interactions, not optimally making use of the load transfer across the CNT-Polymer matrix [25]. Additionally, the better the dispersion of CNTs in the polymer, the higher the performance of the nanocomposite. Both these reasons are the key attribute in numerous research regarding functionalisation of carbon nanotubes. The process causes additional functional groups at the sides/ends of the carbon nanotubes, modifying their surface properties. A schematic representation of the two most common functionalisations is shown in Figure II.5.

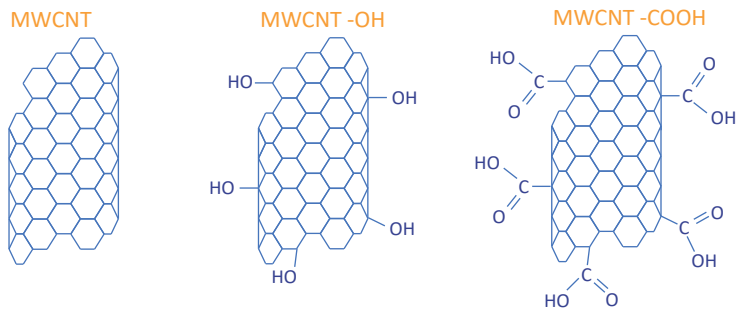

Figure II.5: Examples of CNT functionalisation groups.

II.4.2 Ultrasonic Dispersion of Carbon Nanotubes

In the commonly used ultrasonic dispersion method for incorporating CNTs into polymers, the choice of solvents plays a crucial role in achieving successful dispersion while maintaining compatibility with the polymer matrix. Some solvents, such as chloroform, are known to dissolve the PDMS base polymer, resulting in a significant reduction in viscosity and improved dispersion of CNTs. Research has shown that even up to 9 wt% of CNTs can be uniformly dispersed in the polymer matrix using this approach [22].

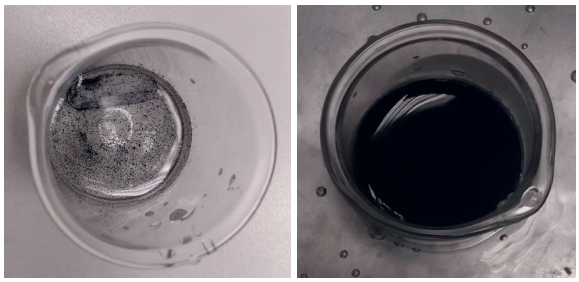

Figure II.6: Effect of ultrasonic dispersion of CNTs. Initially, large agglomerated carbon nanotube clusters are visible. After only several minutes in the ultrasonic bath, a homogeneous black coloured mixture is created.

However, the major drawback is the high toxicity of chloroform, as to why this solvent was not utilised for this research.

The impact of ultrasonic dispersion can be observed in Figure II.6, where a water-CNT solution is subjected to sonication for several minutes. The initially agglomerated CNTs in the transparent liquid transform into a completely black and well-dispersed solution. The images also clearly demonstrate that although the initial amount of added CNTs may appear insufficient (as seen in the left figure of Figure II.6), proper dispersion results in a non-transparent solution throughout.

The typical procedure for dispersing CNTs in polymers is illustrated in Figure II.7. First, both the polymer and the CNTs are mixed with a compatible solvent. This step serves to reduce the viscosity of the solution and disperse the CNT agglomerates. Subsequently, the carbon nanotubes and polymer solutions are combined and subjected to an ultrasonic bath. This ultrasonication process promotes the dispersion of CNTs within the polymer matrix.

Once the dispersion of CNTs in the polymer is completed, the solvent needs to be removed. This is accomplished by mechanically stirring the solution while gradually heating it, allowing the solvents to evaporate. Only after this solvent removal process is complete, the resulting mixture can be utilised for fabrication purposes. Figure II.7 provides a general overview of this concept.

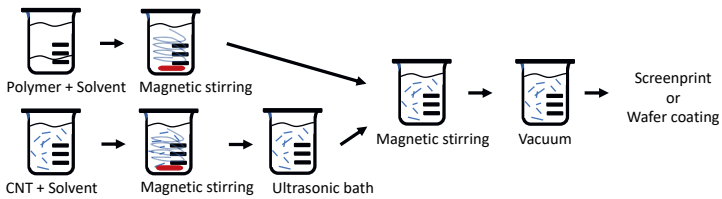

Figure II.7: Ultrasonic CNT dispersion method in polymers

This research specifically targeted solvents that are considered (relatively) user-friendly and readily available. The compatibility between solvents and PDMS was investigated, considering the following list of solvents:

- 2-Propanol (IPA)
- Isopropyl acetate
- Propylene glycol methyl ether acetate (PGMEA)
- Toluene
- Dimethyl sulfoxide (DMSO)
- Acetone
- Ethanol
- N-Butyl acetate

To investigate the solvent compatibility with PDMS and achieve dispersion of CNTs, the solvents were mixed with the PDMS base polymer and CNTs for 30 minutes at a stirring speed of 700 min^{-1} using magnetic stirring. Following this, the solutions were subjected to ultrasonic treatment in an ultrasonic bath (ROAG FASELLEC AG) for 30 minutes. The mixtures were then placed on a table and monitored for a period of 180 minutes. The observations are summarised in Figure II.8.

Among the solvents tested, IPA (Isopropyl Alcohol) and Isopropyl Acetate exhibited no visible changes or settling effects during the specified time period. However, the other solvents displayed clear separation of materials within the vial, sometimes occurring within minutes (see Figure II.8b). Based on these initial results, IPA was selected for the ultrasonic-solvent mixing approach due to its favourable compatibility and lack of visible separation or settling effects.

As mentioned earlier, a major drawback of this method is the requirement to remove solvents from the mixture before further processing. The choice of IPA as the solvent was based on its ease of evaporation by placing the mixture on a hotplate and heating it to 100°C. However, since IPA was often mixed with the polymer at a ratio of 100:1, the evaporation process could take up to 3.5 hours.

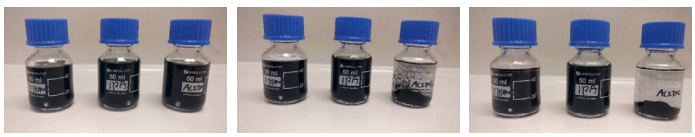

(a) Dispersion quality of CNTs mixed in Ethanol (left), Isopropanol (middle), and Acetone (right). The nanotubes settle almost instantly in the acetone mixture.

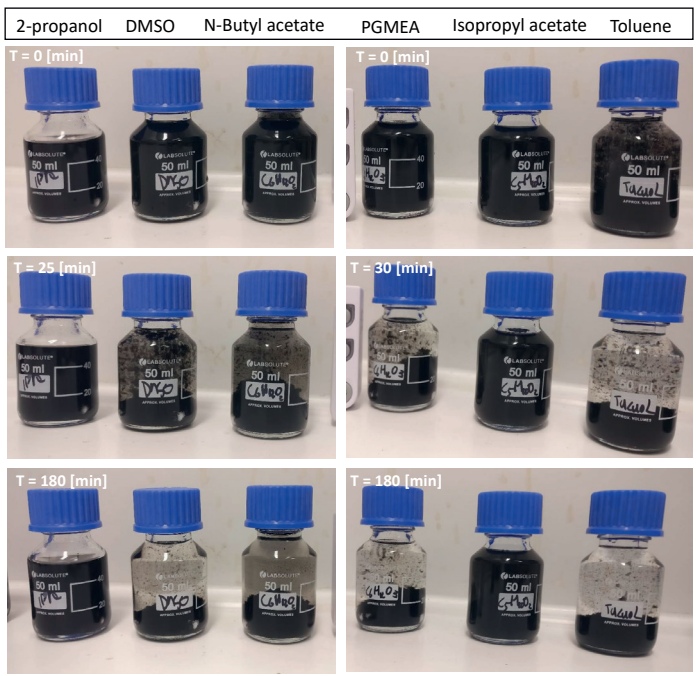

(b) Different solvents mixed with the PDMS base polymer.

Figure II.8: Carbon nanotubes dispersed in numerous organic solvents. Different sedimentation times of the nanotubes is clearly present for different solvents. Isopropanol and Isoproyl acetate show no CNT settling after 3 hours.

After the solvents were removed and the CNTs were dispersed in the polymer, the curing agent was added and briefly mixed into the solution. As a final step, the glass beaker containing the mixture was placed inside a vacuum chamber for 30 minutes to eliminate any air bubbles caused by the mixing process.

In conclusion, this technique enables the incorporation of high concentrations of CNTs into the polymer matrix (up to 8 wt% was tested) due to the reduced viscosity achieved through solvent addition. However, the process is time-consuming, and the need for solvent removal increases the possibility of CNT re-agglomeration, which was observed in some cases. This leads to the formation of large clusters, potentially resulting in reduced sensitivity of the resulting pressure or strain sensitive layers. The dispersion quality was optically assessed by examining the cluster sizes (Figure II.9), and the results are presented in the subsequent section (in Figure II.11).

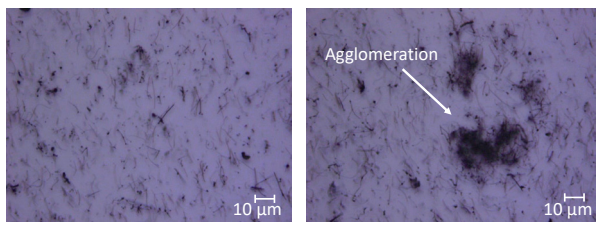

Figure II.9: Agglomeration of CNTs dispersed in a polymer.

II.4.3 Direct Mechanical Mixing Process

A colleague at IMSAS, M. Cen Puc, developed an alternative method known as the "direct mixing" process, which eliminates the need for solvents to disperse CNTs in the polymer [7]. This approach incorporates a custom 3D-printed mixer paddle with 45° pitched blades designed to enhance radial and axial flow [45]. The blades of the mixer paddle fit precisely within a 25ml glass beaker, where the polymer and the specified weight percentage of CNTs are placed. The beaker is then mounted on the mechanical stirrer IKA RW 20n (IKA Works GmbH) and stirred at speeds up to 1200 RPM for 30 minutes.

The high shear forces generated during this process directly disperses the CNTs and break up large agglomerations without the need to lower the viscosity of the polymer. Subsequently, the mixture is placed in a vacuum chamber for 10 minutes to minimise the presence of trapped air bubbles in the final layer. A graphical representation of the direct mixing process is depicted in Figure II.10.

The effectiveness of the newly discovered direct mixing approach was visually demonstrated by significantly improved dispersion of CNTs. The cluster sizes were smaller, and

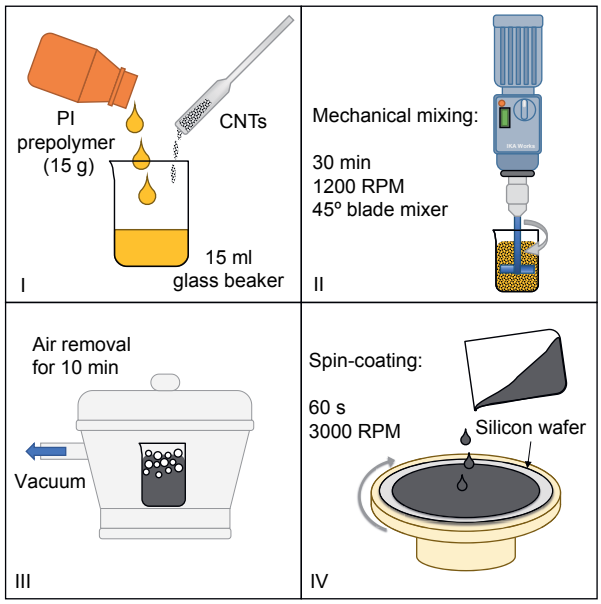

Figure II.10: Direct mixing approach (©2021 IEEE [7]).

a greater number of individual CNTs were observed within the polymer layer. The contrast between the two methods is illustrated in Figure II.11, where the presence of large dense clusters in the solvent method is clearly present for the solvent mixing method.

Furthermore, the previous mixing method, which involved solvent addition and ultrasonic treatment, resulted in a percolation threshold above 1 wt%. In contrast, the faster and more efficient direct mixing method reduced the percolation threshold to approximately 0.45 wt%. This change in percolation is attributed to the improved dispersion.

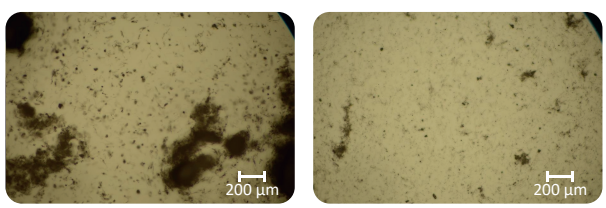

Figure II.11: Difference between solvent method and direction mixing approach ©2021 IEEE.

II.4.4 Detection of Agglomerated Carbon Nanotubes

The optimal dispersion parameters were investigated by varying the mixing speed and mixing time using the direct mixing technique. This section focuses solely on the direct mixing method, as it has been established as superior to the solvent and ultrasonic method. Two types of carbon nanotubes were used: multi-walled carbon nanotubes (MWCNTs) with an outer diameter (OD) of 50nm and lengths (L) ranging from 5-10μm, and functionalised MWCNT-OH with an OD of 50nm and lengths ranging from 5-12μm. These nanotubes were mixed with PDMS and Polyimide.

The mixing times were varied in three steps: 2, 10, and 30 minutes, with both low speed (240 RPM) and high speed (1200 RPM) mixing conditions. The optical results, obtained using a 5x optical microscope and filtered to black and white images to enhance contrast, are presented in Figure II.12, clearly showing the differences in cluster sizes. The optical results reveal the presence of large clusters at low mixing speeds and short mixing times, while smaller cluster sizes are observed at higher speeds and longer mixing times. An interesting finding is that the influence of mixing speed on cluster size does not appear to be time-dependent. In fact, the results indicate that for the standard MWCNTs in PDMS and Polyimide, the cluster sizes may slightly worsen with longer mixing times, but optical inspection alone was insufficient to draw definitive conclusions.

It is well known in the literature that functionalised CNTs feature a greater ability to disperse in liquid media than their regular counterparts [44] [49]. This was briefly

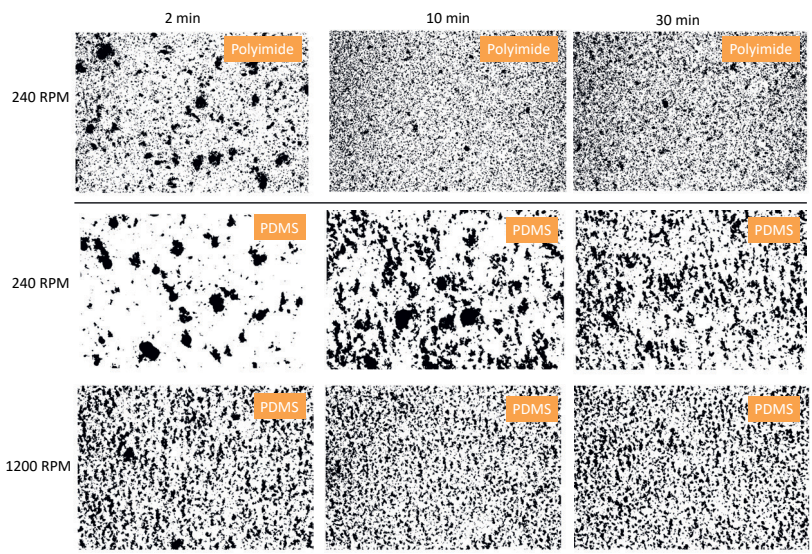

Figure II.12: CNT dispersion in PDMS and Polyimide at different mixing times and speed.

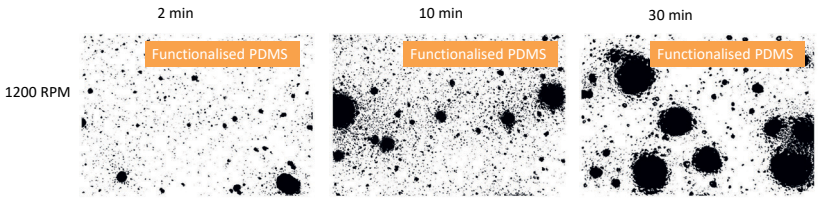

Figure II.13: Functionalised CNT dispersion in PDMS.

investigated by mixing functionalised CNTs according to the same parameters as with the regular CNTs shown in Figure II.12. It was immediately observed that the initial dispersion of CNTs was greatly improved but with increasing time, it drastically worsened. Inspecting the layers more closely (see Figure II.13), it became apparent that with all mixing times, very large and dense clusters were present. Both implemented types of nanotubes featured roughly the same outer dimensions, yet the dispersion seemed completely different.

The results indicated that initial dispersion of the functionalised CNT was greatly improved, as literature suggested. However, due ot the remaining very dense clusters, it was decided to continue the research with the regular CNTs. This bought the additional advantage of being able to compare results with colleague M. Cen-Puc.

Several methods were employed to more qualitatively determine the dispersion quality of the polymer-CNT mixtures. Initially, the clusters were manually measured using the KEYENCE optical microscope. A specific region was selected in each image, and the clusters within that region were measured. The results of these measurements are presented in Figure II.15a. The graph clearly demonstrates the significant differences observed for low-speed mixing, corresponding to the visual observations. However, the differences in cluster sizes for high-speed mixing were not detected in the analysis.

To quantify the effect of the dispersion parameters further, a MATLAB script was developed to analyse the images and determine the size of individual clusters. The implemented steps in the script are outlined as follows:

- Convert the picture into a binary image
- Identify all separate clusters by detecting connected pixels.
- Determine the maximum length of each cluster by finding the outer edges and calculating the longest vector.
- Visualise the individual clusters by marking them with circles and plotting the maximum vector.
- Plot the resulting arrays containing the size and location data of all clusters.

By following these steps, the MATLAB script allows for the analysis and visualisation of cluster size and distribution in the dispersion samples.

Figure II.14 provides a visual representation of the method employed to determine the longest vector for each cluster. The top-left image illustrates the process of identifying the outer edges of the clusters and calculating all possible vectors. The lengths of these vectors are recorded in a matrix, from which the longest vector and its corresponding location and size are determined for further analysis.

The individual clusters are marked with red circles, and the longest vector for each cluster is indicated by a blue line in the image. Additionally, the graph in the bottom-right corner presents a list of cluster lengths, demonstrating the detection of clusters with similar sizes. In the graph, one line with a size range between 23 and 30 μm represents two objects, resulting in a 25% count for that size range. This showcases the ability of the implemented script to identify individual clusters and categorise them based on their approximate sizes.

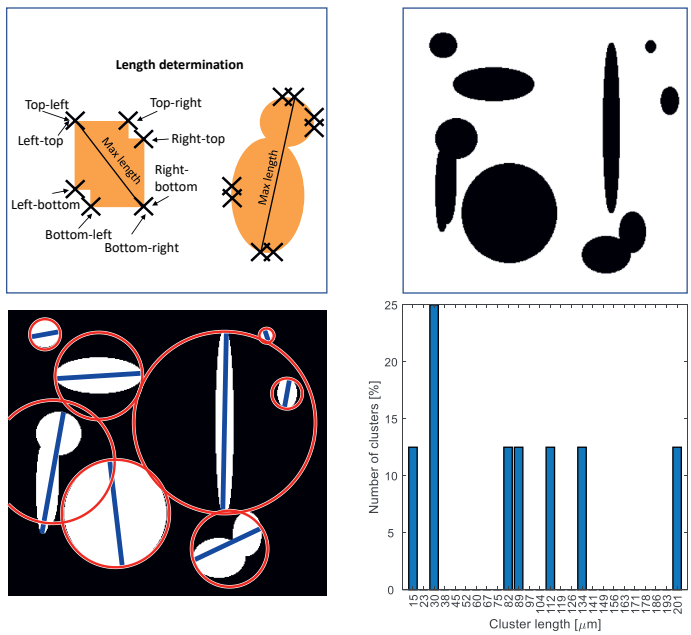

Figure II.14: Cluster size detection algorithm. The outer corners are determined and the longest vector is calculated and plotted. Finally, all cluster lengths are visualised in a graph.

Continuing the analysis using actual data, the results are shown in Figure II.15b. The data used in this graph corresponds to the mixing of PDMS at high speed for 2 and 10 minutes. This approach provided valuable insights, where it can be seen that mixing for 10 minutes significantly improves dispersion by reducing the number of clusters for each size. Consequently, as the mixing time increases, the number of clusters for each length decreases.

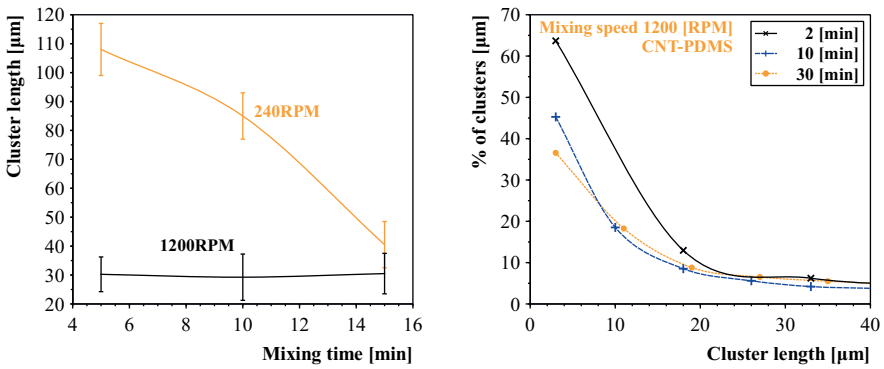

(a) Manually determining clusters. Low-speed mixing (240RPM) shows a great ability to dissolve the clusters. With high speed mixing, no large differences appear.

(b) Cluster length detection in PDMS. More details are now visible and longer mixing does decrease the clusters, but at 30 minutes a small increase seems to happen again.

Figure II.15: Determination of clusters dimensions: manual (left) and with the MATLAB program (right).

However, the current method of determining cluster sizes has limitations when dealing with more complex-shaped clusters. For instance, clusters with an L-shaped structure can lead to the longest vector being connected to points that are not connected along the entire length of the vector. This issue is already visible in the example shown in Figure II.14, where an L-shaped structure is formed towards the bottom.

To enhance the algorithm further, an additional approach was employed, involving the calculation and visualisation of the cluster areas in a graph categorised by size regions (in μm^2). The outcomes are illustrated in Figure II.16. The data is presented by indicating a specific range of cluster sizes (in μm^2) relative to the total number of pixels in the image. This method now allows to observe that, after 10 minutes of high-speed mixing, the occurrence of larger clusters decreases. Moreover, the continued mixing does not yield further improvements; instead, the clusters begin to re-agglomerate and increase in size once again (weighted average 1080, 450, 675 μm^2 resp. for 2, 10 and 30min).

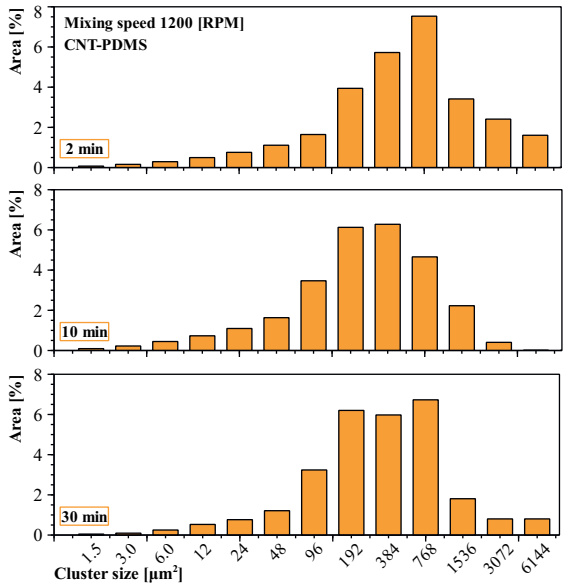

(a) high-speed mixing in PDMS. Weighted averages: 1080, 450, 675 for 2, 10, and 30min.

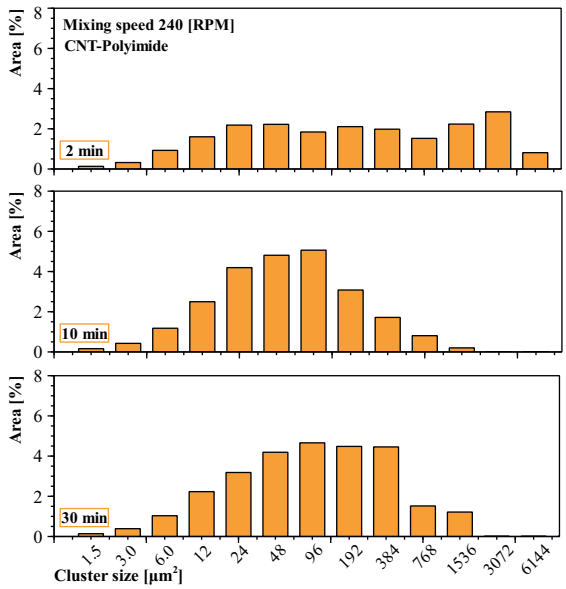

(b) Low-speed mixing in Polyimide. Weighted averages: 975, 129, 234 for 2, 10, and 30min.

Figure II.16: Cluster are detection for CNTs in a polymer.

A similar phenomenon of excessive mixing can be observed when incorporating MWCNTs into Polyimide, as depicted in Figure II.16b. Mixing for 10 minutes demonstrates significant improvement in dispersion, as indicated by the leftward shift of the columns. This enhancement is also visually evident. However, prolonging the mixing time beyond this point leads to an increase in cluster agglomeration (weighted average 975, 129, 234 μm^2 resp. for 2, 10 and 30min). These findings align with existing literature, which highlights that excessive shear forces or prolonged mixing can have negative effects on CNTs and their networks [3] [14]. According to [36], entanglement of CNTs was observed up to 25 minutes of mixing, beyond which the CNTs began to bundle together once again.

II.4.5 Dispersal Quality Differences between PDMS and PI

The dispersion quality of PDMS and PI was investigated using identical concentrations (0.2 wt%) and layer thicknesses (5 μm) but varying mechanical mixing speeds (240 and 1200 RPM).

Upon examining the optical images of PDMS and Polyimide (Figure II.12) it became evident that the cluster sizes in PDMS are significantly larger during low-speed mixing, compared to Polyimide. Interestingly, even at low mixing speeds, the average cluster sizes in Polyimide are smaller than those in PDMS during high-speed mixing, as illustrated in Figures II.16a and II.16b. The improvement in CNT dispersion observed in Polyimide is largely attributed to the presence of 80% solvent volume in the mixture. This results in lower viscosity, facilitating higher shear and mixing forces during the dispersion process.

II.4.6 Surface Topography of Carbon Nanotube-Polymer Layers

The impact of mixing time on the surface layer roughness is apparent when examining Figure II.17. At a mixing time of 2 minutes, peaks on the layer's surface reach a height of 17 μm (Max Peak). However, with longer mixing times, this value decreases significantly. Figure II.17 also displays other roughness parameters, namely Ra (Arithmetic mean roughness), Rq (Root mean square), and Rp (height of tallest profile peak), which indicate the smoothness of the layer. Lower values of these parameters correspond to reduced surface topography of the layer.

Agglomerated carbon nanotubes (clusters) do not attribute to the possible high sensitivities of the piezoresistive sensing layers. Additionally, it is expected that the clusters cannot behave similarly as to individual clusters in the presence of the electrical field for alignment. Therefore, it is key to minimise the number of clusters and isolate the nanotubes as good as possible.

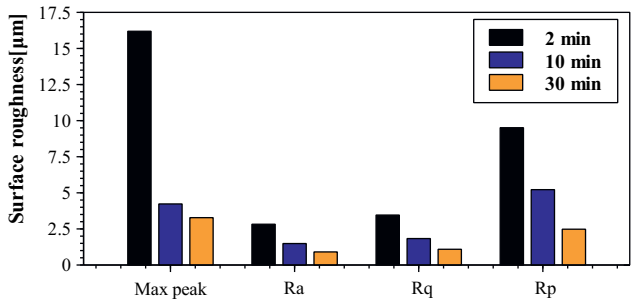

Figure II.17: Surface roughness of CNT-PDMS layers vs. mixing time. Increasing the mixing time, decreases the surface roughness of the top CNT-polymer layer.

II.5 Surface Properties of Polydimethylsiloxane

II.5.1 Surface Modification of PDMS Layer

The inherent hydrophobic nature of PDMS poses challenges when attempting to directly spincoat photoresist onto the polymer surface. Upon coating, the liquid photoresist tends to retract, resulting in the formation of open spaces. To address this issue, a surface modification technique involving oxygen plasma treatment was employed to enhance the hydrophilicity of the PDMS surface.

The effectiveness of the treatment was evaluated by measuring the contact angle of a water droplet placed on the surface. A more upright water droplet indicates a hydrophobic surface, while increased relaxation and spreading of the water droplet indicates improved hydrophilicity. The results of this evaluation can be seen in Figure II.18.

There is no significant difference in contact angles observed with varying concentrations of CNTs in the PDMS polymer. Five measurements were conducted at each step, and the contact angles were recorded. The results of these measurements are depicted in the graph shown in Figure II.19. Minor deviations can be observed in the data without any added carbon nanotubes after the first 5 minutes. However, a noticeable trend is apparent when looking at the other concentrations, indicating a surface modification after 5 minutes of treatment. Further exposure to oxygen plasma only slowly changes the surface further.

With the understanding that the surface modification induced by oxygen plasma treatment is only temporary and reverts to its original state over time [6], the decision was made to proceed directly to the photolithography steps after a 10-minute exposure to plasma.

However, a new challenge arose during the cooling phase after the pre-bake step due to the high thermal expansion coefficient of the PDMS (see Table II.2). The sudden shock of placing the wafer on a 100°C hotplate leads to cracking of the resist surface, caused by

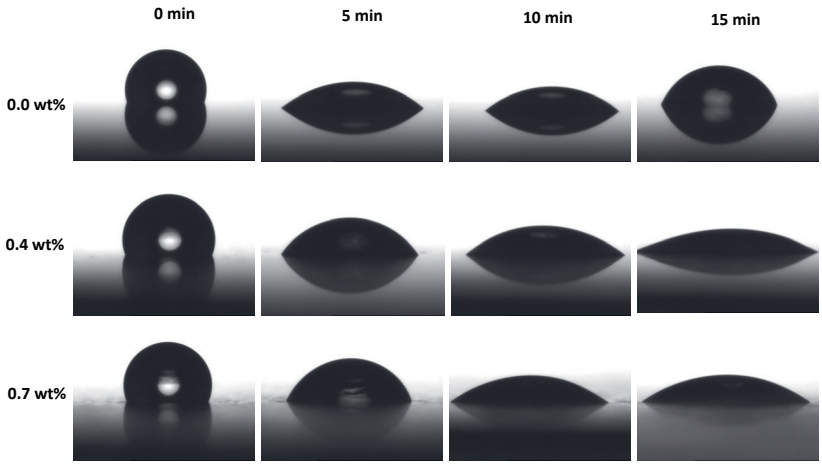

Figure II.18: Contact angle measurements of water droplet for different times of O2-plasma. The PDMS surface changes from hydrophobic to hydrophilic, as can be seen by the relaxation of the water droplets. No real effect of carbon nanotube concentrations is measured.

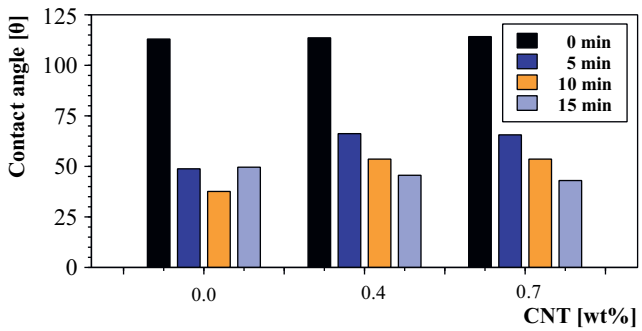

Figure II.19: Contact angle results of water droplet for different times of O2-plasma.

the expansion of the PDMS. To address this issue, an alternative approach was adopted, involving the curing of the resist in a convection oven with a gradual temperature increase and natural cooling. This method significantly improved the integrity of the resin layer, as depicted in Figure II.20. The figure highlights the difference between the photoresist cured on a hotplate and the one cured in an oven.

Table II.2: Thermal expansion coefficients [42] [47] [52] [30].

Polymer	Thermal expansion coefficient	Unit
PDMS	310	$\mu m\, m^{-1}\, °C^{-1}$
PI	0.3	$\mu m\, m^{-1}\, °C^{-1}$
Gold	14.2	$\mu m\, m^{-1}\, °C^{-1}$
Titanium	8.6	$\mu m\, m^{-1}\, °C^{-1}$
Chrome	5.9	$\mu m\, m^{-1}\, °C^{-1}$

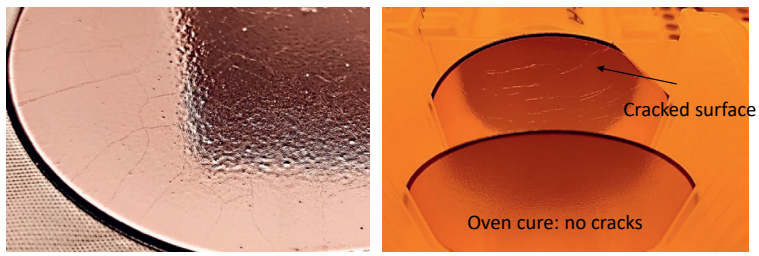

Figure II.20: Photoresist cracks during hotplate prebake. No cracking occurs with oven curing. The right figure indicates a wafer with oven curing (front, without cracks), and hotplate curing (back).

Moreover, the adhesion of the resist to the PDMS remained imperfect, as evidenced by the detachment of thin structures from the surface (Figure II.21). Unfortunately, the exposure of PDMS to oxygen plasma also caused superficial cracks in the layer.

It appears that during the plasma treatment, the silicon molecules present in PDMS react with oxygen, resulting in the formation of a nanometer-thin silica layer. This phenomenon has been extensively documented in existing literature [40] [32] [27]. Depending on the dosage and exposure duration, the mechanical stress can cause cracking of this silica layer.

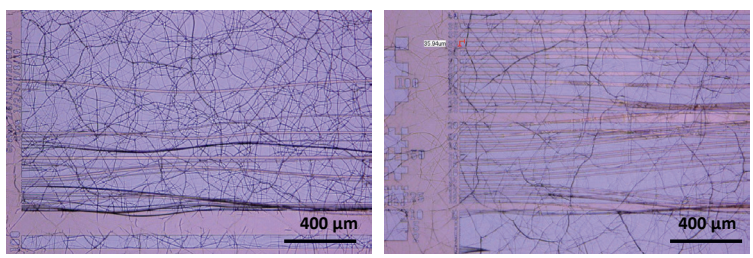

Figure II.21: Bad adhesion of photoresist to PDMS after oxygen plasma treatment.

To further evaluate this observation, a simple PDMS layer was manufactured, on which a structured gold layer (80nm thickness) was deposited using shadow mask deposition. This technique allowed to avoid the use of photolithography and minimise temperature changes on the wafer. Subsequently, the wafer was subjected to a brief etching process using oxygen plasma (after the gold was already sputtered on the PDMS), followed by microscopic inspection. Cracks on the PDMS surface were clearly visible in the areas that were exposed during the etching process. However, under the regions where the gold layer provided protection, no cracks were observed. The results are presented in Figure II.22a. The figure on the right showcases the abrupt termination of cracks in the PDMS layer, precisely at the border where the gold layer was located (with the gold pad on the left side). The cracks cease just shy of the area previously covered by the gold layer. So, it was clear that etching with oxygen plasma directly on the PDMS surface, caused cracking, and the gold layer was able to shield the PDMS underneath.

Additionally, it was observed that the cracked PDMS surface is transferred to the gold layer above. This result is shown in Figure II.22b. Two wafers were spin-coated with PDMS, after which one wafer was subjected to an oxygen plasma for 15 minutes (500W). Both wafers were sputtered with gold (thin 80 nm) and results clearly showed that the non-exposed wafer experienced wrinkles in the gold layer but no cracks. The other oxygen-exposed wafer transferred the cracks from the PDMS layer in the gold layer.

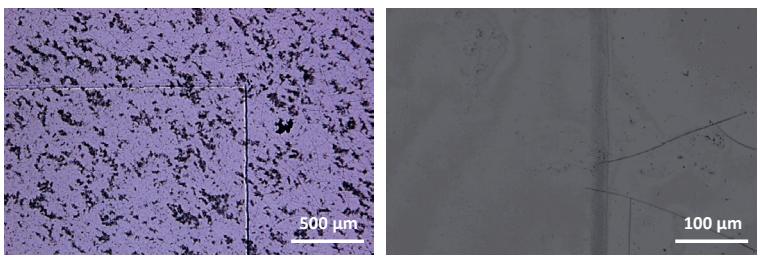

(a) Cracks in PDMS surface due to oxygen plasma. No cracks are visible on PDMS where the protection of the gold layer was.

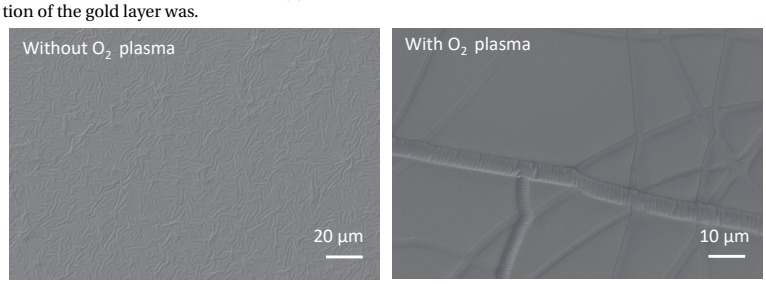

(b) State of sputtered gold layer after native PDMS wafer or with oxygen treated.

Figure II.22: Effect of oxygen plasma on the PDMS surface.

II.5.2 Adhesion Properties of Sputtered Metals to PDMS

Several metallic layers with varying thicknesses were sputtered directly on PDMS to investigate the adhesion properties. The results were used to determine the most suitable process for the electronic connections.

Gold Initially, a 200nm thick gold layer was directly sputtered onto the untreated CNT-PDMS layer. The gold layer was subsequently patterned using standard photolithography steps, followed by dry etching using the following recipe:

$$8\,sccm\,O_2 + 40\,sccm\,CF_4, 800W\,for\,10\,min \tag{II.3}$$

Figure II.23 illustrates the gold layer immediately after sputtering. Noticeable wrinkles are observed on the top surface. The top right side image visualises the result of the last photolithography step: cleaning. After photolithography, the wafers are cleaned in a device resembling a washing machine where water jets and fast moving water are employed. The remaining large structures served as a hard mask for the subsequent dry etching step. However, SEM results indicate poor adhesion to PDMS, with floating gold structures observed on the polymer surface (Figure II.23 bottom images).

Reducing the gold thickness improved the wrinkling effect of the layers but it did not completely address the adhesion problems. Consequently, it was decided that an adhesion layer was necessary to improve adhesion between the metal and PDMS surface.

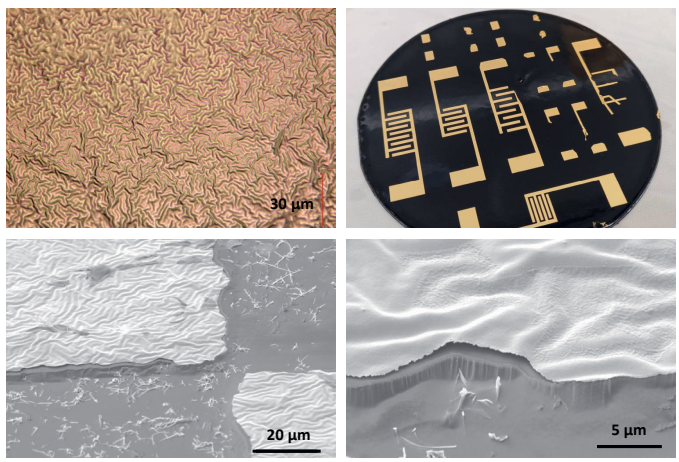

Figure II.23: Gold adhesion to untreated CNT-PDMS. Wrinkles are present on the surface and a bad adhesion to the PDMS polymer underneath.

Chrome-Gold Chromium is a common IC technology adhesion promoter. Typically, a thin layer (15nm) is sufficient to enhance the adhesion to the substrate. However, surface cracks appeared directly after sputtering both layers, as depicted in Figure II.24. Nevertheless, after the manufacturing progressed, it became evident that the adhesion of the Chromium-Gold layer to the PDMS sufficed. Therefore, it is assumed that this is because the PDMS elastomer features a high thermal expansion coefficient. Especially compared to metals like gold and chromium (see Table II.2). The wafers are exposed to elevated temperatures during the sputtering and photolithography processes. The induced stress causes cracks in the top gold layer.

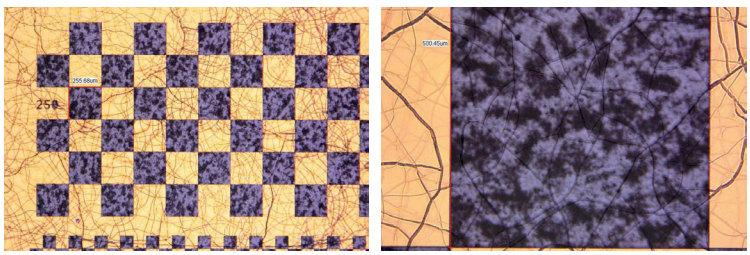

Figure II.24: Chrome-gold cracks to untreated CNT-PDMS.

Titanium-Gold Titanium is another common adhesion promoter for metals. Initial tests did not reveal cracks on the surface. However, immediately after it was observed that this was caused by the poor adhesion between the titanium and PDMS. In fact, the adhesion was so weak that the layers floated away, providing only interesting pictures (Figure II.25) but no useful process. Consequently, titanium was not pursued any further as an adhesion promoter.

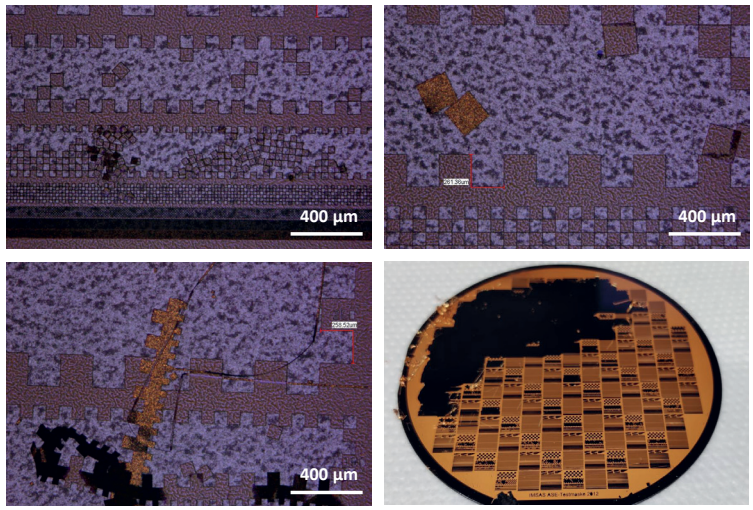

Figure II.25: Titanium-gold adhesion to untreated CNT-PDMS.

II.5.3 Thickness Influence of Sputtered Metal on PDMS

It is well-established that metal layers deposited on polydimethylsiloxane exhibit cracking or buckling effects due to significant differences in temperature expansion coefficients. Colleagues from the Hong Kong University suggested that reducing the thickness of the metal layers could be a potential solution. Thinner layers would decrease the elastic mismatch between the polymer and metal layers, thereby reducing stress.

The standard process for depositing metal connections on sensors involves using 15 nm of chromium as an adhesion layer followed by 100-200 nm of gold sputtered on top. As demonstrated in Chapter II.5.2, sputtering gold directly onto PDMS without an adhesion layer resulted in the formation of wavy patterns due to buckling. Including an adhesion layer significantly improved adhesion; however, cracking occurred immediately after sputtering, likely caused by the large elastic and thermal mismatches. Although temperatures during sputtering are not expected to rise substantially, the utilised sputtering machine possesses a low target-to-wafer distance, which could contribute to sufficient heating of the insulating PDMS layer, causing expansion and subsequent cracking of the overlying, less flexible metal layer.

In a joint effort with Prof. Dr. B. Lüssem, M. Kirsch, and colleagues from Hong Kong University, experiments were conducted by sputtering 5 nm of chromium and 50 nm of gold onto the PDMS layer. The sputtering power was reduced from 100 W to 50 W, resulting in a lower deposition rate that could potentially enhance the layer's quality.

The sputtering time was doubled since it is linearly related to the sputtering power. No cracks were observed in the metal layer. Although some buckling was detected at 100x magnification, cracking was not evident. Unfortunately, the sputter deposition was not entirely homogeneous across the wafer's surface, with noticeable optical differences in the deposited layers. A yellowish color was present in the wafer's centre, whereas the outer 2 cm appeared more silver-coloured and possibly had thinner gold layers.

A positive resist (1.8 μm) was spin-coated directly onto the gold layer and cured in an oven at 85°C for 30 minutes. The wafer was placed in a convection oven to gradually increase the wafer's temperature, in contrast to the standard hotplate technique. Despite this, large cracks appeared in the photoresist layer as the wafer cooled down, presumably due to temperature and mismatch-induced stress. Nevertheless, the gold and chromium layers were successfully etched, and the strain sensor structures were patterned correctly and appeared functional.

Due to the thin layers and short wet etching times, the risk of over-etching or completely removing the structures was high. Combined with the sputtering in-homogeneity's, initial structures yielded non-conductive results (>40MΩ) when tested with a standard multimeter. It is probable that manual testing using needles resulted in the destruction of the thin conductive layers, preventing successful measurements.

There seems to be a trade-off in layer thickness and cracking of the surface. Increasing the metallic layers would increase the conductivity but causes cracking. More profound experiments and different sputtering parameters are necessary to investigate the possibilities in manufacturing thicker metallic layers onto PDMS.

II.5.4 Etching of Carbon Nanotube - PDMS Layers

The etching process of the PDMS layer features a mixture of CF4 and oxygen gas (shown in Equation II.3). The presence of oxygen causes the surface to crack due to the formed SiO2 layer (cracks are depicted in Figure II.26), as discussed previously in the above sections. However, the organic component of PDMS (the chemical name is: $(C_2H_6OS_i)_n$) must be etched with oxygen plasma. This assumption was experimentally determined by etching with different gas mixtures, as shown in Table II.3. No removal of the PDMS layer was detected without an oxygen presence in the plasma mixture.

Table II.3: Experimentally determined PDMS etch rates.

CF_4 [sccm]	O_2 [sccm]	Etchrate [μm/min]
40	0	0.0
40	8	0.2
40	40	0.7

Even if the oxygen surface treatment of PDMS were to provide perfect adhesion of the photoresist, the issue of the formed silica layer still remains. This thin layer acts as an insulating barrier on the surface, rendering it unsuitable for gold interconnects. To test this, two PDMS wafers were prepared with a gold layer sputtered directly onto the surface using a shadow mask (creating a matrix of 1x1 cm gold pads). One of the wafers was exposed to 15 minutes of oxygen plasma just before deposition. The results, presented in Figure II.27 as a heat map, clearly demonstrate an increase in resistance (up to infinity) for the wafer that was exposed to oxygen plasma. The black-coloured edges are due to the wafer's circular shape, and the outer regions exhibit higher normalised resistivity. This can be attributed to the fact that the outer sides of the layer are thinner due spin coating in-homogeneity's.

Due to the inability to directly apply photoresist on the PDMS layer, it was key to find another material to shield the structures for the dry etching step. A hard mask out

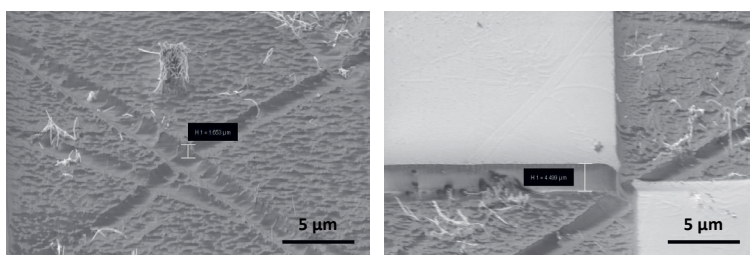

Figure II.26: Chrome-gold layer after PDMS dry etching. Cracks appear on the PDMS surface. The depth of the cracks seem to be only a few nanometers and not completely through.

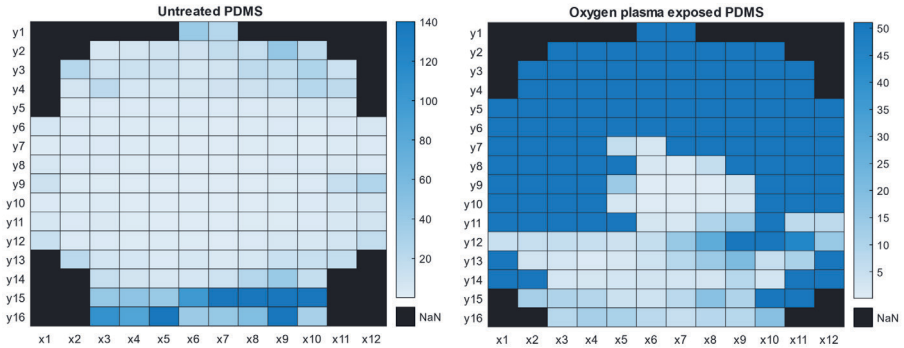

(a) Untreated PDMS (b) Treated PDMS

Figure II.27: Effect on oxygen plasma. Thin silica layer causes a thin isolation layer (b). The dark blue color indicates no measurable resistivity (inf resistance). Values are the normalised resistance.

of gold was chosen to be directly sputtered on the PDMS, eliminating the need for the photoresist directly on the PDMS. The hard mask itself can be structured with regular photoresist as the resist does not come into contact with the PDMS.

The etching of the CNT-PDMS layers was performed using two different reactive gases: SF6 and CF4. The gas flow is regulated by multiple valves, precisely controlling the rate of flow in order to achieve a controllable etch rate. It was observed that the reaction of the SF6 gas was so intense, that the machine was not able to regulate the pressure and flow rates. This resulted in far less etching control and less smooth sidewalls. The differences to the CF4 gas mixture is shown in Figure II.28. This gas mixture showed far smoother sidewalls and more control in pressure regulation.

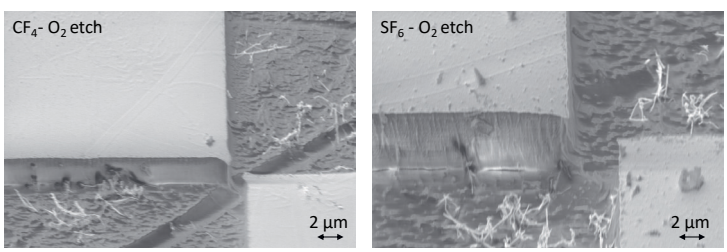

Figure II.28: Etching of CNT-PDMS layers with two different reactive gas mixtures. Etching PDMS with the SF_6 gas is extremely unstable and creates rough edges.

II.5.5 Etching of Carbon Nanotube - Polyimide Layers

The nanotube-Polyimide layers are etched via dry etching with the following gases:

$$40\ sccm\ O_2\ \&\ 8\ sccm\ CF_4 \tag{II.4}$$

The acquired etch-rate was found to be roughly 0.5 μm/min for 2 wt% CNT-PI layers. All layers were slightly over-etched to ensure complete removal of the targeted polymer layer. This is done because results showed that carbon nanotube clusters were etched slightly slower than the polymer itself, leaving behind small clusters on the silicon surface, as presented in Figure II.29.

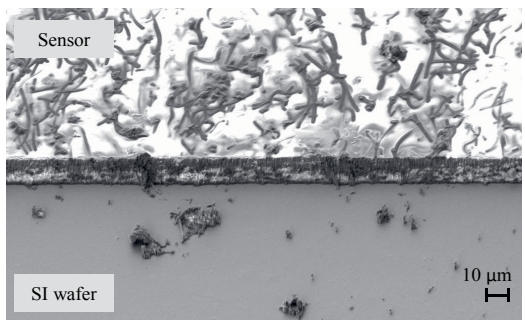

Figure II.29: Etching of CNT-PDMS layers with two different reactive gas mixtures. The random orientation of the carbon nanotubes in the polyimide layer is clearly visible. Some CNT clusters remain on the silicon wafer after etching (bottom part of the figure).

References

[1] Farhang Abbasi, Hamid Mirzadeh, and Ali-Asgar Katbab. Modification of polysiloxane polymers for biomedical applications: a review. 2001.

[2] Moinuddin Ahmed et al. "MEMS sensors on flexible substrates towards a smart skin". In: SENSORS, 2012 IEEE (2012), pp. 1–4.

[3] Alamusi et al. "Piezoresistive strain sensors made from carbon nanotubes based polymer nanocomposites". In: Sensors 11.11 (2011), pp. 10691–10723.

[4] Ronaldo Ariati et al. "Polydimethylsiloxane composites characterization and its applications: a review". In: Polymers 13.23 (2021), p. 4258.

[5] Wolfgang Bauhofer and Josef Z Kovacs. "A review and analysis of electrical percolation in carbon nanotube polymer composites". In: Composites science and technology 69.10 (2009), pp. 1486–1498.

[6] Dhananjay Bodas and Chantal Khan-Malek. "Hydrophilization and hydrophobic recovery of PDMS by oxygen plasma and chemical treatment—An SEM investigation". In: Sensors and actuators B: chemical 123.1 (2007), pp. 368–373.

[7] Marco Cen-Puc et al. "Carbon Nanotubes/Polymer Films for Microsensors Applications". In: 2021 IEEE Sensors. IEEE. 2021, pp. 1–4.

[8] Baodeng Chen et al. "Skin-inspired flexible and high-performance MXene@ polydimethylsiloxane piezoresistive pressure sensor for human motion detection". In: Journal of Colloid and Interface Science 617 (2022), pp. 478–488.

[9] Yuli Chen et al. "Theoretical estimation on the percolation threshold for polymer matrix composites with hybrid fillers". In: Composite structures 124 (2015), pp. 292–299.

[10] Namsun Chou, Jinmo Jeong, and Sohee Kim. "Crack-free and reliable lithographical patterning methods on PDMS substrate". In: Journal of Micromechanics and Microengineering 23.12 (2013), p. 125035.

[11] Nauman Ali Choudhry et al. "Design, development and characterization of textile stitch-based piezoresistive sensors for wearable monitoring". In: IEEE Sensors Journal 20.18 (2020), pp. 10485–10494.

[12] Daniel Gräbner et al. "Screen-Printed Resistive Pressure Sensors: Influence of Electrode Geometry on the Performance and on Cross-Sensitivity to Strain and Temperature". In: Journal of Physics: Conference Series. Vol. 1837. 1. IOP Publishing. 2021, p. 012004.

[13] Samia Hamouni et al. "Alcohol and alkane organic extraction using pervaporation process". In: Macromolecular Symposia. Vol. 386. 1. Wiley Online Library. 2019, p. 1800247.

[14] Yan Yan Huang and Eugene M Terentjev. "Dispersion of carbon nanotubes: mixing, sonication, stabilization, and composite properties". In: Polymers 4.1 (2012), pp. 275–295.

[15] Danish Khan et al. "A review of the challenges and possibilities of using carbon nanotubes in organic solar cells". In: Science of Advanced Materials 10.6 (2018), pp. 747–760.

[16] Saleem Khan, L Lorenzelli, and RS Dahiya. "Bendable piezoresistive sensors by screen printing MWCNT/PDMS composites on flexible substrates". In: 2014 10th Conference on Ph. D. Research in Microelectronics and Electronics (PRIME). IEEE. 2014, pp. 1–4.

[17] Saleem Khan, Leandro Lorenzelli, and Ravinder S Dahiya. "Screen printed flexible pressure sensors skin". In: 25th Annual SEMI Advanced Semiconductor Manufacturing Conference (ASMC 2014). IEEE. 2014, pp. 219–224.

[18] C Lai et al. "Fabrication and performance of full textile-based flexible piezoresistive pressure sensor". In: Journal of Materials Science: Materials in Electronics 33.8 (2022), pp. 4755–4763.

[19] G Latessa et al. "Piezoresistive behaviour of flexible PEDOT: PSS based sensors". In: Sensors and Actuators B: Chemical 139.2 (2009), pp. 304–309.

[20] Jing Li et al. "Correlations between percolation threshold, dispersion state, and aspect ratio of carbon nanotubes". In: Advanced Functional Materials 17.16 (2007), pp. 3207–3215.

[21] Qiuyan Li, Shijing Luo, and Qing-Ming Wang. "Piezoresistive thin film pressure sensor based on carbon nanotube-polyimide nanocomposites". In: Sensors and Actuators A: Physical 295 (2019), pp. 336–342.

[22] Chao-Xuan Liu and Jin-Woo Choi. "Improved dispersion of carbon nanotubes in polymers at high concentrations". In: Nanomaterials 2.4 (2012), pp. 329–347.

[23] Joost Conrad Lötters et al. "The mechanical properties of the rubber elastic polymer polydimethylsiloxane for sensor applications". In: Journal of micromechanics and microengineering 7.3 (1997), p. 145.

[24] Chen Ma et al. "Alignment and dispersion of functionalized carbon nanotubes in polymer composites induced by an electric field". In: Carbon 46.4 (2008), pp. 706–710.

[25] Peng-Cheng Ma et al. "Dispersion and functionalization of carbon nanotubes for polymer-based nanocomposites: A review". In: Composites Part A: Applied Science and Manufacturing 41.10 (2010), pp. 1345–1367.

[26] Stefan CB Mannsfeld et al. "Highly sensitive flexible pressure sensors with microstructured rubber dielectric layers". In: Nature materials 9.10 (2010), pp. 859–864.

[27] KL Mills et al. "The mechanical properties of a surface-modified layer on polydimethylsiloxane". In: Journal of materials research 23.1 (2008), pp. 37–48.

[28] Leon Mishnaevsky Jr et al. "Materials for wind turbine blades: An overview". In: Materials 10.11 (2017), p. 1285.

[29] Harsha Nallabothula et al. "Processing-mediated different states of dispersion of multiwalled carbon nanotubes in PDMS nanocomposites influence EMI shielding performance". In: ACS omega 4.1 (2019), pp. 1781–1790.

[30] Shun'ichi Numata et al. "Thermal expansion behavior of various aromatic polyimides". In: Journal of applied polymer science 31.1 (1986), pp. 101–110.

[31] The meaterial selection platform Omnexus. Comprehensive Guide on Poyimide (PI). 2021. URL: https://omnexus.specialchem.com/selection-guide/polyimide-pi-plastic (visited on 07/18/2023).

[32] Michael J Owen and Patrick J Smith. "Plasma treatment of polydimethylsiloxane". In: Journal of adhesion science and technology 8.10 (1994), pp. 1063–1075.

[33] Vivek Pandey et al. "Piezoresistive pressure sensor using nanocrystalline silicon thin film on flexible substrate". In: Sensors and Actuators A: Physical 316 (2020), p. 112372.

[34] Sun-Jun Park et al. "Flexible piezoresistive pressure sensor using wrinkled carbon nanotube thin films for human physiological signals". In: Advanced Materials Technologies 3.1 (2018), p. 1700158.

[35] Soonjae Pyo et al. "Development of a flexible three-axis tactile sensor based on screen-printed carbon nanotube-polymer composite". In: Journal of Micromechanics and Microengineering 24.7 (2014), p. 075012.

[36] Harald Rennhofer and Benjamin Zanghellini. "Dispersion state and damage of carbon nanotubes and carbon nanofibers by ultrasonic dispersion: a review". In: Nanomaterials 11.6 (2021), p. 1469.

[37] Tim Mike de Rijk and Walter Lang. "Low-Cost and Highly Sensitive Pressure Sensor with Mold-Printed Multi-Walled Carbon Nanotubes Dispersed in Polydimethylsiloxane". In: Sensors 21.15 (2021), p. 5069.

[38] Smith Salifu et al. "Recent development in the additive manufacturing of polymer-based composites for automotive structures—A review". In: The International Journal of Advanced Manufacturing Technology 119.11-12 (2022), pp. 6877–6891.

[39] Andreas Schander et al. "A flexible 202-channel epidural ECoG array with PEDOT: PSS coated electrodes for chronic recording of the visual cortex". In: IEEE Sensors Journal 19.3 (2018), pp. 820–825.

[40] Rian Seghir and Steve Arscott. "Controlled mud-crack patterning and self-organized cracking of polydimethylsiloxane elastomer surfaces". In: Scientific reports 5.1 (2015), pp. 1–16.

[41] Ayse Sezer Hicyilmaz and Ayse Celik Bedeloglu. "Applications of polyimide coatings: A review". In: SN Applied Sciences 3 (2021), pp. 1–22.

[42] Slygard 184 Silicone Elastomer Technical Data Sheet. https://www.dow.com/content/dam/dcc/documents/en-us/productdatasheet/11/11-31/11-3184-sylgard-184-elastomer.pdf. Accessed: 2020-10-10.

[43] Stefano Stassi et al. "Smart piezoresistive tunnelling composite for flexible robotic sensing skin". In: Smart materials and structures 22.12 (2013), p. 125039.

[44] E Tamburri et al. "Modulation of electrical properties in single-walled carbon nanotube/conducting polymer composites". In: Carbon 43.6 (2005), pp. 1213–1221.

[45] Hamed Tanabi and Merve Erdal. "Effect of CNTs dispersion on electrical, mechanical and strain sensing properties of CNT/epoxy nanocomposites". In: Results in Physics 12 (2019), pp. 486–503.

[46] D Thuau, Vasileios Koutsos, and Rebecca Cheung. "Electrical and mechanical properties of carbon nanotube-polyimide composites". In: Journal of Vacuum Science & Technology B: Microelectronics and Nanometer Structures Processing, Measurement, and Phenomena 27.6 (2009), pp. 3139–3144.

[47] The Engineering Toolbox. Metals - Temperature Expansion Coefficients. https://www.engineeringtoolbox.com/thermal-expansion-metals-d_859.html.

[48] Pavan Kumar Valavala. "Electronic properties of zig-zag carbon nanotubes: a first-principles study". In: (2008).

[49] Luca Valentini et al. "Dynamics of amine functionalized nanotubes/epoxy composites by dielectric relaxation spectroscopy". In: Carbon 42.2 (2004), pp. 323–329.

[50] Luheng Wang, Tianhuai Ding, and Peng Wang. "Thin flexible pressure sensor array based on carbon black/silicone rubber nanocomposite". In: IEEE Sensors Journal 9.9 (2009), pp. 1130–1135.

[51] Yongling Wu et al. "Piezoelectric materials for flexible and wearable electronics: A review". In: Materials & Design 211 (2021), p. 110164.

[52] Yun Xiao et al. "Chapter 12 - Microfluidic Cell Culture Techniques". In: Microfluidic Cell Culture Systems. Ed. by Christopher Bettinger, Jeffrey T. Borenstein, and Sarah L. Tao. Micro and Nano Technologies. Oxford: William Andrew Publishing, 2013, pp. 303–321. ISBN: 978-1-4377-3459-1. DOI: https://doi.org/10.1016/B978-1-4377-3459-1.00012-0. URL: https://www.sciencedirect.com/science/article/pii/B9781437734591000120.

[53] Satoshi Yoda et al. "Preparation of polymer metal composite film as a precursor of metal doped carbon membrane via supercritical impregnation". In: 6th International Symposium on Supercritical Fluids. 2003, pp. 1981–6.

[54] Rui Yu et al. "Highly sensitive flexible piezoresistive sensor with 3D conductive network". In: ACS applied materials & interfaces 12.31 (2020), pp. 35291–35299.

[55] Siu-Ming Yuen et al. "Preparation and morphological, electrical, and mechanical properties of polyimide-grafted MWCNT/polyimide composite". In: Journal of Polymer Science Part A: Polymer Chemistry 45.15 (2007), pp. 3349–3358.

[56] Jia-wen Zhang et al. "Textile-based flexible pressure sensors: A review". In: Polymer Reviews 62.1 (2022), pp. 65–94.

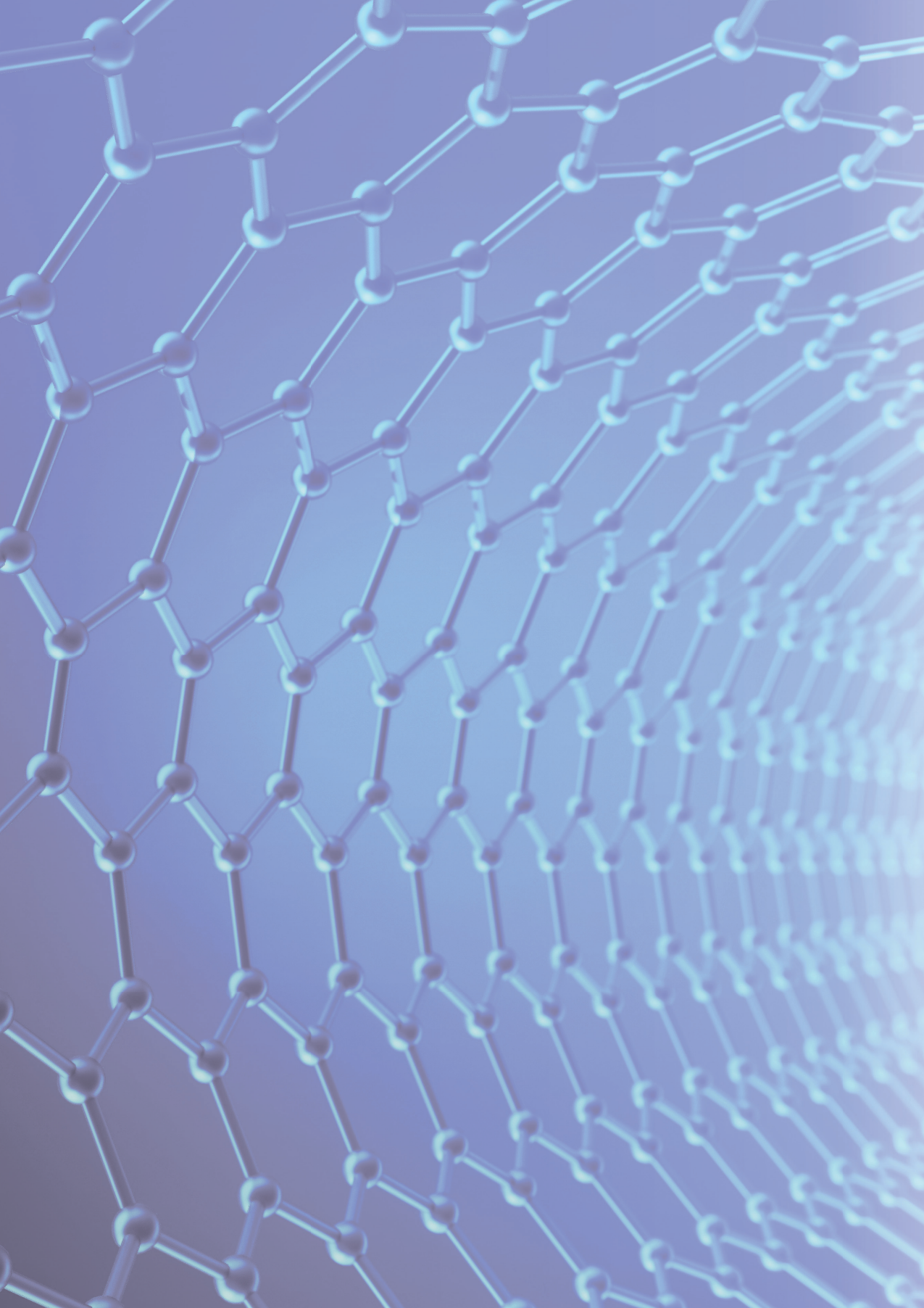

CHAPTER III

Randomly Dispersed Carbon Nanotube-Based Sensors

Parts of this chapter have been published in:
de Rijk, T.M, Cen-Puc, M., Piening, J. K., & Lang, W. (2022, October). Single layer piezoresistive polyimide pressure sensor based on carbon nanotubes. In 2022 IEEE Sensors (pp. 1-4). IEEE.

Cen-Puc, M., de Rijk, T.M., Schander, A., Gleason, M. V., & Lang, W. (2023, October). Strain Microsensors Based on Carbon Nanotube/Polyimide Thin Films. In 2023 IEEE Sensors. IEEE.

Abstract

Compressing the flexible polymer causes the volume to change and the corresponding distances between the rigid carbon nanotubes to decrease. This is the main basis of the introduced sensor in this Chapter. This change in resistance due to an externally applied force is the piezoresistive property. Numerical simulation involving randomly oriented curved nanotubes between two conductive plates with an applied pressure show the first behaviour of a theoretical sensor. Effects of the layer geometries, chance of conduction and layer thicknesses are numerically investigated.

First, thick-film based CNT-PDMS sensors show a corresponding behaviour to the numerical simulation: with an applied compressive force, the resistance drops linearly for the first region. Thinner and smaller PDMS-based sensors show high sensitivity but poor stability and repeatability of the sensors. The sensors are able to follow discrete and continuous pressure changes but a drift is almost always noticeable.

The addition of carbon nanotubes to the polymer changes its flexibility properties, which is measured by investigation the stress-strain relations of CNT-PDMS samples for different CNT weight concentrations. Additionally, results showed an inverse correlation between sensor sensitivity and nanotube concentration: lower concentrations are more sensitive. Similar results were found for layer thickness; thinner layers appear to be more sensitive.

Finally, the more rigid, thin and stable material polyimide is introduced as the basis for the randomly dispersed carbon nanotube piezoresistive pressure sensor. Different geometries and sensor thicknesses, again show the effect on sensor response. Repeatability and stability of the sensor was proven by exposing it to several hundred pressure cycles, after which the resistance values of the sensors hardly changed.

III.1 Introduction

This Chapter characterises the piezoresistive strain and pressure properties of polymer layers with embedded randomly dispersed carbon nanotubes. Sensors were manufactured with both PDMS and Polyimide as a polymer. Results of the more flexible PDMS polymer are compared with the more stable Polyimide.

The sensing principle is based on the fact that the polymer decreases in size with increasing pressure. As a result, the average distances between the carbon nanotube structures decrease, leading to an increase in the material's conductivity. This concept is visually represented in Figure III.1. Gold inter-digital electrodes (IDEs) are fabricated on top of the piezoresistive polymer to measure this material change.

The behaviour of the sensor can be described analytically by Equation III.1, which relates the applied stress σ to Young's Modulus E [5]. This relationship illustrates that a certain applied stress σ causes the inter-particle distance s to decrease.

$$s = s_0(1-\epsilon) = s_0(1-\frac{\sigma}{E}) \tag{III.1}$$

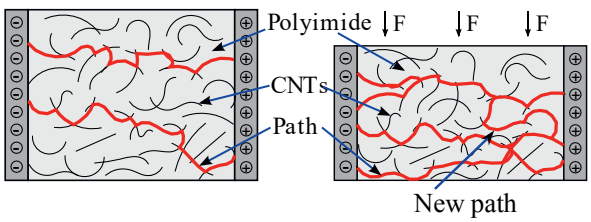

Figure III.1: Sensor principle. With increasing pressure, the piezoresistive layer compresses, increasing its conductivity.

III.2 Numerical Results

The behaviour of the piezoresistive layer containing carbon nanotubes was investigated using the FEM simulation program COMSOL Multiphysics. The simulation included realistic representations of curved CNTs, as shown in Figure III.2a. For better visualisation, the dimensions of the CNTs were enlarged. The fundamental principle remains unchanged: compressing the polymer leads to more connections between carbon nanotubes, resulting in an increased number of conductive paths between the electrodes. This, in turn, causes a change in resistance, which can be measured. If a connection is present between the electrodes via multiple connections carbon nanotubes, COMSOL Multiphysics is able to determine the resistance.

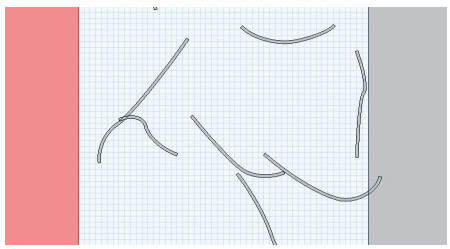

(a) Simulation of curled CNTs.

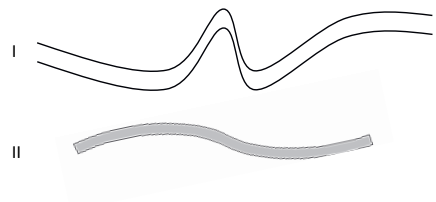

(b) Effect of duplicating a bezier curve (I) and drawing the bezier curves with specified control points (II). A non-constant diameter is observed only in method (I).

Figure III.2: Simulated Carbon nanotubes in COMSOL Multiphysics.

To generate parallel curves, the Bezier curve offset approximation algorithm as proposed by W.J. Brouwer [3] was employed. This algorithm provides an efficient construction of near-parallel Bezier curves. Simply duplicating a bezier curve and moving it does not result in parallel curves even in case of a small bend. If that method would have been employed, it could cause overlapping lines, resulting in negative spaces in the model and resulting in a simulation error. The property is highlighted in Figure III.2b. The figure clearly shows the thickness variations of the top CNT, which was drawn by duplicating the top line. Drawing the CNT with specific control points that determine the curvatures of the lines gives perfectly drawn CNTs. Multiple Bezier curves were connected while ensuring continuity in the lines, thus avoiding any abrupt changes or kinks in the CNTs. Numerous carbon nanotubes are placed between two large electrodes in an arbitrary orientation, with a distance of 100 μm between them.

Key parameters influencing the percolation threshold are the agglomeration percentage and the CNT dimensions. Both parameters are intertwined, as longer and thinner CNTs have a greater tendency of agglomerating together. Numerical calculations were performed to visualise the effect of different CNT dimensions on the CNT-CNT distances. Figure III.3a illustrates the CNT inter-particle distances for four different multi-walled carbon nanotubes, depending on the weight concentration. With an increasing aspect ratio, the CNT inter-particle distance decreases, which, in turn, increases the chance of creat-

ing a conductive polymer. These results gave the recommendation of not utilising the longest CNTs possible, but more in a range of <500, to have the best of both properties.

The chance of conduction was determined and, depending on layer thicknesses, found to be Φ_{sim} = 0.3-0.4 wt% (measured at 50% conduction possibility). This range is in the same order of magnitude as found in this research. Additionally, one should mention that only a small part of the IDE was simulated (a length of 100 μm). It is expected that increasing the length results in higher conductivities at lower concentrations, reducing the (ideally dispersed) percolation threshold even lower. However, to further increase the simulation area (which means adding more CNTs) would cause the computation time to drastically increase. Therefore, it was chosen to keep the 100 μm for the sensor sensitivity and CNT weight percentage influence simulations.

The change in layer thicknesses (50–700 μm) was simulated to find the effect on the sensor response. Conductivity in the thin sensing layers is expected to change rapidly, as the layer is in the same order of magnitude as the lengths of the CNTs. With increasing thickness, it takes relatively more nanoparticles to overcome the longer paths between the electrodes. For example, a sensor with 50 μm thickness and 10 μm CNTs needs at least five consecutive CNTs to form a conductive path between both electrodes. This number increases with increasing sensor thicknesses. In turn, the chance of such long connective paths decreases with the increasing sensor thickness (as presented in Figure III.3b). Applying a directional force to one side of the sensor with a fixed weight percentage of carbon nanotubes effectively increases the nanoparticle weight percentage due to the compressing polymer. The results confirming these expectations are displayed in Figure III.4, where it can be clearly seen that thinner layers exhibit larger conductivity changes with respect to CNT weight percentages. Hence, it can be argued that thinner layers experience higher sensitivities. This could also be intuitively explained because thinner layers feature shorter conductive paths, hence any change in the short paths have a larger influence than thicker layers where more connections are present. One connection loss out of ten results in a larger change than one out of a hundred.

A pressure is applied to a single side to determine the caused resistance change. The outcome is depicted in Figure III.6b. Since the simulation involved a large number (over 1000) of CNTs in COMSOL, utilising the script was necessary to keep simulation times as low as possible. Results of the simulation are depicted in Figure III.6a, where they are compared with the first version pressure sensors.

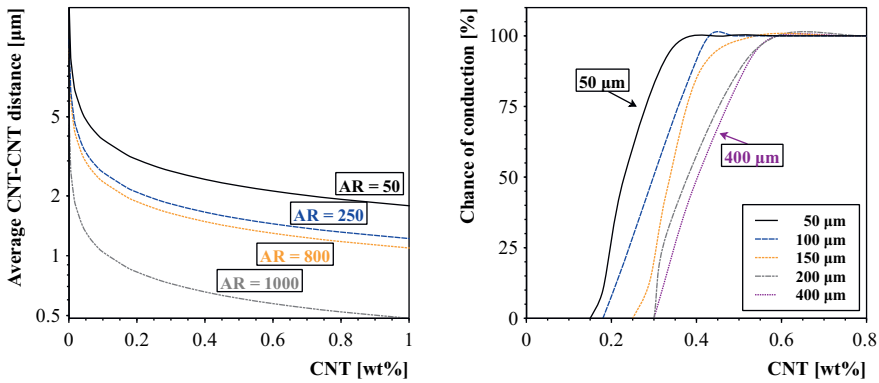

(a) The theoretical CNT inter-particle distance for different CNTs in relation with the wt% in the polymer. Higher aspect ratio nanotube feature smaller CNT-CNT distances and result in lower percolation thresholds.

(b) Statistical chance of formed conductive networks between electrodes with different sensor thicknesses. Thinner layers experience earlier chance of forming conductive networks.

Figure III.3: Theoretically determined impact of aspect ratio (AR) and the layer thickness.

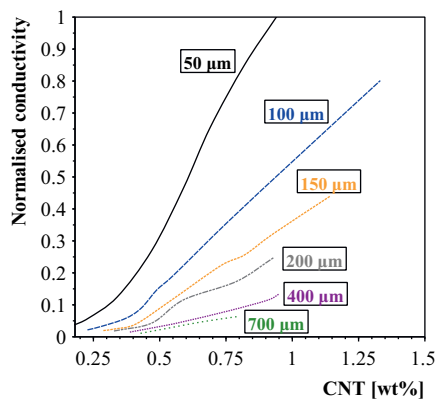

Figure III.4: The theoretical conductivity for different sensors thicknesses. The thicker the layer becomes, the less sensitive the sensor.

III.3 PDMS-based Pressure Sensor

Thick CNT-PDMS layers were manufactured to validate the working principle of flexible piezoresistive-based pressure sensors. High weight percentages of CNTs (6 wt%) were dispersed in isopropanol and then mixed with the PDMS polymer. After proper dispersion, the solvent was removed, and the mixture was placed in a custom 3D-printed mold (as the mixture was too thick for spin-coating). It was then flattened with a squeegee (similar to the device used for screen-printing) and cured at 70°C for 1.5 hours (higher temperatures were not feasible due to the temperature limitation of the PLA filament).

The substrate used was a 3 [mm] thick PMMA sheet that had previously been structured with silver inter-digital electrodes through screen-printing. Several pressure characterisation tests were performed, resulting in multiple proper responses. However, the results were not repeatable for multiple pressure cycles. Figure III.5 shows an image of the first hybrid sensor, combining screen- and mold-printed CNT-PDMS pressure sensor.

Figure III.5: Screen-printed inter-digital electrodes (left). CNT-PDMS composite mold-printed on top of electrodes (right). For clarification purposes a 0.2 CNT wt% solution was printed in order to leave the electrodes visible through the layer.

Results of both the simulation data and the experimental data are shown in Figure III.6. Similar behaviour is observed for both the numerical and experimental results of the initial pressure regions. However, certain differences between the model and the real sensor are present. Disparities in the model can be attributed to the absence of simulated agglomerations (only perfectly dispersed CNTs are implemented in the model) and the limited scope of the simulation, which includes only two electrodes instead of a complete IDE structure. However, the simulation indicates an initial linear pressure response with a slow decrease in sensitivity after a certain point. This behaviour is also in agreement with the first thick high CNT-content pressure sensors.

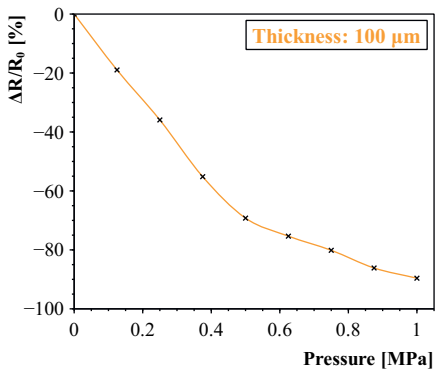

(a) Theoretical sensor response. A linear response is present up to 500kPa, after which the sensitivity decreases slightly.

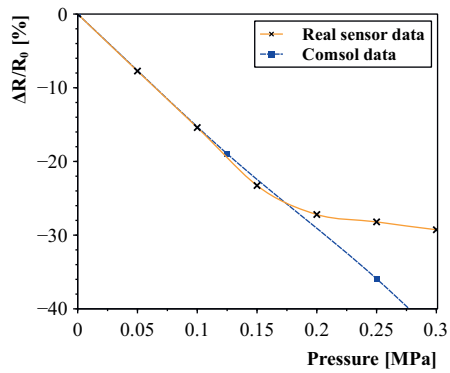

(b) Experimental sensor results following the initial response of the numerical simulation determined by a COMSOL Multiphysics model.

Figure III.6: Results of first generation thick film PDMS-CNT sensors (6wt%).

The results demonstrated the successful creation of a piezoresistive pressure-sensitive layer with carbon nanotubes in PDMS. The subsequent step was to downscale the sensor and produce thinner and smaller sensors. Using the lithography steps discussed in Chapter II.4.3, 60 μm thick layers (0.5 wt%) were spin-coated with sputtered chrome-gold interdigital electrodes (100 μm line-width and thickness). This fabrication process involved the direct mixing approach, which allowed for lower concentrations and made spin-coating feasible.

The sensors were subjected to a pressure of 7 bar inside a pressure chamber. The result is depicted in Figure III.7a. A clear response to pressure is detected, but the sensors drift greatly and the sensitivity decreases after each cycle. However, it is worth noting that different sensors exhibited similar behaviour during their initial pressure cycle, as depicted in Figure III.7b.

The stability of the sensors was investigated by repeatedly exposing them to a certain fixed pressure. While some sensors showed slight repeatable behaviour, unfortunately, most of the sensors exhibited drifting, as shown in Figure III.8.

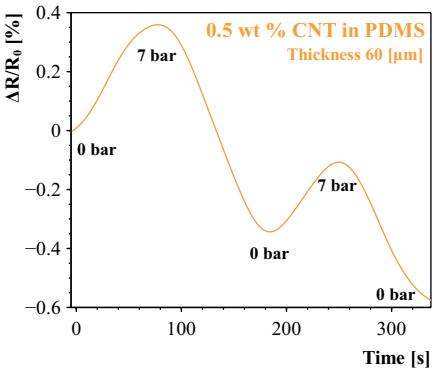

(a) Two pressure cycles inside a pressure chamber. A response to pressure is clearly visible but with a large drift.

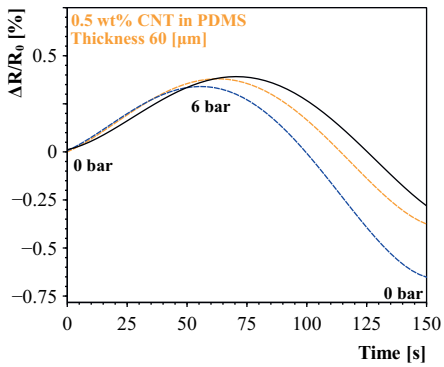

(b) Three different sensors response indicating a repeatable behaviour for the initial pressure cycle.

Figure III.7: Sensor responses to pressure chamber. A clear response to the ambient pressure is present. However, the sensor layers experience a irreversible change of resistance after each pressure cycle.

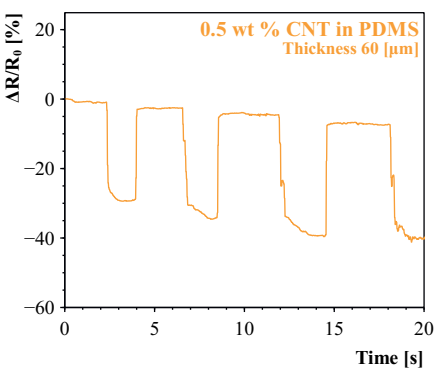

(a) Response to discrete pressure changes.

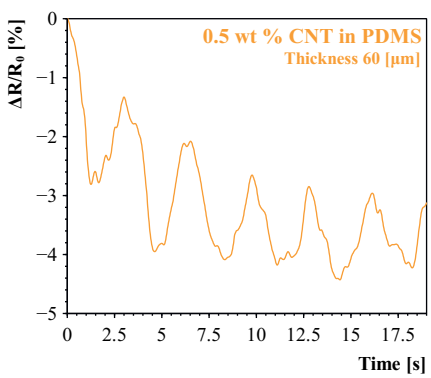

(b) Response to continuous pressure changes.

Figure III.8: Sensor responses to direct applied pressure on the sensors.

III.3.1 Experimental Percolation Threshold

The addition of solvents to the PDMS-CNT mixtures helps to reduce the viscosity of the solutions and improve the suitability for proper spin-coating. On the other hand, increasing the CNT weight content will eventually result in a viscosity that is too thick for spin-coating. In the direct mechanical mixing approach used in this research, there are no additional solvents to reduce the viscosity. Through experimentation, the threshold was found to be around 0.8 wt% (for PDMS). Beyond this point, the mixture becomes too thick, and after spin-coating, noticeable thickness variations occur (thicker layers in the middle and thinner layers at the sides).

Therefore, the conductivity of different CNT weight percentage layers was investigated, with concentrations up to this threshold, as shown in Figure III.9. As expected, thinner layers exhibited higher sheet resistances.

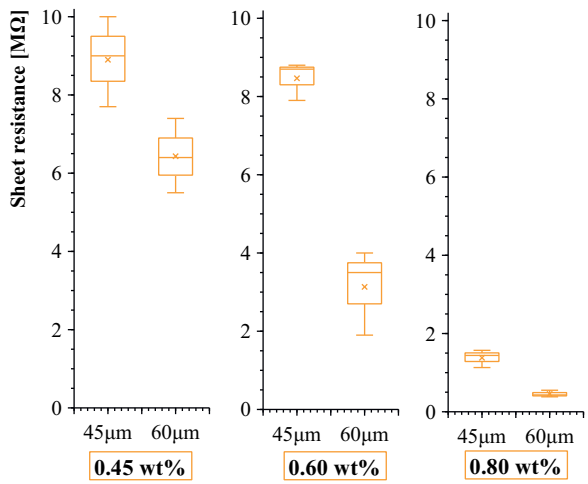

Figure III.9: Carbon nanotube concentration in relation to the samples sheet resistance.

The polyimide used in this research was based on a precursor U-Varnish-S (UBE Europe GmbH) with 20 wt% polyamic acid content. This means that the initial solution hold 80% of solvent, which greatly enhances the ability to mix CNTs into the polymer. A colleague at IMSAS University Bremen (M. Cen-Puc) experimentally found good CNT dispersion in polyimide layers up to 6 wt%. The percolation was found to be similar as with PDMS: ≈0.5 wt%.

However, clear differences were found in the CNT dispersion for both polymers. Identical concentrations, mixing techniques and spin-coating parameters were implemented to investigate the differences in dispersion quality. The influence of mixing speed is shown in Figure III.10. The graphs indicate that, for 10 minutes of high speed mixing, the average cluster size decreases (shifts more to the left), but increases again after 30 minutes. For low-speed mixing, it seems that longer mixing is needed to partly dissolve the agglomerations. These results correspond to current literature, where it is stated that too high shear forces or prolonged mixing can damage the CNTs and their networks [1] [6]. Entanglement of CNTS occurred up to 25 minutes of mixing, after which the CNTs started bundling together again [8].

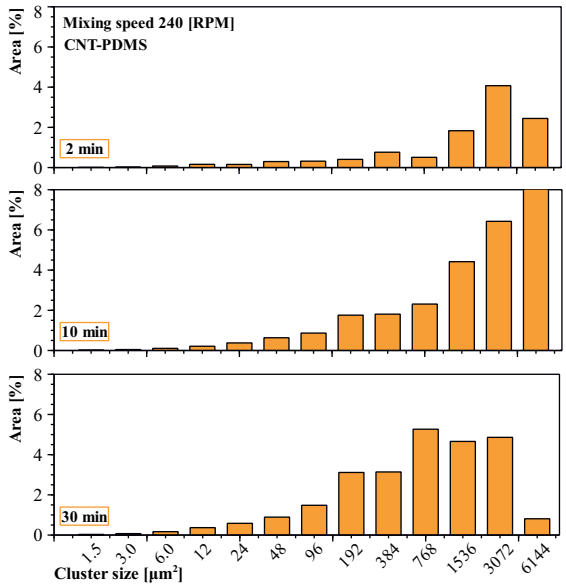

(a) Low-speed mixing of PDMS.

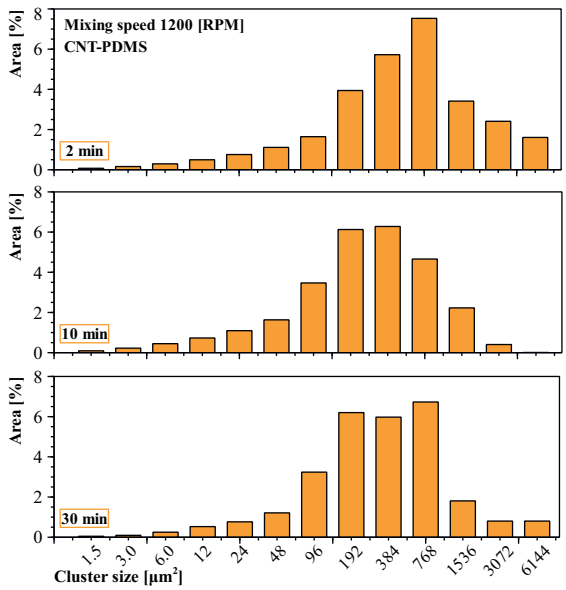

(b) High-speed mixing of PDMS.

Figure III.10: Cluster area detection to compare low and high-speed mixing of CNTs in PDMS.

III.3.2 Filler Influence on Polymer Mechanical Properties

To achieve conductive foils with still flexible properties, it is necessary to select metallic fillers which achieve a low percolation threshold. The more weight percentage of filler is needed, the higher the mechanical change in the polymer. Therefore, CNTs are highly suitable to add, and only small deviations in the flexibility, stiffness and strain resistance are expected.

The mechanical properties of the foils are measured with the XYZTEK Condor 100 which is able to precisely control the motion, and measure the force. A schematic overview of the measurement setup is shown in Figure III.11. Simultaneously, the change in resistance is measured by a precise multimeter (Keithley DMM6500). Therefore, the mechanical and electrical properties are continuously measured during the strain tests. The samples are clamped with custom 3D printed grippers [4]. Sandpaper is added to ensure a tight grip between the copper electrodes and the gripper. Figure III.12 shows a sample in the strain test setup.

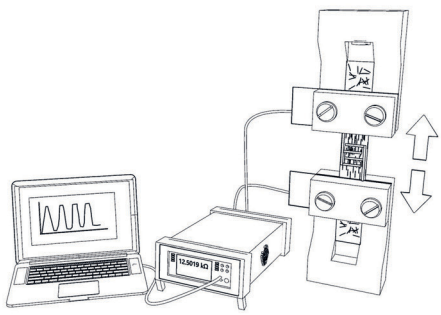

Figure III.11: Schematic overview of pull test setup.

The samples were divided into different groups based on the carbon nanotube weight percentage (0, 2, and 4 wt% CNTs). These samples were created using the earlier solvent method, allowing for larger concentrations of CNTs. It was observed that the mechanical differences between the newer direct mechanical mixing method and the solvent method were minimal due to the very small differences in carbon nanotube contents. Moreover, as discussed earlier, the direct mechanical mixing method improved dispersion, leading to increased conductivity of the layer, and consequently requiring less filler material.

To investigate the mechanical properties of the various samples, they were subjected to tensile testing, where they were pulled apart up to 30% strain. The Young's Modulus of the samples was determined using the following relation:

$$E = \sigma/\epsilon = (FL_0)/A(L_n - L_0) \tag{III.2}$$

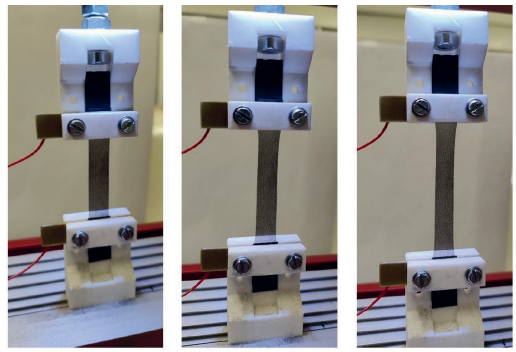

Figure III.12: PDMS-CNT pull test samples at different strain stages.

The influence for CNTs with higher concentrations is shown in Figure III.13a. It is clear that the addition of carbon nanotubes changes the mechanical properties (the material becomes stiffer), but still a linear stress-strain relation is observed, and flexibility properties are still linear up to 30%. The Young's Modulus increases as shown in Figure III.13b. The found value for pristine PDMS (3 MPa) corresponds to literature values [2].

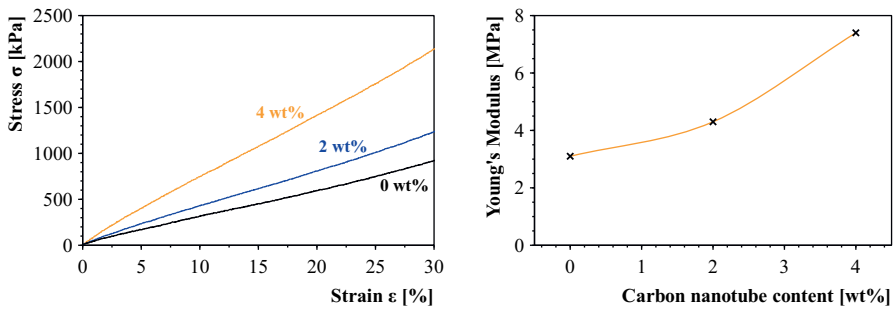

(a) Force-strain relation of high CNT concentrations. The CNT loading influences the polymer layers.

(b) Determined Young's Modulus of samples. Higher CNT loadings increase the stiffness.

Figure III.13: Mechanical changes of CNT-filled PDMS composites.

III.3.3 Strain Characterisation

The electrical measurements are performed with a high precision multimeter Keithley DM6500, which can measure the resistance and store the results immediately in a digital .csv file for further data processing. Figure III.14a show the strain results for 60 μm thick samples. The sensitive behaviour changes depending on the carbon nanotube concentration. Results show that a decrease in carbon nanotube content leads to more strain sensitive layers. The found Gauge factors for these layers are 1.4, 1.5, and 3.4 respectively for 0.8, 0.6 and 0.45 wt%. The Gauge factor is a measure for the sensitivity of piezoresistive strain materials. It is determined by the following relation:

$$K = \frac{\Delta R/R}{\Delta L/L} \tag{III.3}$$

In this equation, R is the initial resistance and ΔR is the change in resistance. This is similar for the L (initial length) and ΔL (change in length). For metals, the gauge factor is about 2. This means that a 0.1% strain applied to a 100Ω strain gauge sees a 0.2% change in resistance.

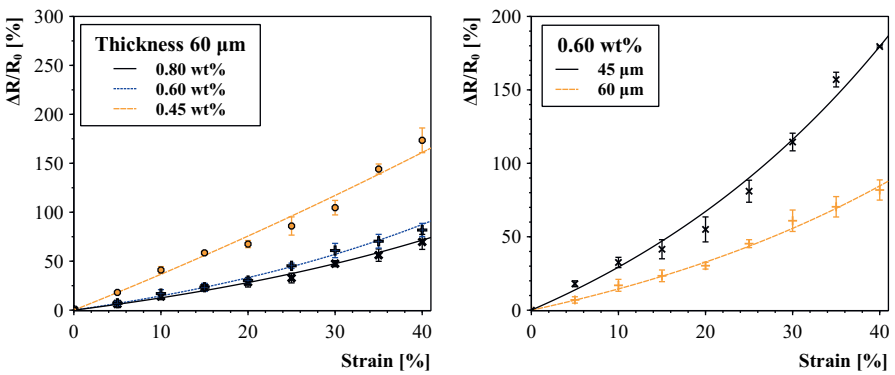

(a) Strain response for 60 μm thick layers. Lower carbon nanotube concentrations yield higher responses.

(b) Strain response for 0.6 wt% CNT-PDMS layers. Thinner layers give higher sensitivity.

Figure III.14: Strain response of the piezoresistive layers.

The influence of layer thickness on the piezoresistive sensitivity was investigated by creating two identical layers but with different thicknesses (45 μm and 60 μm). As expected and consistent with literature and numerical analysis (as discussed in previous sections), the thinner layers exhibited higher sensitivity to strain, with a relatively small Gauge factor ranging from 1.5 to 3.5. The results are presented in Figure III.14b.

III.4 Polyimide-based Pressure Sensor

Polyimide possesses a high elastic modulus, resulting in a more rigid piezoresistive layer compared to other polymers such as PDMS, which has an elastic modulus of only 360-870 kPa [7].

The multiwalled carbon nanotubes (CNT) used in the experiment have a diameter of 50-90 nm and an aspect ratio greater than 100 (Sigma-Aldrich Chemie GmbH). These CNTs (2wt%) are dispersed in the polymer for 30 minutes using the mechanical mixing method discussed in Chapter II. Subsequently, the films are spin-coated for 60 seconds at 3000 RPM and directly cured in a vacuum hotplate at 450 °C. This process yields a final sensor thickness of 4.7 μm.

The piezoresistive films are structured with 200nm thick gold interdigital electrodes, featuring an area of 1.8 mm2, a linewidth of 100 μm, and a gap size of 200 μm (as shown in Figure III.15a). To isolate the multiple sensors on the wafer, plasma etching is carried out using 40 sccm O2 and 8 sccm CF4 for 12 minutes. The etch rate of the 2 wt% CNT-PI layers was measured to be 0.5 μm/min. Due to the presence of added CNTs in the polymer, slight local in-homogeneities in the etch rate may occur. Consequently, brief over-etching is performed to ensure the complete removal of the PI-CNT layer around the sensors. This step guarantees isolation and well-defined sensor structures.

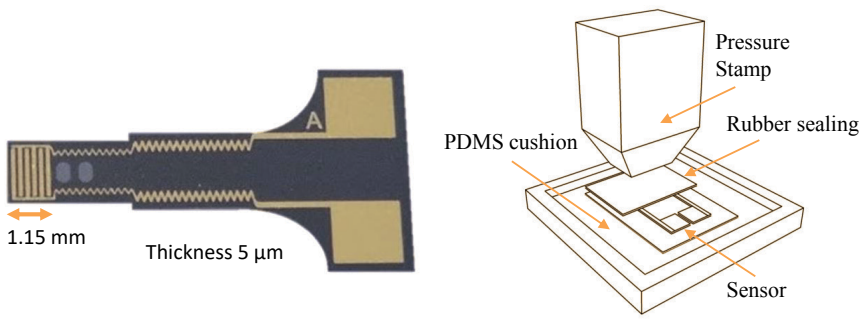

(a) Actual flexible pressure sensor made from a single layer of carbon nanotube-polyimide and gold electrodes. The inter-digital electrodes are visible on the left with a linewidth of 100 μm, and a gap size of 200 μm.

(b) Measurement setup. The sensor is placed on a PDMS cushion and isolated with a 100 μm thin HNBR rubber sheet. The pressure exposure is performed with a 1x1cm stamp.

Figure III.15: Actual pressure sensor (a). Measurement setup for pressure characterisation (b).

The sensors are placed between two custom made 100 μm thick hydrogenated nitrile rubber (HNBR) parts, simulating the integration of a sensor inside a rubber sealing. The rubber films (fabricated by our partners at the German Kautschuk Institute (DIK) in Hannover) are produced by means of a film press tool consisting of two circular molds with a 100 μm spacer. The HNBR mixture was vulcanised at 170°C at a pressure of 50 bar.

Copper wires are connected to the sensors using silver glue Elecolite 414 and then linked to a digital Multimeter (DMM6500, Keysight). Prior to each measurement, the multimeter undergoes calibration with a 100 Ω metal film resistor. A 3D printed stamp with a 1x1 cm area is affixed to the bond tester Condor 100 (XYZTEC). This bond tester is capable of performing multiple automated pull/push cycles, ensuring precise and repeatable pressure control.

To prevent damage to the sensors, a custom-made 6 mm thick PDMS cushion is employed to absorb the force. The stamp moves at a speed of 50 μm/min until it reaches the predefined force, at which point it holds for a specified period. Afterwards, the stamp is retracted at the same speed until it is completely clear from the sensor.

Figure III.15b provides an overview of the measurement setup, and Figure III.16 shows the results of the applied force and the sensor's response.

The average sensor responses for pressures up to 70N are presented in Figure III.17a. Sensors with a 50 μm interdigital electrode distance exhibited a linear sensitivity of 0.12‰/N up to a region of 55N. On the other hand, increasing the interdigital electrode distance (200 μm) resulted in higher sensitivity (0.45‰/N), but with a lower linear region, reaching almost 10N. Beyond this point, the change in pressure response gradually declined.

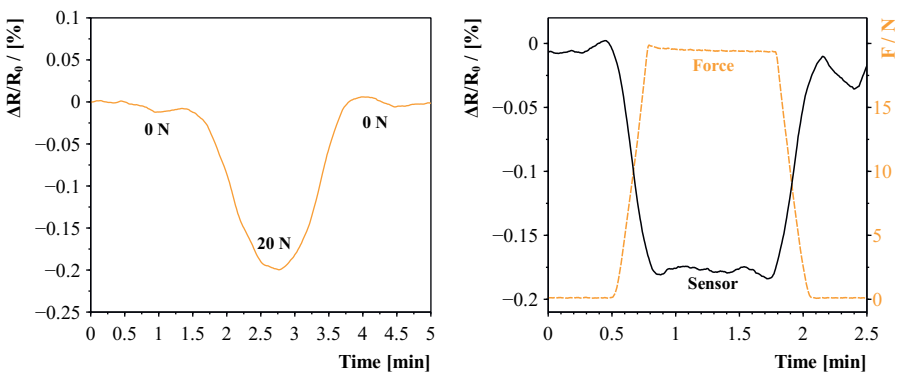

(a) Response to continuous pressure.

(b) Sensor response with shown actual applied force.

Figure III.16: Sensor responses to pressure.

The saturation of the sensor can be explained by the fact that with compressive strain, the CNTs can only move so far until they reach each other. This restricts their movement and results in the saturation point, where the minimum distance between the CNTs has been reached. On the other hand, with tensile strain, the distance is theoretically unlimited, potentially leading to a more efficient sensor range [6].

To investigate the effect of the piezoresistive layer thickness, identical sensors with two different thicknesses of 5 and 7 μm were manufactured. It was found that decreasing the thickness increased the sensitivity of the sensor (from 0.12‰/N to 0.33‰/N, Figure III.17b). However, it also lowered the detectable force range of the sensor. Results in Section III.2 had already shown that the probability of forming CNT-CNT connections with pressure increases with decreasing layer thickness. It is believed that the thinner layers can only absorb pressure up to a certain point, after which they become saturated, preventing further rearrangement within the piezoresistive layer and thus limiting the effective pressure region.

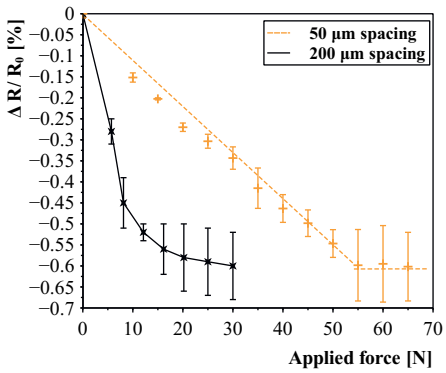

(a) Geometry influence. Larger inter-digital spacing increases the sensitivity but seems to reduce the sensitive regions.

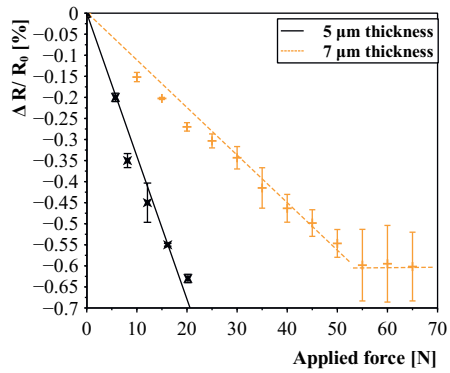

(b) Thickness influence. Thinner layers experience a higher sensitivity to pressure, with a smaller sensitive region.

Figure III.17: Effect on sensor geometry and thickness changes to its sensitivity.

The base resistance of the sensors was compared before and after the pressure characterization, which involved 7 cycles per force step, up to 70N. It was observed that the thinner sensors (5 μm) exhibited less irreversible change in base resistance (0.5%) compared to the thicker ones (7 μm) with 1.7% change.

Furthermore, the long-term stability of the sensors was determined by subjecting them to 500 continuous cycles of 20N, using the same machine parameters. The results revealed no noticeable changes in the sensor properties over the entire duration of the test (Figure III.18a).

Several tests with different CNT concentrations yielded insight in the pressure-sensitivity dependency of the sensors. Results showed larger resistance changes for the lower CNT concentrations, but the overall sensitivity did not seem to change greatly (as shown in Figure III.19b). These results are different than the found sensitivity influence due to different CNT wt% for the tensile strain samples, which showed an influence with the CNT weight content.

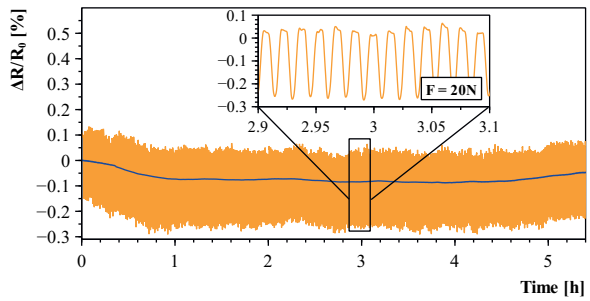

(a) Cyclic response of pressure sensor. The sensor shows stable and repeatable responses for the tested 500 pressure cycles of 20N.

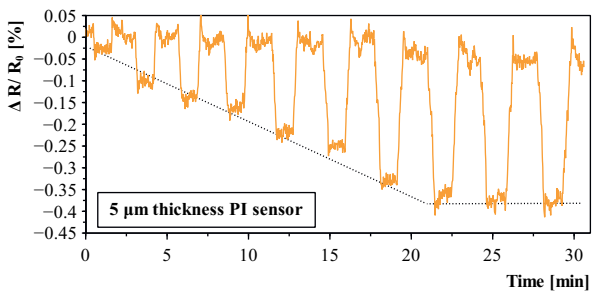

(b) Sensor response showing the different tested pressure cycles (in steps of 5N).

Figure III.18: Polyimide-based pressure sensor results.

III.4.1 Temperature Response of Polyimide Sensors

A sensor could be integrated into a sealing for monitoring changes in pressure, indicating failure or a leak. In order to accurately detect these changes, sensor long-term stability and drifts should be known in order for proper compensation. Therefore, the sensors are heated to 70°C for 112 hours as part of investigating the ageing effects of the sensor. The sensor response is measured every 15 seconds and the results are shown in Figure III.19a. The figure clearly shows an inverse relation to temperature. At 70°C, the sensor response shows a minimal linear decline over the 112 hours. After cooling down, the sensors base-resistance increased by 0.22%. This can be partly attributed by different beginning and ending temperatures (24.0°C vs. 22.9°C).

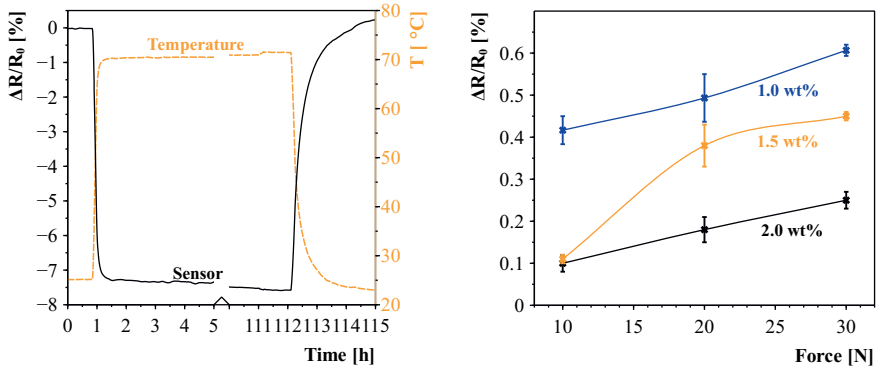

(a) Sensor response to temperature.

(b) Sensor response with different CNT concentrations.

Figure III.19: Base resistances dependency on temperature (left) and sensor response of different nanotube concentration layers (right).

References

[1] Alamusi et al. "Piezoresistive strain sensors made from carbon nanotubes based polymer nanocomposites". In: Sensors 11.11 (2011), pp. 10691–10723.

[2] Ronaldo Ariati et al. "Polydimethylsiloxane composites characterization and its applications: a review". In: Polymers 13.23 (2021), p. 4258.

[3] W.J. Brouwer. Identifying and Reducing visual Clutter for Process Graph Layouts. 2020.

[4] Marco Cen-Puc et al. "Carbon Nanotubes/Polymer Films for Microsensors Applications". In: 2021 IEEE Sensors. IEEE. 2021, pp. 1–4.

[5] Xingyi Huang and Chunyi Zhi. "Polymer nanocomposites". In: doi 10 (2016), pp. 978–3.

[6] Yan Yan Huang and Eugene M Terentjev. "Dispersion of carbon nanotubes: mixing, sonication, stabilization, and composite properties". In: Polymers 4.1 (2012), pp. 275–295.

[7] Kamal Izdihar et al. "Structural, mechanical, and dielectric properties of polydimethylsiloxane and silicone elastomer for the fabrication of clinical-grade kidney phantom". In: Applied Sciences 11.3 (2021), p. 1172.

[8] Harald Rennhofer and Benjamin Zanghellini. "Dispersion state and damage of carbon nanotubes and carbon nanofibers by ultrasonic dispersion: a review". In: Nanomaterials 11.6 (2021), p. 1469.

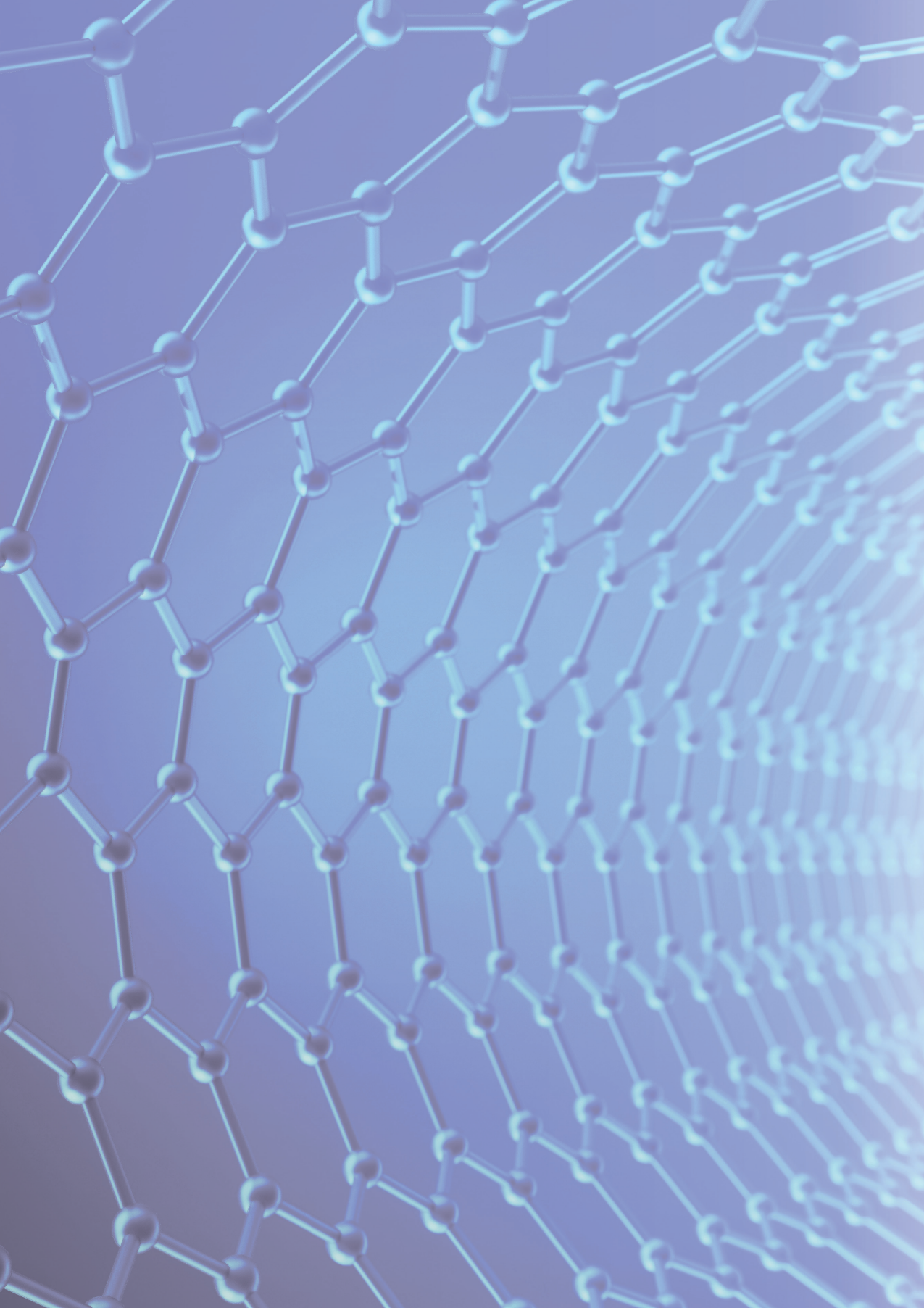

CHAPTER IV

Aligned Carbon Nanotube-Based Sensors

The contents of this chapter have been published in:
de Rijk, T. M., Schewzow, A., Schander, A., & Lang, W. (2023).
Unidirectional Electron-Tunneling Polymer Strain Sensor Based on aligned Carbon Nanotubes.
Sensors Vol 23., No 20., October 2023.

Abstract

High aspect ratio carbon nanotubes can be directly mixed into polymers to create piezoresistive polymers. Reducing the cross-sensitivity and creating unidirectional sensitive sensors can be achieved by aligning the nanotubes before they are cured in the polymer layer. This research presents and characterises this alignment of carbon nanotubes inside polydimethylsiloxane and gives the corresponding strain sensor results. The influence on the alignment method, as well as the field strength, frequency and time is shown. An analytical model is created to investigate the sensors behaviour and determine the effect of electron-tunneling in the sensor. A numerical model gives insight into the necessary applied field strength, frequency and time to facilitate alignment in viscous liquids. The experimental data shows a two-phase piezoresistive response. First a linear strain response after which the more dominant electron-tunneling piezoresistive phase starts with high gauge factors up to $k \approx 4500$ in the preferential direction, depending on carbon nanotube concentration. Gauge factors in the orthogonal direction remain low ($k \approx 22$). Finally, the dynamic stability of the sensors is proven by exposing the sensors to cyclic strain. Small initial drifts are observed but appear to stabilise after several cycles.

IV.1 Introduction

The orientation of the CNTs within their host material can be altered by applying an external electric field. The possible advantages of aligned CNTs can already be intuitively visualised to create connections of high aspect ratio CNTs over long, predefined, directions. Thermal or electrical conduction paths can be created in a preferred direction, as where in all other directions the conductivity is decreased. These selective conductive paths can be utilised for directional strain sensing with very high Gauge factors. Regular carbon nanotube based sensors often feature relatively low Gauge factors (in the order of 0.5-4) [31] [29] [5] [32]. Aligned carbon nanotube polymer layers show up to 10-fold resistance differences compared to the orthogonal direction, proving a preferential direction inside the polymer [2] [4]. Measured Gauge factors of aligned carbon nanotube compounds show far greater potential than regular other metallic piezoresistive materials [3] [28].

Even higher sensitivities for very small strain regions (up to 0.10%) are found in literature that are based on piezotronic tunneling junctions and shown to be up to a Gauge factor of $4.8x10^5$ [3].

This study aims to investigate, characterise, and optimise the alignment of carbon nanotubes within polydimethylsiloxane and assesses its effects on the performance of piezoresistive sensors. This alignment of carbon nanotubes in a specified direction minimises the cross-sensitivity of the sensor. An ideal sensor features no electrical connections in all other directions and only reacts to the direction of the applied strain. The experimental data is supported by extensive numerical and analytical models, yielding key insights into the working principle of the carbon nanotube alignment due to an applied electric field and the possible high sensitivities due to formed electron tunneling connections.

IV.2 CNT Alignment Methods

There are various techniques available for aligning carbon nanotubes (CNTs) within their medium. The following are the two most commonly used methods:

IV.2.1 Magnetic Alignment

In this method, an externally applied magnetic field is used to align the dispersed CNTs within the polymer. Generally, very high magnetic fields (7-10 Tesla [16] [24]) are required to achieve the rotational movement of CNTs. The alignment concept relies on the different diamagnetic susceptibilities (parallel $\chi_\parallel$ and perpendicular $\chi_\perp$) of the CNTs. If $\chi_\perp > \chi_\parallel$, then the CNTs will align parallel to the magnetic field, as demonstrated by [16].

Table IV.1 presents experimentally determined magnetic susceptibilities for various polymer-CNT composites. A distinct difference was observed for the low CNT concentration mixtures. The addition of CNTs reduced the magnetic anisotropy of the mixtures. This reduction in anisotropy was attributed to insufficient dispersion quality and the

Table IV.1: Magnetic susceptibilities of nanotube composites for different CNT concentrations [16].

Concentration [wt %]	$\chi_{\parallel}$ [x10^{-6} emu g^{-1}]	$\chi_{\perp}$ [x10^{-6} emu g^{-1}]	$\chi_{\parallel}$ - $\chi_{\perp}$
1	-5.2	-6.2	1
2	-6.7	-6.8	0.13
5	-4.2	-4.3	0.11

formation of clusters in high wt% CNT mixtures. When CNTs agglomerate, strong tube-tube van der Waals interactions limit their rotation along the applied magnetic field [16].

The alignment of CNTs by the applied external magnetic field can be verified by determining the conductivity in both the parallel and perpendicular directions. As early as 2002, research conducted by T. Kimura demonstrated a difference of more than one order of magnitude between the conductivity measurements in the parallel and perpendicular directions. This substantial difference in conductivity clearly indicated a change in CNT orientation in the presence of the applied magnetic field. Furthermore, the effect of alignment decreased with an increase in CNT concentration, as illustrated in Figure IV.1.

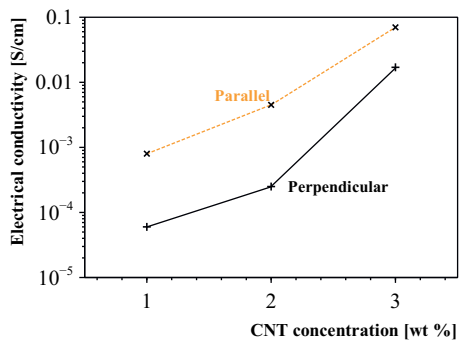

Figure IV.1: Conductivity of aligned CNT-Polymer composites in parallel and perpendicular direction. Image recreated from [16].

Another study by Ajiki and Ando in 1993 demonstrated that the diamagnetism perpendicular to the CNT axis can be up to three orders of magnitude larger than in the parallel direction, further confirming the alignment effect [1].

Additionally, the shape and size of the carbon nanotubes also play a role in their alignment. A study conducted by Jang and Sakka found that thick straight CNTs had a greater tendency to align than thin curved CNTs [12].

Furthermore, the addition of magnetic nanoparticles, such as magnetic maghemite ($\gamma - Fe_2O_3$), has been shown to enhance the magnetic susceptibility and increase the aligning ability of CNTs [1] [15]. These magnetic nanoparticles can assist in aligning CNTs under the influence of an external magnetic field, further improving the alignment process.

IV.2.2 Electric Field Alignment

The most common and possible most practical method to align CNTs is by exposing the uncured polymer mixture to an externally applied electric field. This method will be discussed further in this Chapter.

IV.3 Theoretical Principle

There are two basic principles of aligning CNTs with the help of an electric field: direct current-assisted alignment and indirect voltage-assisted alignment. Both methods are based on inducing a dipole moment within the CNTs, allowing them to gradually align with the applied electric field. However, due to the slight polarisation of the liquid medium itself, the alignment may not be completely parallel.

Figure IV.2 provides a graphical representation of the different steps involved in aligning CNTs in a liquid medium using the direct approach. Initially, the CNTs are randomly dispersed within the medium (1). After applying the electric field, the polarised CNTs experience a dipole moment, creating translational and rotational force that aligns the CNTs in the liquid due to the re-distribution of free electrons [18] (2). The polarised CNTs can connect to each other and form long connections (3). Depending on the alignment method used, the CNTs can form connections to the electrodes (4), or in the case of the indirect alignment method (which will be discussed later), they may not form direct connections to the electrodes.

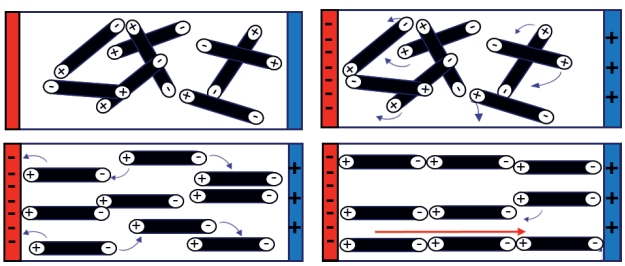

Figure IV.2: Alignment principle. The first randomly oriented carbon nanotubes rotate in the presence of an electric field due to their polarisation and acquired dipole moment. Afterwards, the polarised and aligned nanotubes form long connections.

The direct approach involves using two electrodes that are in direct contact with the liquid, allowing the possibility of current flowing through the solution. With this method, CNTs can form connections directly at the electrodes, creating local high electric fields (possibly changing the homogeneity of the field) and increasing the field strength at those locations. Other CNTs can then connect to the ones already attached to the electrodes, and this process continues until a connection is made between both poles. However, this approach can result in thicker conductive paths between the electrodes and carries the risk of creating shorts between the electrodes, which could halt the alignment process.

On the other hand, the indirect approach only utilises the electric field to induce the dipole moment within the CNTs. As there is no risk of creating a short between the electrodes, the alignment can continue without any time restraint. The CNTs slowly rotate and align in the direction of the electric field and can form connections, but this method does not create fast and uncontrollable long connections between the poles. In the indirect approach, the CNTs solely experience the electric field and align.

The effects of aligning CNTs using either the direct current-assisted approach or the indirect approach are shown in Figure IV.3. After the initial alignment is complete, the CNTs aligned with the indirect method will have rotated and possibly connected to nearby neighbour CNTs. In contrast, the current-assisted direct approach features more aligned agglomerations due to the local strong electric fields and current transfer when polarised CNTs attach to the electrodes and form connections.

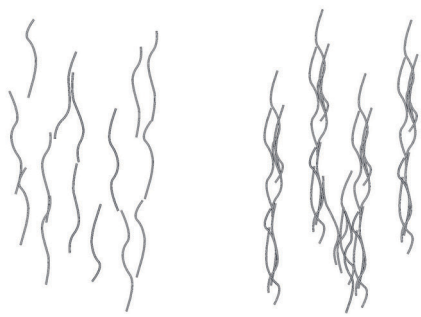

Figure IV.3: Alignment of CNTs in a vertical electric field with (left) indirect alignment and (right) with current-assisted direct alignment.

IV.4 Principle of Translational and Rotational Movement

IV.4.1 Translational Movement

The translational movement of carbon nanotubes can be explained by either the additional charged functional groups to carbon nanotube or by means of the electrophoresis theory. This is the case when a static DC electric field is applied.

Depending on the manufacturing process of the carbon nanotubes, they can become charged. For example, if the CNTs are treated with acidic functional groups, they can become positively charged. Basic groups can cause for negatively charged CNTs [23]. This has to do with the fact that acidic groups tend to donate protons and become negatively charged. The donated protons adhere to the CNT surface, giving them a net positive charge, which can cause the translational movement of carbon nanotubes.

The electrophoresis theory proposes a two layer system, the so-called double layer theory. Ions of a single kind collect at the particles' surface while around the CNT, the counter-ions shield this net charge from the bulk. With the applied DC electric field, these mobile counter-ions set in motion and create a directional liquid flow. The CNT moves due to the transferred viscous stress (the electrophoretic force) [22] [17]. This process is graphically shown in Figure IV.4. This so-called electrophoretic mobility μ is given by the following relation [9]:

$$\mu = \frac{v}{E} = \frac{\epsilon\zeta}{\eta} \tag{IV.1}$$

With, v denoted for the drift velocity, ϵ the dielectric constant, ζ the zeta potential of the carbon nanotube and η the viscosity of the polymer. The zeta potential is a measure of the surface charge, which for an AC field is equal to zero (no net electrophoretic mobility) [9].

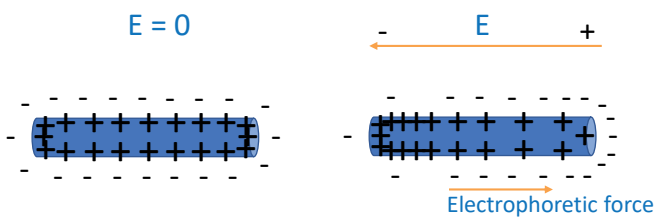

Figure IV.4: Principle of Electrophoresis. The double layer theory shows that suspended particles (with net null charge) feature an electric surface charge with a diffused layer of counter-ions around the suspended particle.

However, the mere presence of the carbon nanotubes within the electric field (inside the liquid medium) causes field in-homogeneities. The major force behind the CNT-CNT connections is due to the Coulombic attraction between oppositely charged ends of carbon nanotubes [9] [20]. Due to the hexagonal interlinked carbon atom structure of the nanotubes, each carbon atom is bonded to its neighbours by three valence electrons, leaving one electron free to move [27]. The polarised CNTs have an opposite increased charge density at the outer ends, causing local electric fields that can cause movement of other nanotubes in close proximity (dielectrophoresis). This principle is shown in Figure IV.5. This figure only presents the field lines connecting the CNTs. The field lines between the poles of the nanotube are removed for clarification. Due to the accumulated charges at the poles, these region exhibit the highest field strength and are the 'docking places' for other nanotubes. This effect thus yields the characteristic head to head CNT connections, forming long lines.

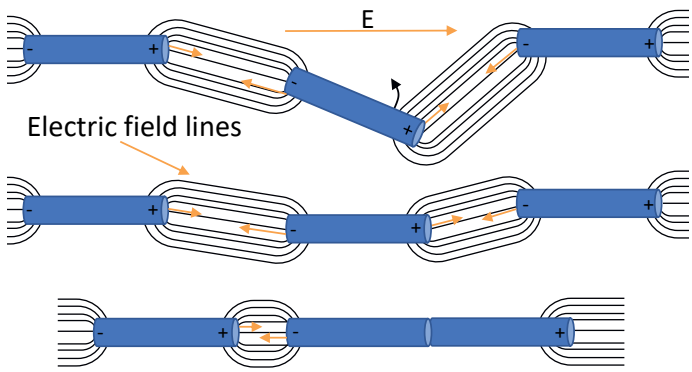

Figure IV.5: CNT head-to-head alignment due to an externally applied electric field. First, the nanotubes align themselves with the electric field due to the polarised nanotube ends. Secondly, the translational movement causes long connecting pathways to form between the electrodes.

IV.4.2 Rotational movement

In the presence of an electric field, the conductive carbon nanotubes are polarised and experience a dipole moment. The induced torque acts on the carbon nanotube and aligns it with the electric field [18] [8]. This process is graphically shown in Figure IV.6. The maximum torque is present when the dipole is perpendicular to the applied electric field ($max\tau$). The smaller the angle between the polarisation vector and the electric field, the smaller the induced torque (minimum when $sin(\theta = 0) = 0$). The alignment will continue until an equilibrium has been reached. This is either when the dipole is fully aligned or when the alignment force is not strong enough to facilitate the movement (weak electric field or too viscous medium).

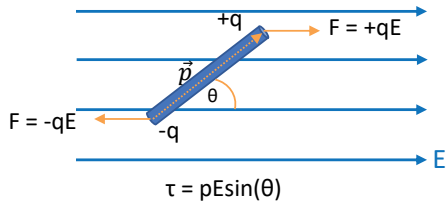

Figure IV.6: Principle of rotational forces on a dipole.

IV.5 Materials and Methods

Polydimethylsiloxane (PDMS) Slygard 184 was chosen as a suitable polymer to form the basis of the piezoresistive sensing layer. The main reason for this choice was the fact that the elastomer has no additional solvent that needs to evaporate whilst curing the final layer and it is well known in the ic-technology industry. It was expected that this removal of solvent negatively influences the alignment quality. Additionally, the molecular structures of elastomers (like PDMS) comprise of very loose, wide and long polymer chains, causing its flexibility properties.

The sensor fabrication is completely performed inside the cleanroom with regulated temperature and humidity. The characterisation of the sensors is performed in a climate-controlled laboratory. It is known that humidity changes the resistivity of carbon nanotube-polymer layers [25] [33]. To fabricate and test all samples inside climate-controlled environments ensured this effect was minimised.

The manufacturing process needs two sets of electrodes: alignment electrodes and measurement electrodes. The first are sputtered directly onto a 4-inch glass wafer and isolated by a 5 μm polyimide layer. This isolation is necessary to ensure no connections are possible between the alignment electrodes via the nanotube-polymer mixture, which could cause short circuits and stop the alignment process. The CNT-PDMS mixture is spin-coated directly (without any surface treatment) on top of the polyimide layer. The carbon nanotubes (Sigma-Aldrich Chemie GmbH) in this research feature a diameter OD of 50-90nm with an aspect ratio of >100. The CNTs are mixed with the direct mixing approach, discussed in Section II.4.3. The gold contact pads of the alignment electrodes are freed of polymer and a voltage is applied to the uncured PDMS layer to align the CNTs. Afterwards, the piezoresistive layer is cured at 90°C for 45 minutes. A low curing temperature is chosen to minimise the induced stress within the polymer layer. The second set of electrodes are the inter-digital electrodes used for measuring the sensor response. This chrome-gold layer is deposited via the sputtering process and structured with standard lithography processes. The only exception is that the photoresist is pre-baked in an oven to slowly ramp the temperature to 90°C. The standard process

would allow the resist to cure on a hotplate, but previous experience showed the layers underneath to crack due to the high temperature expansion coefficient of the PDMS. After the top inter-digital electrodes are structured, the sensors are cut and easily removed from the bottom polyimide layer. A simplified version of the sensor layers is shown in Figure IV.7.

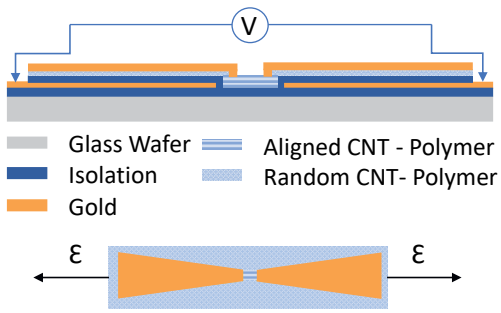

Figure IV.7: View of the individual sensor layers. The top part shows the fabrication layers on top of the glass wafer. The alignment electrodes are isolated with a polyimide layer (purple). The measurement electrodes are sputtered on top of the cured CNT-PDMS layer. After the sensors are complete, they are detached from the wafer, leaving the glass wafer, alignment electrodes and polyimide layer behind.

The sensor is based on the fact that with applying tensile strain, the distance between the conductive particles increases and the conductivity decreases. Ideally, with the aligned CNTs, the sensitivity is increased in the preferred direction, and reduced to zero in all others. The individual sensors are placed in a custom-made gripper with copper plates to continuously measure its resistance (shown previously in Section II.4.3). The whole setup is placed in the CONDOR 100 Bond tester (XYZTEC), which is completely programmable to preciously pull the samples apart while measuring the applied force. The speed was 20 μm/sec and the samples were stretched up to 1.0% strain. The resistance was continuously measured with a digital multimeter (Keithley DMM6500). An overview of the measurement setup and a picture of the actual setup with a strain sensor is shown in Figure IV.8.

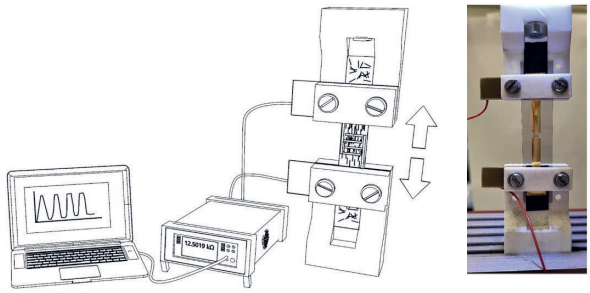

Figure IV.8: Measurement setup for characterising the strain sensors. The samples are placed inside a custom made gripper (shown in Section II.4.3 [6]) and connected to the digital multimeter.

IV.6 Analytical Model for the Piezoresistive Effect

Two main principles of piezoresistivity are expected to occur while the sensors are experiencing tensile strain:

- Loss of conductive networks due to reorientation of CNTs within the polymer matrix. The CNTs change their orientation and position due to the applied strain. In general, it is assumed that the CNT-CNT connections start breaking up with increasing strain. As the polymer matrix is highly flexible, the effects are reversible with decreasing strain. This relation is shown by Equation IV.2, where the applied stress (σ) causes the decrease of the inter-particle distance s.

$$s = s_0(1-\epsilon) = s_0(1-\frac{\sigma}{E}) \tag{IV.2}$$

- Electron tunneling when the CNT-CNT distance is closer than 1.0 nm. The carbon nanotubes within this distance can conduct current, which with increasing strain will abruptly stop when the distance becomes too great.

The more interesting effect due to the alignment of CNTs is the electron tunneling effect, which could theoretically increase the Gauge factor multiple orders of magnitude. The electric field causes the CNTs to rotate and align in the direction of the induced field. If the CNTs come close together (<1.0 nm) a current can flow between the CNT-isolation-CNT barrier. This tunneling effect depends on the distance between the media and its barrier height. The tunnel resistance is shown in Equation IV.3, based on Simmon's theory [26]:

$$R_{tunnel} = \frac{V}{AJ} = \frac{h^2 d}{Ae^2\sqrt{2m\lambda}} exp(\frac{4\pi d}{h}\sqrt{2m\lambda}) \tag{IV.3}$$

The cross-sectional area of the CNT is denoted by A (OD = 50nm), tunneling current density J, Plank's constant h, tunneling distance d, mass of the electron m and the barrier height λ. The barrier height, according to literature, was approximated between 0.5 eV and 2.5 eV for epoxy [26]. The CNTs in the polymer experience a poor stress transfer from the polymer matrix due to the large elastic mismatch (CNT: 270- 950GPa [34], PDMS: 0.57-3.7MPa [30]) and weak interface strength [26]. Hence, the deformation of the CNTs due to the applied strain is assumed to be neglectable, and the piezoresistivity is mainly attributed to the tunneling effect. Figure IV.9 shows the relation between the tunnel distance and the corresponding change in resistance (based on Equation IV.3). The exponential relation is clearly visible. High changes in conductivity occur when the distance between individual tunneling CNTs is changed slowly. This effect is far greater than the regular piezoresistive property using conductive CNT networks that break up with applied strain. Hence, it can be assumed that if high resistances are measured with large (non-linear) resistance changes, this is attributed by electron tunneling. This effect will outweigh the change of resistance due to disconnecting CNTs that change their orientation.

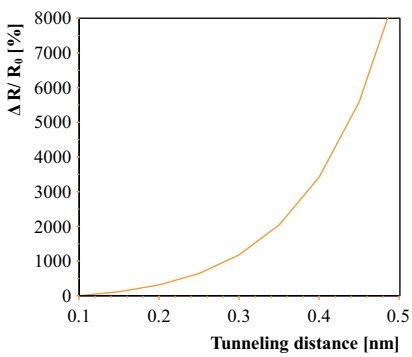

Figure IV.9: Relation between electron tunneling distance and the change in resistance for a single carbon nanotube pair. This relation follows from Equation IV.3. R_0 is the resistance value at a distance of 0.1 nm.

A more detailed analytical model was created to show the effect of aligned carbon nanotubes and their CNT-CNT interactions via either direct contact or electron tunneling. The large difference in sensitivity in the alignment direction and the orthogonal direction is validated. The general concept of the model is shown in Figure IV.10. The model consists out of two vertical electrodes with a specified amount of carbon nanotubes (high aspect ratio rectangles). The nanotubes are placed vertically aligned in several conductive paths as shown in the figure. Variation in both x and y directions are included to ensure slight random positioning. A valid electrical connection is determined when either the nanotubes are in direct contact or close enough for tunneling (<2.5nm in this model).

The conductive paths are determined (that are classified as a valid connection) and the resistance is calculated for each connection. This is done either via determining the resistance of the connecting 'wires' ($R = \rho(L/A)$) or by the exponential electron tunneling relation shown in Equation IV.3.

A summery and a brief overview of the analytical method is presented below.

- Parameter definition including CNT dimensions, maximum tunnel distance and number or objects.
- Creation of rectangles (simplified CNTs). Two main electrodes at the top and bottom and a specified number of random or aligned rectangles.
- Determination of the closest distances between all rectangles. The rectangle borders are implemented for this, not the centre points.
- The shortest path is determined between the electrodes via Dijkstra's shortest path algorithm.
- A strain on the sensors is simulated by changing the y-coordinates of all objects, just as with a real applied strain.
- The distances and shortest paths are determined once again for all applied strains.
- The resistance of each connection is determined; either via tunneling or direct contact. Electron tunneling is possible for distances lower than 2.5nm, featuring the exponential relation between resistance and distance. Direct contact resistance is determined by the length and width of the connection.
- Finally, multiple parallel conductive connections are modelled and their parallel resistance is determined.

It is expected that after the alignment of carbon nanotubes in the polymer is complete, conductive paths have been formed. Initially, this would mean the nanotubes are in contact before the applied strain. The nanotubes are slowly pulled apart until the first connections break and electron tunneling occurs that suddenly jumps the linear strain response to an exponential growth. This property is also seen in the analytical simulations and shown in Figure IV.11. The left figure shows the relation between the expected resistance change for different number of connecting CNTs. All results show an initial low Gauge factor ($\approx$ 1, see inset) up and until the strain is large enough and the direct connections break. The longer the CNT paths between the electrodes are, the higher the sensitivity appears to be. Figure IV.11b presents the effect of the aspect ratio on the sensitivity. This effectively confirms the previous figure because low aspect ratio connected CNTs feature more connections over the same distance and hence feature higher sensitivity. The carbon nanotubes in this research feature an aspect ratio of $>$150. Additionally, the aspect ratio correlates closely with the percolation threshold of the mixture. The relation can be mathematically represented by the relation shown in Equation IV.4 [7], which clearly shows the inverse dependency between the aspect ratio and percolation threshold.

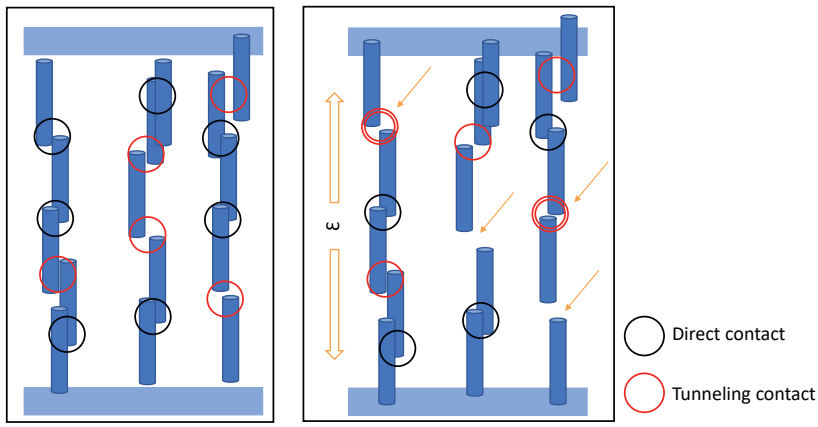

Figure IV.10: Analytical model principle. With applied tensile strain, previously connected CNTs detach and become an electron tunneling connection. Or previous electron tunneling connections become too large and result in CNT-CNT disconnection. New or changed connections are indicated by a double coloured circle and an arrow.

$$\Phi_{pc} = \frac{(3+\delta_d^2)}{6AR} \tag{IV.4}$$

Ideally, if all vertically conductive paths are perfectly aligned, a strain in the orthogonal direction (horizontal in this case) should have no effect on the sensor. However, due to possible cross-connections, a small change is still expected. The results of the strain sensitivity in the direction orthogonal to the alignment direction is shown in Figure IV.12a, showing the low changes as suspected (please mind the larger applied strain up to 40% on the x-axis).

The loss of connections is shown in Figure IV.12b. This map indicates all CNT-CNT electron-tunnel connections (in this case 20). The connections, indicated by the orange colour, decrease with increasing strain, causing the large increase in measured resistivity. After a certain amount of strain, all connections will be too far away and no conductance is measured.

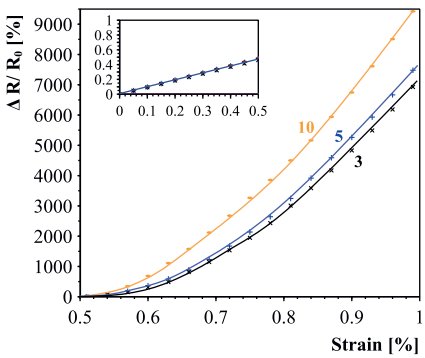

(a) Influence on sensitivity with varying number of CNT-CNT connections (10, 5 and 3). Results show an increase in sensitivity for higher number of connecting nanotubes (similar to wider inter-digital gaps).

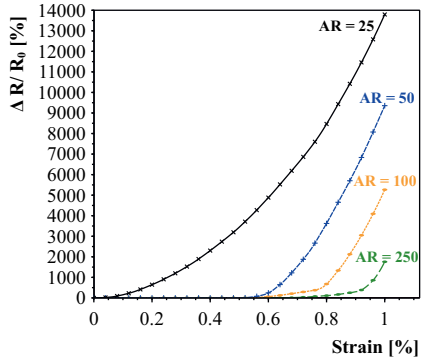

(b) Influence on sensitivity by varying the aspect ratio of CNTs. A fixed electrode distance was chosen with varying aspect ratio CNTs. The initial linear low Gauge Factor response seems to lengthen with increasing aspect ratio.

Figure IV.11: Analytical results to model the response of aligned carbon nanotube networks. The inset of (a) shows the linear initial low Gauge Factor response up to 0.5%, after which electron tunneling becomes more dominant and the response drastically increases.

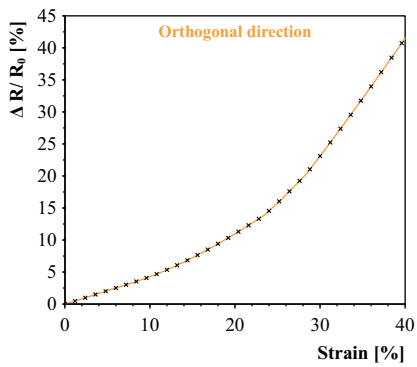

(a) Strain sensitivity response by pulling orthogonal to the alignment direction. Responses shows far lower sensitivity than for in the alignment direction shown in Figure IV.11a.

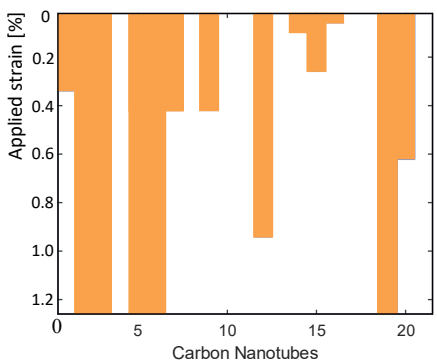

(b) Visualisation of the available tunneling connections (in orange) decreasing with applied strain. Vertically, a decrease in tunneling connections is visible due to increasing strain.

Figure IV.12: Numerical simulation results and model principle. Left: Low sensitivity in the orthogonal direction. Right: Visualisation of the loss of connection (parallel to alignment) with applied strain. The figure shows the connections for a total of 20 carbon nanotubes on the x-axis and their present connection status (orange or white).

IV.7 Numerical Simulation for Nanotube Rotation

The concept of rotating CNTs inside a liquid medium using an external electric field was validated through a COMSOL Multiphysics model. The model consisted of a single CNT (with outer diameter 30μm and length 600μm) placed in a liquid (water) under the influence of a 2kV/m, 2Hz AC field. This first model featured these larger CNT dimensions in order to keep computation times short. Figure IV.13a illustrates the load on the nanotube in the x and y direction. The applied electric field is in the y-direction and the CNT has a starting angle of 30° with respect to the x-axis. With alignment, the x-component of the load decreases, as the y-component increases. Eventually, the nanotube stabilises in the aligned direction. Furthermore, as depicted in Figure IV.13b, it can be observed that the nanotube become polarised, and the polarisation increases until an equilibrium has been reached.

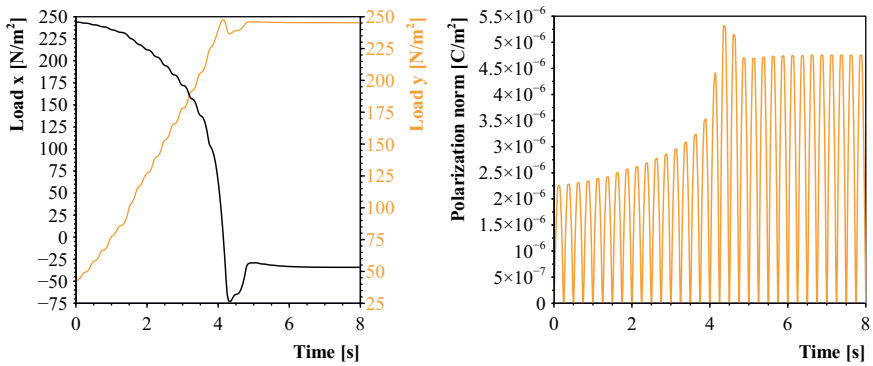

(a) Load on CNT-ends while aligning in the electric field (in y-direction). Initially, the CNT is angled 30° to the electric field. The load on the y-direction increases as the load on the x-direction decreases with alignment.

(b) Polarisation of the CNT during alignment in an electric field (2kV/m AC, 2Hz). The cyclic behaviour of the AC field is visible in the polarisation graph. The polarisation increases with alignment until it stabilises.

Figure IV.13: Applied forces on the carbon nanotube due to applied electric field.

In a more detailed and realistic model, the same CNT dimensions as the real CNTs used in this research were considered: an outer diameter of 50 nm and a length of 5 μm. The influence of frequency with a fixed voltage was investigated, and the results are presented in Figure IV.14. The results indicate that the rotational movement of the CNT decreases with increasing frequency.

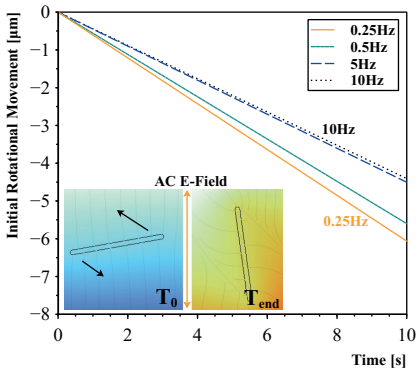

Figure IV.14: Rotational movement of CNTs in a polymer with different electric field frequencies. The higher frequencies show lower rotation movement. The inset shows the rotation of the carbon nanotube. The color differences in the background are due to the AC field.

The rotational movement of the CNT is not a straight line and corresponds to the applied frequency waveform. For clarity, a straight line is shown to visualise the differences. The initial movements were linear until the rotation exceeded a certain threshold, after which the rotation decreased.

It is believed that the CNTs have a certain threshold after which they have enough energy to rotate within the liquid. The highest polarisation occurs at the peaks of the AC voltage, during which the length surpassing this threshold decreases with increasing frequency. Therefore, it is thought that a frequency too high may not be able to fully polarise the CNT in time and stop or slow down the alignment.

The influence of viscosity and electric field strength on the CNT alignment is demonstrated in Figure IV.15a. The figure illustrates the load on both ends of the CNT. Since the opposing ends rotate in opposite directions, the relation between the loads have opposite signs. The crossing point indicates the parallel position of the CNT in relation to the applied field.

In the simulation, viscosities and parameters were selected to correspond to the properties of PDMS. The data reveals that an increase in viscosity (from 1 to 3 pas) results in a longer alignment time. Conversely, an increase in electric field strength decreases the alignment time. These observations suggest that higher viscosity requires more time for the CNTs to align with the applied field, while stronger electric fields expedite the alignment process. This information provides insights into how viscosity and electric field strength can influence the alignment kinetics of CNTs in a liquid medium. Additionally, first values of the needed field strengths and frequencies for the experiments are now known.

If carbon nanotubes attach to the conductive electrodes, they can create local areas of increased electric field strengths and cause alignment imperfections. This effect is simulated and demonstrated in Figure IV.15b, where the increase in field strength (e2) is clearly visible. It can also be clearly seen that the direction of the electric field strength changes. This is due to the fact that the growth of CNT connections changes over time, leading to variations in local electric field strengths and directions.

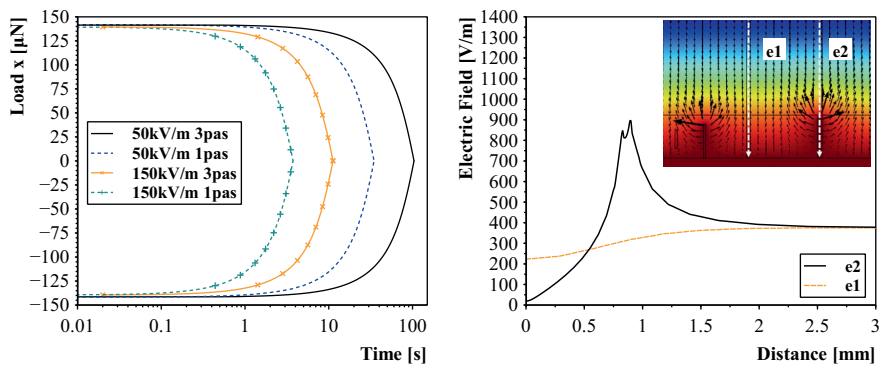

(a) Influence of viscosity and E-field on CNT-alignment. Viscosities are chosen to correspond to uncured PDMS.

(b) Effect of connected CNTs to the outer electrodes. Local high electric fields disturb the alignment.

Figure IV.15: Numerical simulation results of rotating carbon nanotubes in an electric field.

IV.8 Characterisation of Alignment Parameters

Carbon nanotubes were mixed in de-ionised water and aligned with two electrodes on either side in a 3D printed mold (1 cm spacing). The results are shown in Figure IV.16. It can be seen that the first homogeneous solution is non-transparent and after the alignment continues, more and more thick connections form. At the end, it looks like all CNTs are in thickly formed 'highways' between both electrodes. This test was performed with placing the electrodes directly into the solution, enabling for a current to flow once connections were formed. The applied AC voltage was 13.3kV/m at 1Hz.

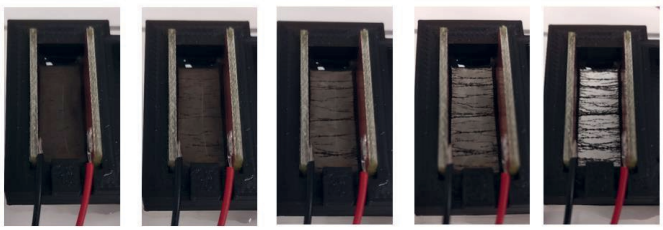

Figure IV.16: Carbon nanotube alignment in DI-water as Proof of Concept. The electrodes (1cm apart) are placed directly into the solution.

Using a DC voltage yielded the same alignment effect but with the major disadvantage of slowly pulling all charged CNTs to a single side. This was experimentally proven by applying a DC voltage of 13.3kV/m and measure the current during alignment. Figure IV.17a clearly shows a very sharp increase in current, after which the CNTs start to pull to one side and the current decreases slowly until it stabilises. It is thought that at this saturation point, there is a formed connection present between both electrodes via the sidewalls of the mold.

It is expected that the migration of nanotubes when positioned in a DC electric field is caused by the initial charge of the nanotubes. Depending on the manufacturing process of the carbon nanotubes, they can become charged. For example, if the CNTs are treated with acidic functional groups, they can become positively charged. Basic groups can cause for negatively charged CNTs [23]. This has to do with the fact that acidic groups tend to donate protons and become negatively charged. The donated protons adhere to the CNT surface, giving them a net positive charge, which can cause the translational movement of carbon nanotubes. This effect is the main reason why low alternating voltages were implemented in this research to align the carbon nanotubes.

The CNT concentration was lowered even more to try and visualise the effect of alignment on the conductivity of the solution. Two different frequencies were applied and the results are depicted in Figure IV.17b. Results confirm previous experiments that the alignment with higher frequencies (1 vs. 2 Hz) decreases. The most controllable alignment speed seems to be with the lower frequencies, which corresponds to the performed numerical simulations.

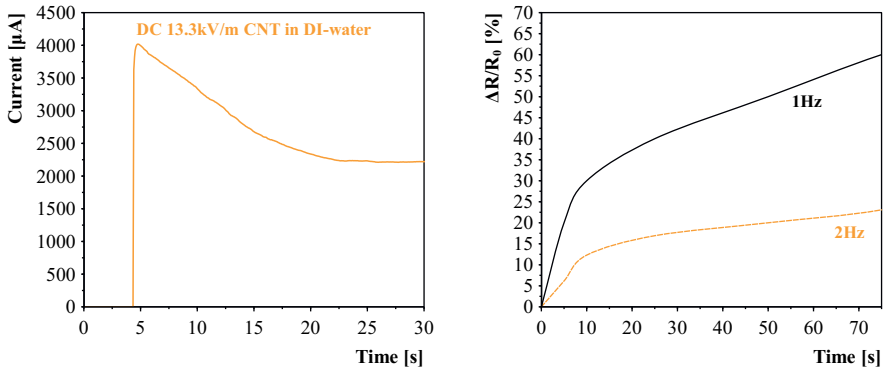

(a) Dc alignment shows migration of carbon nanotubes. The conductivity decreases due to the nanotube migration.

(b) Frequency influence on CNT alignment for 0.02 wt% in de-ionised water. In PDMS, a lower electric field frequency shows faster alignment.

Figure IV.17: DC and AC Alignment in de-ionised water.

After the initial experiments, the alignment parameter characterisation was performed with a manufactured mold featuring an electrode distance of 3 mm and a length of 1.5 cm. Two alignment methods were characterised: with the direct current application (electrodes inside the liquid) or indirect alignment where the electrodes were isolated from the liquid. The alignment process was investigated for the following parameters: electric field strength, alignment time, indirect vs. direct alignment and frequency influence.

For the piezoresistive layer, PDMS with a 1:5 curing agent ratio was chosen. Normally, the standard ratio for the curing agent is 1:10. However, in this case, the proportion of the curing agent was increased to the maximum value that still yielded proper layers, which was a ratio of 1 to 5. This adjustment was made to create the least viscous solution possible, which is beneficial for the alignment process.

Electric Field Strength The necessary electric field strength required to induce optical alignment of CNTs was investigated. A fixed frequency of 1Hz was used for this study. If, after 60 minutes, no optical change in CNT alignment was observed, it was assumed that the applied field strength was not sufficient. Results showed a very precise window of field strength needed for aligning the CNTs in PDMS. An induced electric field of 460 kV/m did not result in an optical change in the CNT orientation, while with 500 kV/m, alignment occurred almost instantly.

As suspected, the speed of alignment increased with higher field strengths. To achieve better control in the alignment process, a field strength of 480 kV/m was chosen. This specific field strength produced an optical change in CNT alignment after several minutes, which was deemed feasible for later wafer fabrication and sensor production.

Alignment Time The CNT-polymer samples were subjected to an indirect electric field of 480 kV/m at 1Hz for up to 60 minutes. Microscopic images were taken at intervals of 5 minutes, capturing the starting position, alignment after 5 minutes, and alignment after 60 minutes, as shown in Figure IV.18. The results clearly demonstrate a noticeable change in alignment even after just 5 minutes, with a more pronounced effect after 60 minutes. As the electric field is applied for longer duration's, the CNTs agglomerate and create thicker carbon nanotube bundles.

Furthermore, it was found that as the CNT weight percentage (wt%) in the polymer increased, the alignment of CNTs took longer. Beyond a certain CNT concentration, no visible optical alignment was observed anymore due the large clusters in the mixture.

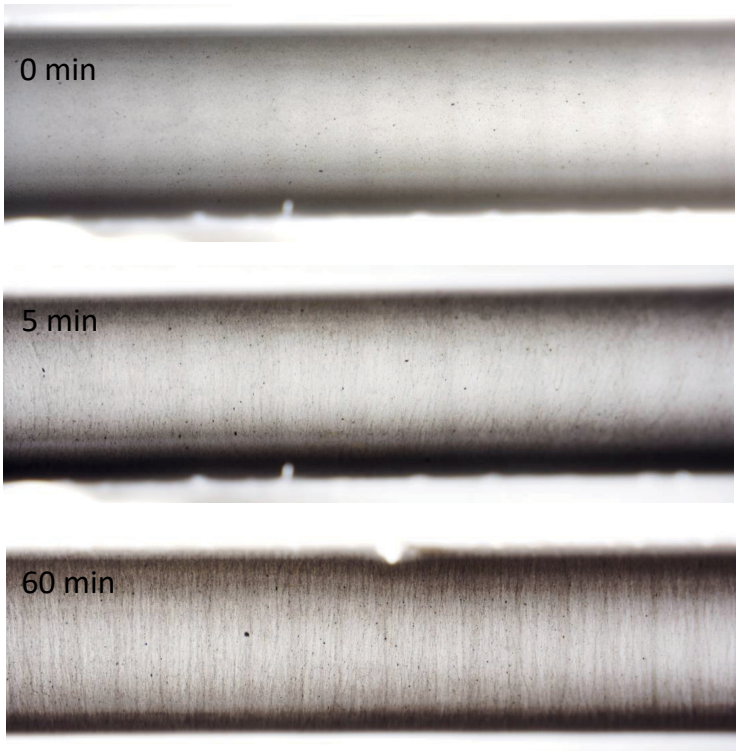

Figure IV.18: Carbon nanotube alignment for different times (0, 5 and 60 minutes). With an electrode distance of 3 mm. First, a randomly dispersed solution is visible. After 5 minutes, the first conductive paths are visible, which become more pronounced after 60 minutes.

Indirect vs. direct alignment As mentioned before, two alignment methods are possible. Either the electrodes are placed in the solution, enabling a current to flow between the electrodes once conductive paths are formed, or with isolated electrodes. Both methods were investigated and the results were clear. The indirect method was able to align the CNTs in the same (optical) way as the direct method. However, difficulties arose with the direct method, specifically with the sudden connection between both electrodes and the high required voltages. Figure IV.19a shows a measurement performed while aligning the CNTs in PDMS. After some time, there was an increase in current flow, but suddenly, it dropped back to zero. At the instant a connection was created between both poles, the released energy due to the short-circuit was so significant that a small visible shock-wave ran through the solution, instantly curing the PDMS at the location of the short-circuit and destroying the alignment.

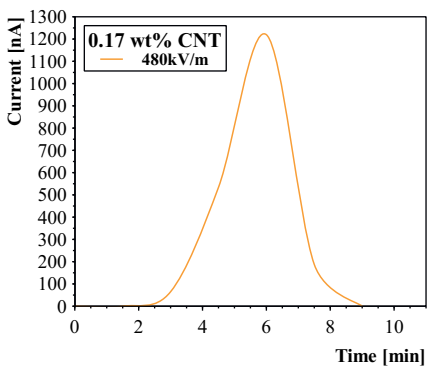

(a) Measured current during the direct-method alignment process. The high voltages and the created connection between the electrodes caused a electrical short circuit, destroying the nanotube alignment.

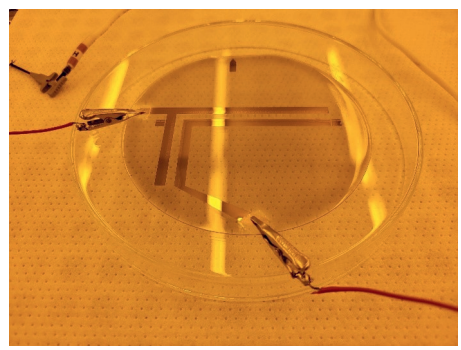

(b) Wafer alignment setup. The large parallel gold electrodes are the alignment electrodes. Between them, the nanotubes are aligned. The polymer is manually removed in order to have an electrical contact between the electrodes and the clamps connected to the high voltage generator.

Figure IV.19: Carbon nanotube alignment results and alignment setup.

Additionally, with the direct alignment method, it was observed that after the solution was optically aligned, the edges on either side started moving turbulently. A circular motion was visible on either side, while no movement was visible in the middle. It is theorised that this effect is caused by the change in the local electric field orientation due to the CNTs attached to the electrodes, as previously discussed and shown in Figure IV.15b.

Due to these results and the challenges encountered with the direct method, the indirect method was chosen for aligning the CNTs in the wafer-fabricated sensors. The indirect method demonstrated successful carbon nanotube alignment without the associated complications .

Frequency Influence Frequencies of 1Hz, 10Hz, 100Hz and 1kHz were investigated with a fixed voltage of 480kV/m for up to 60 minutes. The time it took to optically move and align the CNTs was taken as a comparative study between the frequencies. Results are shown in Table IV.2. Similar to the simulation results, the alignment time increased with increasing frequency.

Table IV.2: Time to optical alignment of CNTs in PDMS polymer.

Frequency	Time to align [min]
1Hz	3
10Hz	18
100Hz	>60
1000Hz	>60

IV.8.1 Effect of Air bubbles in the mixture

Before placing the mixtures inside the electric field, it is essential to remove all air bubbles through vacuum treatment. Any remaining air bubbles can have a significant impact on the electric field, causing it to change its direction, as depicted in Figure IV.20a. The presence of air bubbles can disrupt the alignment process of CNTs over time, leading to undesirable outcomes, as illustrated in Figure IV.20b.

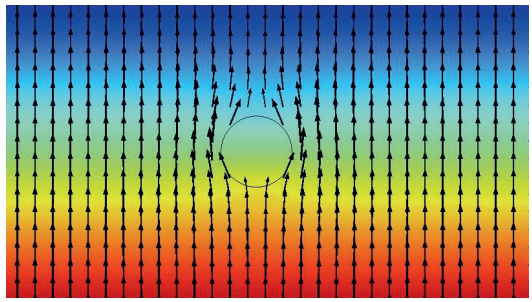

(a) Numerical model showing the effect on the electric field with an air bubble in the polymer.

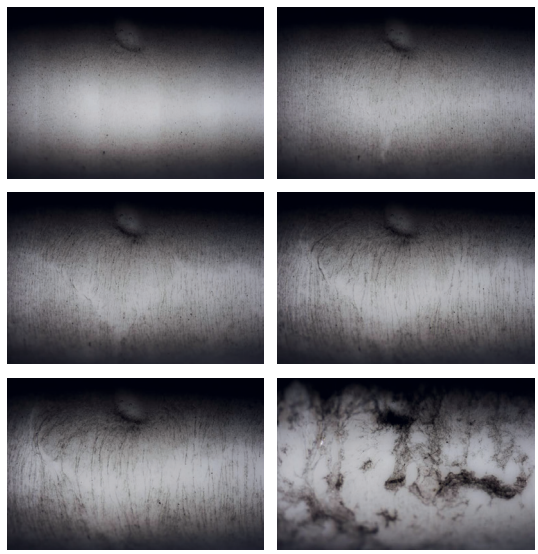

(b) Experiment with an air-bubble in the mixture. The artefact distorts the electric field and subsequiently, the alignment.

Figure IV.20: Effect of air-bubbles in the alignment mixture.

IV.8.2 Nanotube Alignment in Elastomers and Duroplastics

This research showed that, as suspected, the viscosity of the solution plays a major role in the alignment process. This was shown in numerical simulations, as well as in the experimental results. For DI-water, an electric field strength of 13.3kV/m was already suitable for aligning the CNTs. For PDMS however, the alignment started above 460k/m. The effect of different polymers was investigated by trying to manufacture aligned strain sensors in polyimide. The polyimide solution was prepared from precursor U-Varnish-S with 20 wt% polyamic acid content. The CNTs were mixed in the duroplastic via the direct mixing method explained in Chapter II.4.3. After several tries with different layer thicknesses, electric field strengths and frequencies it was found that no alignment or even nanotube movement was present after several hours. A highly likely explanation is the major difference between both solutions. PDMS is an elastomer with very loose and long molecule chains that are relatively far apart. This property of elastomers makes them so highly flexible, which is a key advantage of PDMS. The polyimide used in this research is from the duroplastic family and is created using a two step process which includes roughly 80% polar solvent. After spin-coating, the solvent is evaporated after which the polyimide will harden and form a dense matrix of molecular chains with multiple cross-connections between chains. This gives the final cured polyimide layer its highly stable mechanical properties. It is expected that due to the dense molecular matrix (also already before hardening), the nanotubes do not have the freedom of aligning within the matrix. In combination with the high amounts of polar solvents (which also polarise within the electric field), this could cause the inability of rotating and aligning the CNTs in the duroplastic solution.

Figures graphically indicating the difference between elastomers (PDMS) and duroplastics (Polyimide) are shown in Figure IV.21. This explanation would also confirm the reason why the CNTs align very quickly within the DI-water, as the viscosity is very low and the CNTs are not hindered by dens molecular chains.

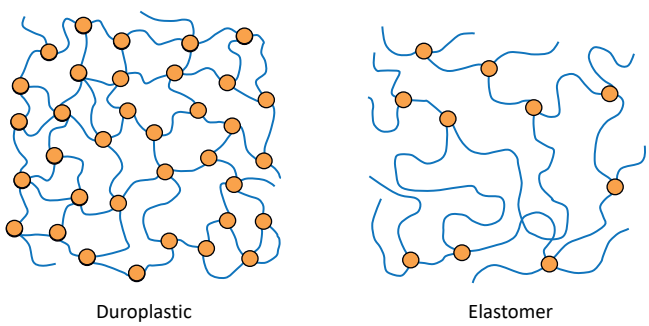

Figure IV.21: Schematic representation of polymer chains for duroplastics and elastomers.

The gas permeability could also serve as a indication for how dense the molecular structure is. The oxygen permeability of a 1 mm thick PDMS membrane is around $3.1 - 3.4^{-4} \frac{m^2}{day}$ depending on the curing agent ratio (more curing agent gives a denser matrix and less permeability) [19]. For Polyimides the oxygen permeability is found to be around $2.5 - 10^{-9} \frac{m^2}{day}$, depending on the specific type [21].

IV.9 Experimental Sensor Results

Sensors were fabricated with four different CNT concentrations (0.04, 0.08, 0.17, and 0.33 wt%) to investigate their influence on sensor quality. Typically, concentrations below 0.2 wt% were considered to be non-conductive. Therefore, any measured conductivity change was attributed to the alignment process.

The glass wafers (featuring the isolated gold alignment electrodes) were placed on the spin-coater and a 65 μm thick CNT-PDMS layer was deposited. The wafer was placed on an upside-down petri-dish where both electrodes were connected to the Labsmith HV3000 high voltage generator, which was set to 480kV/m at 1Hz. The alignment time was set to 60 minutes, after which te electric field was turned off and the PDMS layer was slowly cured at 90°C for 45 minutes. The alignment setup is shown in Figure IV.19b.

Depending on the added CNT concentration, the layers were optically transparent (<0.2 wt%), or almost black coloured (0.33 wt%), as shown in Figure IV.22. On the right side of the figure, the bottom horizontal alignment electrodes are still visible. On top, the vertical strain sensor with its large connections is shown.

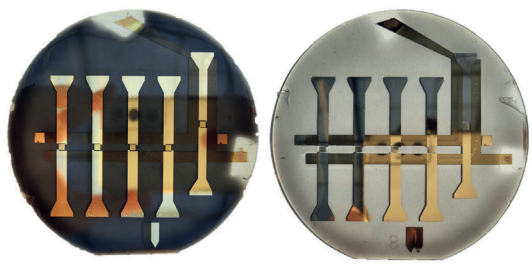

Figure IV.22: Strain sensors on the wafer. Different CNT concentrations cause changes in transparency (left 0.33 wt%, right 0.08 wt%)..

The alignment was inspected via an optical light microscope. The results immediately before and after alignment are shown in Figure IV.23a. The carbon nanotubes are randomly oriented before the alignment. After 5 minutes, clear first alignment of the CNTs is detected, with stronger pathways after 60 minutes. Multiple sensors were manufactured on a single wafer. Half of the sensors were aligned in the horizontal direction, the other half in the vertical direction, as shown in Figure IV.23a. This figure also shows

that after 60 alignment minutes, still no movement was visible outside the alignment area (top right image). With help of the scanning electron microscope, the alignment of the CNTs was confirmed inside the material by looking with a parallel view, or directly from the front, as shown in Figure IV.23b. Only a few carbon nanotubes are visible due to the very low concentrations of carbon nanotubes.

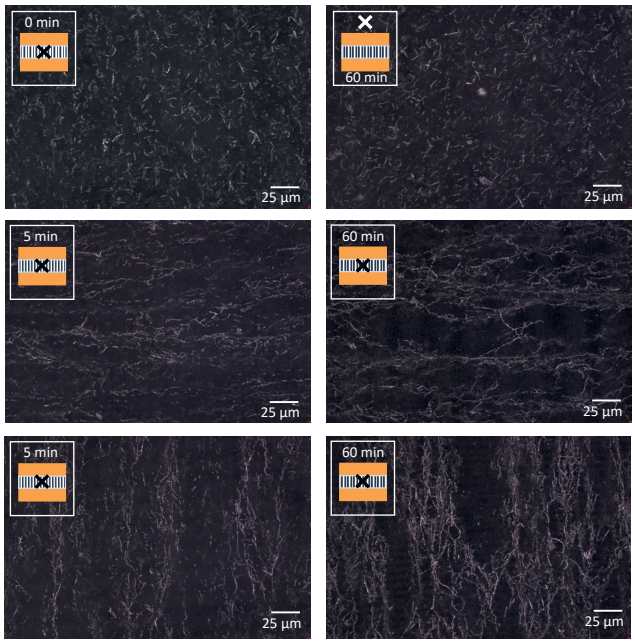

(a) Optical results of CNT alignment in PDMS. The insets indicate location of picture. More agglomerated conductive networks form after 60 minutes.

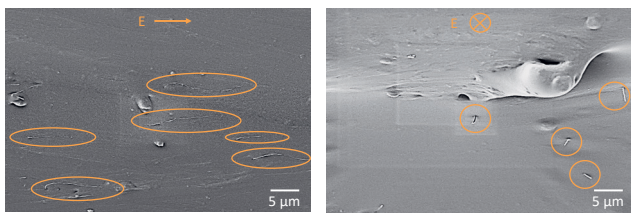

(b) Scanning electron microscope view of aligned CNTs, viewed from both directions. The left picture shows a parallel view to the alignment direction, as the right image shows a frontal view of the aligned nanotubes.

Figure IV.23: Microscopic results depicting the carbon nanotube alignment in the cured PDMS layer.

The unidirectional behaviour of the sensor was investigated by creating two different IDE-design structures on top of the sensing layer. The sensor is based on the fact that with applying strain, the distance between the conductive particles increases and the conductivity decreases. Ideally, with the aligned CNTs, the sensitivity is increased in the preferred direction, and remains unchanged in all others. This is explained more clearly in Figure IV.24b. The carbon nanotubes in the left part are aligned in the same direction as the inter-digital electrodes. If strain is applied in the vertical direction, the CNTs are pulled apart but the conductivity difference of both parts of the IDE is not greatly affected. If the IDEs are rotated 90 degrees and the aligned CNTs cross both IDEs and connect them together, the resistance change should be increased.

IV.9.1 Base Resistance Change

The base resistance of all samples was measured and plotted in Figure IV.24a. The sensors with the parallel IDE orientation featured a far greater base resistance than its counterpart. This is expected as it was thought the parallel IDE orientation has less connections between them via the aligned CNTs. With increasing wt% in the piezoresistive layer, a decrease in base resistance was measured. Without any carbon nanotube alignment, the solution showed a resistance of $>1G\Omega$.

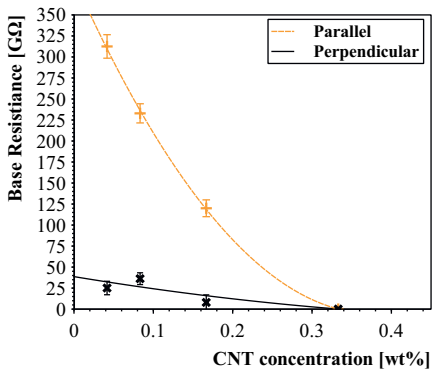

(a) Initial resistance of strain sensors. The perpendicular IDE structures yield more connections, as suspected, and show greatly lower resistances as the parallel counterpart. Higher CNT wt% result in lower sensor resistances, as expected.

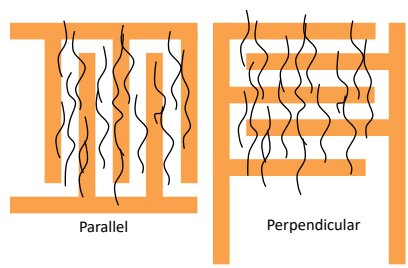

(b) Sensor design with two IDE orientations. The perpendicularly rotated IDE structure to the alignment direction causes more CNT pathways connections and is expected to be more sensitive to strain than the parallel setup.

Figure IV.24: Base resistances of sensors with different nanotube concentrations (left) and view of the inter-digital electrode setup (right).

IV.9.2 Alignment Quantification

The alignment was also investigated via determining the average color intensities in the horizontal and vertical direction. This process converted the taken microscopic images to grey-scale images and determined average intensity for each orientation. For ideal vertically aligned CNTs, a repeated pattern should occur with low and high intensities when scanning the image horizontally. Scanning the image in parallel to the aligned CNTs, should not emphasise any repeatable pattern. Exactly this observation was realised and is shown in DI-water (Figure IV.25) and in PDMS (Figure IV.26).

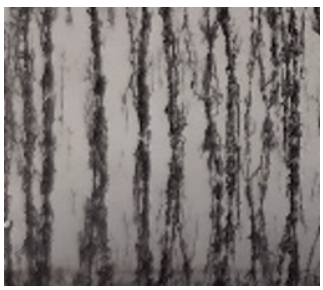

(a) Alignment of CNTs in DI-water.

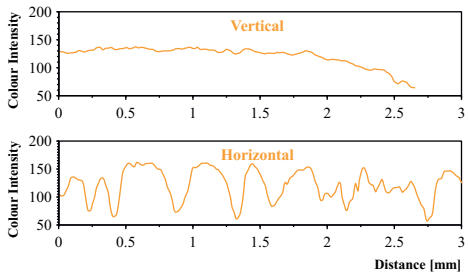

(b) Colour intensity result for both directions.

Figure IV.25: Alignment quantification in water.

(a) After 60 min of alignment.

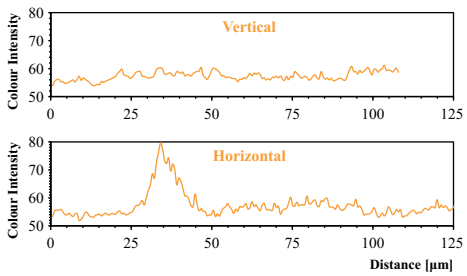

(b) Colour intensity result for both directions.

Figure IV.26: Alignment quantification in PDMS sensors.

IV.9.3 Two-phase Piezoresistive Response

The carbon nanotube aligned piezoresistive strain sensors exhibited, similar to the analytical simulations, a two-phase response. For the first small strain range, the electron-tunneling effect appears not to be the dominant factor and is combined with the regular piezoresistive effect. It is theorised that a large part of the CNT-CNT connections stay connected and only shift, resulting in linear resistance changes. After a certain threshold has been reached, electron tunneling occurs due to the increased change of disconnecting CNT-CNTs, drastically increasing the response of the sensors up until a point where no conductive paths are present anymore.

Results of all sensors clearly indicate a great sensitivity change within the measured strain regions (up to 0.7%). Results, with an inter-digital electrode distance of 200 μm, are shown in Figures IV.27 and IV.28a. Large differences in sensor responses are present for both measured directions. The unidirectional sensitivity of the sensors is proven when looking at the responses for both the parallel and perpendicular directions. Small sensor responses in the parallel direction are caused by the cross-connections in the aligned pathways.

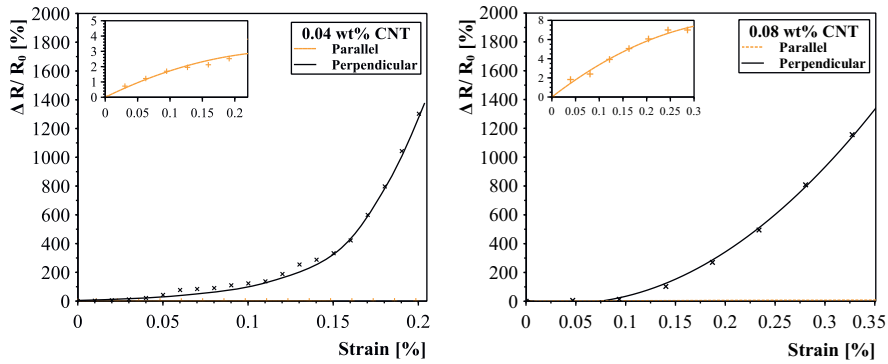

(a) Results for 0.04 CNT wt% sensors.

(b) Results for 0.08 CNT wt% sensors.

Figure IV.27: Strain results for different carbon nanotube concentrations with inter-digital electrode distance of 200μm. A clear distinction in sensitivity is present between the parallel and perpendicular IDE orientation.

Additionally, the effect of inter-digital electrode spacing is shown in Figure IV.28b, confirming analytical calculations that shorter distances yield less sensitive sensors. The maximum found k-factor for the linear region was found to be 60 (in contrast to 550) and saturating at almost 300% resistance change (instead of 1600% for the 200μm inter-digital electrode spacing sensors). However, results do show a more smoother response and far greater sensitive region than the 200 μm IDE-spaced sensors (1% to 0.25% strain).

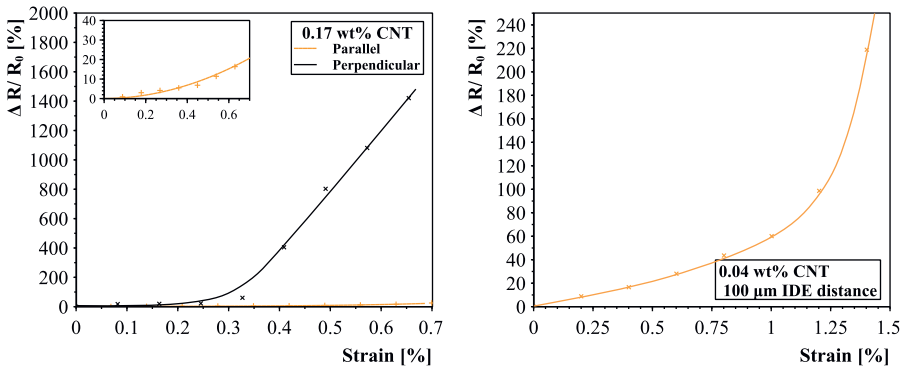

(a) Results for 0.17 CNT wt% sensors.

(b) Sensor response with smaller IDE distance.

Figure IV.28: 0.17% sensor result with 200 and 100 μm inter-digital electrode distance.

It is found that the concentration of carbon nanotubes does not play a major role in the maximum achievable resistance change. All nanotube concentration sensors saturated around a resistance change of 1600%. This is mainly caused due to the fact that all aligned sensors featured a starting resistance in the same order of magnitude, and the upper limit was set by the maximum measurable resistance of the high precision multimeter (<1TΩ). Results did show however, that higher concentrations yield longer linear regions, as can be seen for the 0.17wt% (up to 0.3% strain, see Figure IV.29). It is thought that with higher concentrations, thicker and more bundled networks are created, needing more applied tensile strain to reach the second 'electron tunneling' phase.

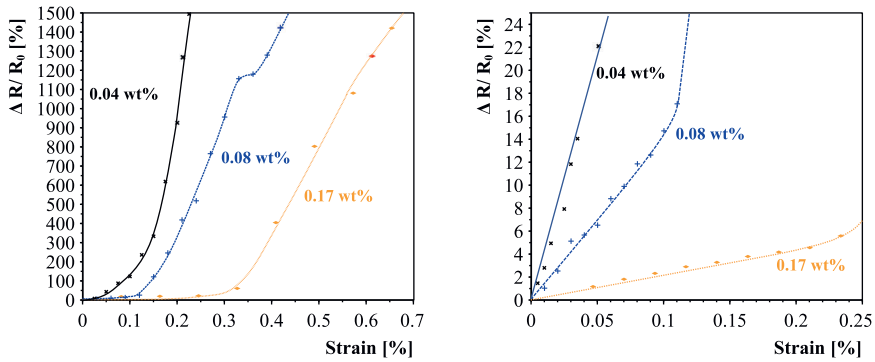

(a) Complete sensor response overview for different nanotube concentrations.

(b) Zoom-in of the initial first phase piezoresistive responses.

Figure IV.29: Sensor responses for different carbon nanotube concentrations.

Results in this study give very high Gauge factors, which correspond to the theoretical and analytical findings of creating a piezoresistive polymer based on tunneling electrons that hop between individual carbon nanotubes. The large initial resistances of the sensors is attributed to the fact that due to the alignment of CNTs and the very low percentages of added nanotubes, only a few very thin (<10um) and long (200μm) connections are created. This in combination with possible CNT-CNT connections via electron tunneling gives rise to the high resistances.

The effect on large clusters within the layer is apparent when looking at the results for the aligned carbon nanotube sensor with a concentration of 0.33 wt%. This viscosity of the CNT-PDMS solution was already so much thicker that the spin-coated layers thickened greatly, as is shown in Figure IV.30a. The responses of the sensors show large jumps in resistivity change, as is depicted in Figure IV.30b. All tested sensors for this concentration showed these sudden increases. It is therefore thought, in combination with the large clusters due to the high CNT-concentration, that the cause is due to sudden disconnects between clusters. A suspicion is that the large clusters are connected via regular individually aligned CNT networks that get suddenly broken off due to the applied strain, causing sharp increases in measured resistance. Similar effects, yet far less pronounced, can be seen looking at the 0.08 wt% line in Figure IV.29a. This effect acknowledges once again the necessity for perfect dispersion of carbon nanotubes in order to create as much as possible continuous and smooth sensor responses.

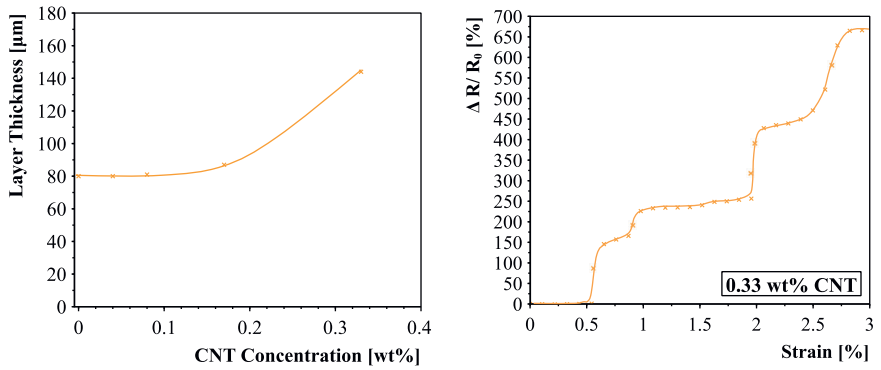

(a) Sensor layer thickness in relation to CNT content.

(b) Response for aligned 0.33% CNT sensor.

Figure IV.30: Nanotube concentration influence on layer thickness and on sensor reponse.

The depth location of the carbon nanotube networks in the layers was investigated by scanning through the transparent sensing layer and taking pictures at several height intervals. It became apparent that, although the layers are very thin, the carbon nanotubes are slightly pulled down toward the bottom electrodes (where the field strength is the strongest). Figure IV.31 presents the results of the microscopic images at several height intervals, clearly showing most CNTs are at the bottom layers. This is not the case everywhere but a general tendency is visible. There are less pathways at the top of the layer.

Due to the non-ideal alignment behaviour of the regular multi-walled carbon nanotubes, high sensitivities (compared to regular metallic Gauge factors) are measured in both directions. Nevertheless, the difference between both orientations is great, and a preferential direction is clearly detected. It is assumed that the cross-connections form additional (electron tunneling) connections perpendicular to the alignment, causing the sensitivity in this direction.

IV.9.4 Piezoresistive Tunneling Effects

Both the numerical results as the sensor results show an exponential relation between the applied strain and resistance change and show that very high Gauge factors are possible due to electron tunneling. A bias voltage sweep is applied to the sensors to confirm the sensors do indeed experience electron tunneling. A 15kΩ resistor is taken as a reference. The results of the non-linearity of the sensors, indicating a non-linear resistance due to tunneling effects, is shown in Figure IV.32.

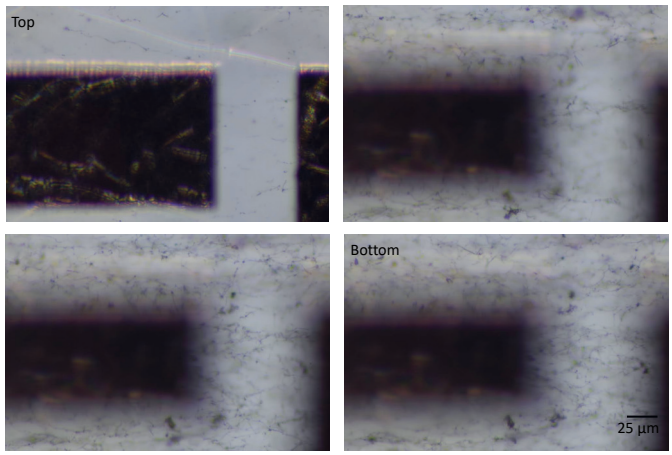

Figure IV.31: Location of the aligned carbon nanotubes in the piezoresistive layer. Observations show the CNTs are pulled down toward their alignment electrodes and away from the surface where the gold sensor electrodes are sputtered.

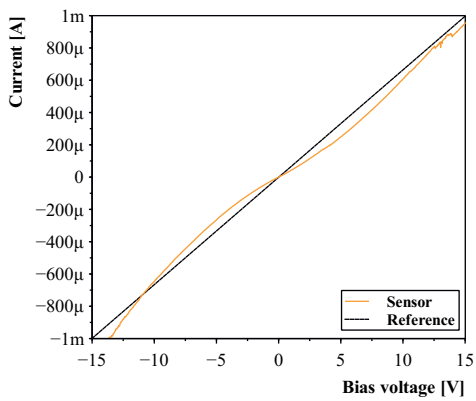

Figure IV.32: Non-linear sensor behaviour indicating the presence of electron tunneling connections in the carbon nanotube - polymer sensor layer.

The dynamic stability and repeatability of the strain sensors was investigated by exposing the sensors to a repeated strain of 0.7% for up to 100 cycles (Figure IV.33). Responses show a slight upward drift until it appears to stabilise and show a highly stable dynamic response.

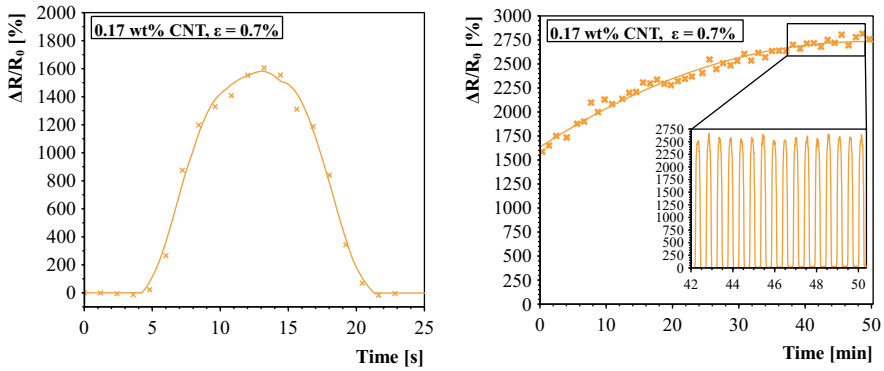

(a) Individual strain cycle. The sensors show similar responses for tensile strain phase and relaxing of the sensor.

(b) Cyclic strain response. An initial small drift upwards is visible, after the sensor stabilises.

Figure IV.33: Aligned sensor response to (repeated) strain exposure.

IV

IV.9.5 Effect of Functionalised Carbon Nanotubes

The effect on the dispersion and alignment quality of functional groups attached to the carbon nanotubes was investigated. Oxidised carbon nanotubes with a length of 5-12 μm were utilised in this research. Literature suggests that the -OH and -COOH functional groups result in a repulsive interaction between the aligning CNTs and yield better aligned connections. The functional groups cause an increase amount of charge on the multi-walled carbon nanotubes, which in turn increases their dipole moment [13].

Three different concentrations of carbon nanotubes (0.05, 0.1 and 0.02 wt%) were dispersed in PDMS via the mechanical mixing method and spin-coated on the glass wafers featuring the gold alignment electrodes. The mixing of the nanotubes in the polymer was kept brief (5min), as previous results showed worsening agglomerations with increasing time. The mixture was aligned with the identical parameters as with the regular nanotubes: with an indirect electric field of 480kV/m for 60 minutes. The alignment results for the oxidised nanotubes are presented in Figure IV.34 and compared with regular carbon nanotubes.

The alignment differences between both types of carbon nanotubes couldn't be more clear. Immediate observations show clear and thin conductive paths versus more agglomerated aligned connections. As literature suggested, the functionalised carbon nanotubes form more clean connective paths with a highly repetitive distance interval. It seems there are individually (not connected) aligned CNTs throughout the whole thickness of the layer, with the exception of well-defined connected pathways. The corresponding alignment quantification (detection of horizontal and vertical pathways) is shown in Figure IV.36. Comparing the results to the regular nanotubes aligned in PDMS, shown in Figure IV.26, a much clearer quantification is found.

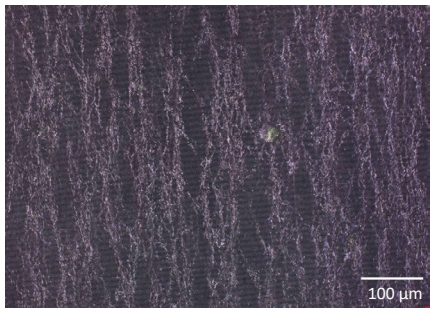

(a) Regular nanotubes.

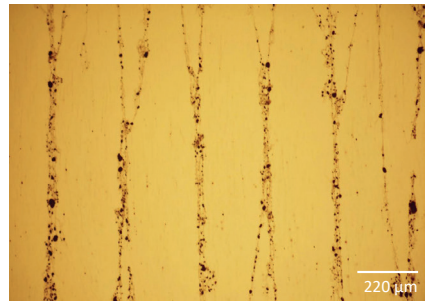

(b) Oxidised nanotubes.

Figure IV.34: Comparing alignment of regular and oxidised carbon nanotubes (0.2 wt%). Please mind the different scale-bar.

Secondly, it seems that the distance between conductive paths depends on the added concentration of carbon nanotubes. Looking at two microscopic pictures shown in Figure IV.35, a clear difference in horizontal path interval is observed, which is confirmed by looking at Figures IV.36 and IV.37. The peaks in the figure indicates a conductive path. Clearly, more peaks are present (although of lower intensity) for the lower concentration of carbon nanotubes. A possible explanation regarding the difference in pathway interval distance could be due to the fact that the thicker the CNT pathways get, the stronger the electric fields and their attractive force are. This would mean that by prolonged alignment, smaller pathways merge into thicker pathways. A possible confirmation is shown by the optical microscope images, showing thicker nanotube pathways with higher concentrations (Figure IV.35).

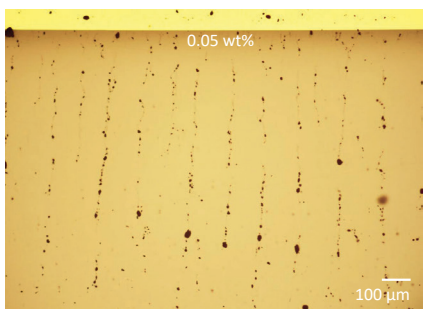

(a) 0.05 wt%.

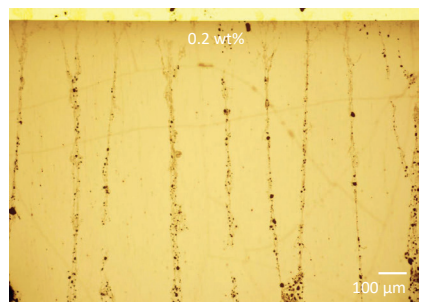

(b) 0.2 wt%.

Figure IV.35: Possible conductive path interval dependency on nanotube concentration.

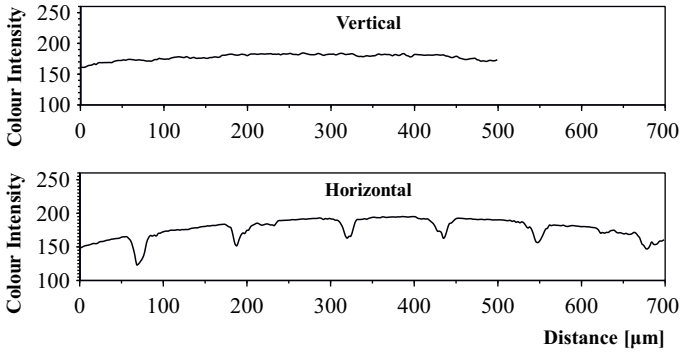

Figure IV.36: Alignment quantification of oxidised nanotubes in PDMS. No paths are found when scanning vertically through the images. Scanning through the image horizontally, yields repeatable peaks indicating CNT pathways.

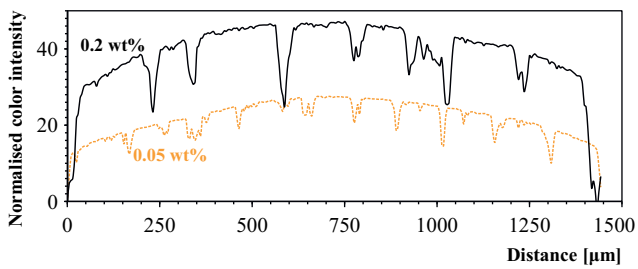

Figure IV.37: Alignment quantification of two different concentrations of oxidised CNT in PDMS.

Thirdly, the behaviour of the growing CNT network was observed when looking at the alignment process at different time intervals. First, the individual CNTs align in the direction of the electric field. Hereafter, the first CNTs connect at the edges of electrodes, after which they slowly grow toward the middle until they connect. It was found that the nanotubes align at the edges in a more orderly fashion then in the middle. The lateral cross-connections between conductive paths increase further away from the electrodes. This is clearly presented in Figure IV.38 , which presents the alignment after 5 and 60 minutes (0.2 wt% CNT). After 5 minutes of alignment, a preferential direction is visible, with at the edges already first formed CNT-pathways. After 60 minutes this has increased to fully grown pathways with visible cross-connections in the middle area. Additionally, it is shown that the CNTs follow the electric field due to the curvature in the electrodes. The distance at the corner is still not fully connected after 60 minutes. Alignment of individual nanotubes is visible, but pathways are not yet fully formed.

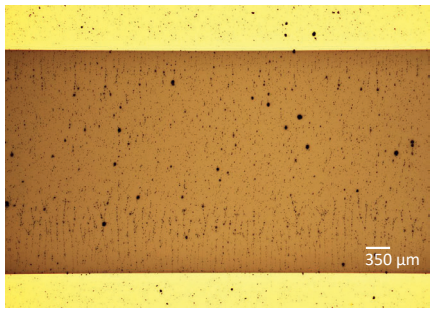

(a) 5 minutes alignment.

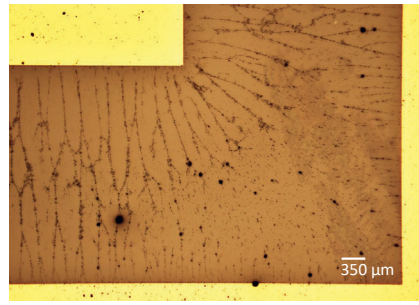

(b) 60 minutes alignment.

Figure IV.38: Growing nanotube pathways for different alignment times.

Additionally, it seems that the lower concentrations need more time to align, as is clearly visible when looking back at Figure IV.35. It is assumed that the alignment process increases with the formation of thicker pathways. With an initial increase of nanotubes, the alignment process has an initial boost and creates faster pathways. Looking at Figure IV.39, it can be seen that the 0.05 wt% concentration has very thin connections. Most pathways have not yet reached the full distance (FigureIV.39b). With the higher concentration mixture, more fully grown pathways are visible.

The final observation would be the increased amount of clusters within the CNT-polymer mixture. This was already found and presented in Chapter II.4.4, where it was stated that the agglomerations were much larger for the functionalised nanotubes. Increasing the mixing time only seems to worsen the dispersion. It seems that the dispersion of the functionalised carbon nanotubes was already very great, and mixing causes additional agglomerations. It is assumed that the curled nanotubes knot/bundle together during mixing, forming clusters.

The large clusters are very noticeable on all Figures in the section. A keen observation is the fact that it looks like the nanotube pathways follow the clusters, as can be seen especially well in Figure IV.39. It is thought that the large clusters experience large polarisation and are beacons of local electric fields. Due to the low aspect ratio's they probably only rotate and migrate slowly but attract other nanotubes from further away. Isolated clusters with no attached nanotubes were not detected. All clusters were aligned in a straight line with attached isolated carbon nanotubes connecting them together. This principle is also shown in the numerical COMSOL simulation in Figure IV.40. The more powerful large clusters create a stronger electric field that is engulfing the small nanotube. Therefore, it is expected that individual nanotubes align to the large clusters, and subsequently, the clusters align in straight lines as well.

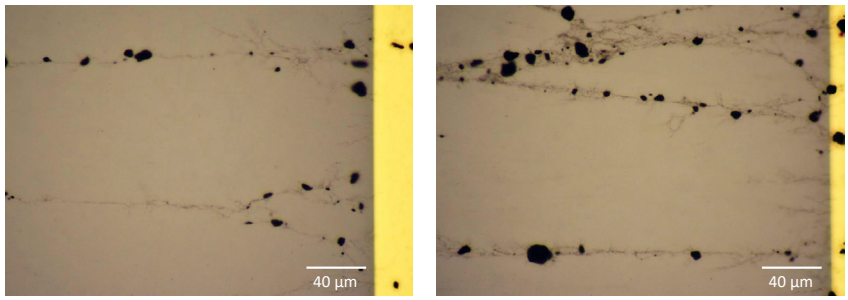

(a) 0.05 wt% vs. 0.2 wt%

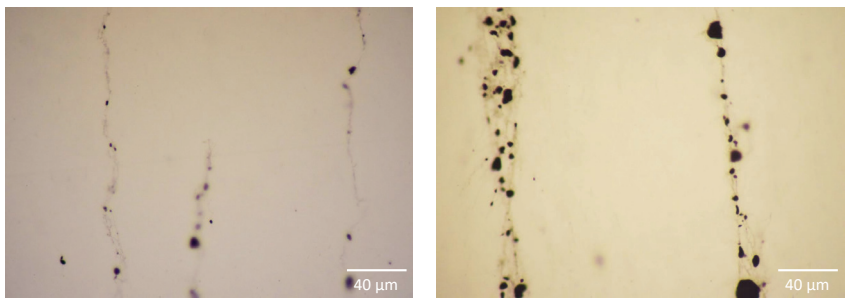

(b) 0.05 wt% vs. 0.2 wt%

Figure IV.39: Individual carbon nanotube pathways after 60 alignment minutes.

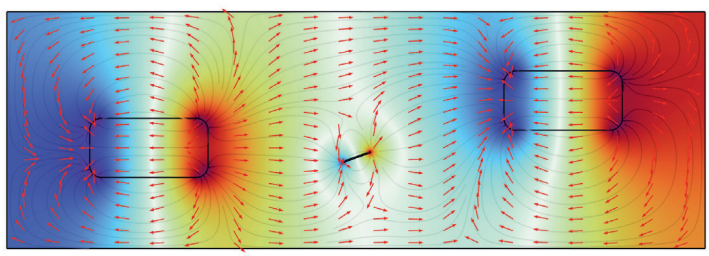

Figure IV.40: Influence on a single carbon nanotube by two large clusters. The red color indicates a positive charge, the blue indicates a negative charge. The arrows show the direction of the electric field.

As can be seen in all the figures above, the alignment of the functionalised nanotubes is drastically different. More ideal conductive paths are formed with less cross-connections at the electrode sides. Just as with the regular nanotubes, there are more cross-connections in the middle. It is thought that this is due to the fact that how further away from the electrodes, the impurer the homogeneity of the field gets due to the already formed nanotube pathways. However, the pathways that are formed, show thick bundled and attached carbon nanotube networks reaching form cluster to cluster. This is also confirmed when looking at the strain results IV.41, that in contrast to their aligned regular nanotube counterparts, do not show very large (exponential) changes in resistivity. The found Gauge factors for the 0.17 CNT wt% sensors were 10 and 80 ($\epsilon = 2$), for respectively the parallel and perpendicular direction. The sensors showed a linear response to strain up to 2%, which is greatly increased when comparing to the smaller (up to 0.5) strain regions for the regular aligned nanotube sensors. When looking more closely to results, it can be seen that the overall trend of the sensors is linear, but small jumps are present in the line. It is expected that this occurs due to sudden loss of conductive networks, therefore jumping the resistance upwards. Once again, the still present ability to detect strain in the parallel direction is attributed due to the cross-connections between conductive paths.

A voltage-bias sweep was performed because the sensor behaviour did not show any of the tunneling traits that were found with the regular carbon nanotube sensors (Figure IV.42. Immediate results showed no non-linearity in the current behaviour with sweeping voltages, indicating no change in resistance due to electron hopping. It is expected that the improved alignment quality, combined with the dense formation of conductive paths, is able to form proper electrical connections. The effect that while sweeping the voltage from -10 to 10V a current is measured at 0V is attributed due to possible charging or capacitive effects in the sensor.

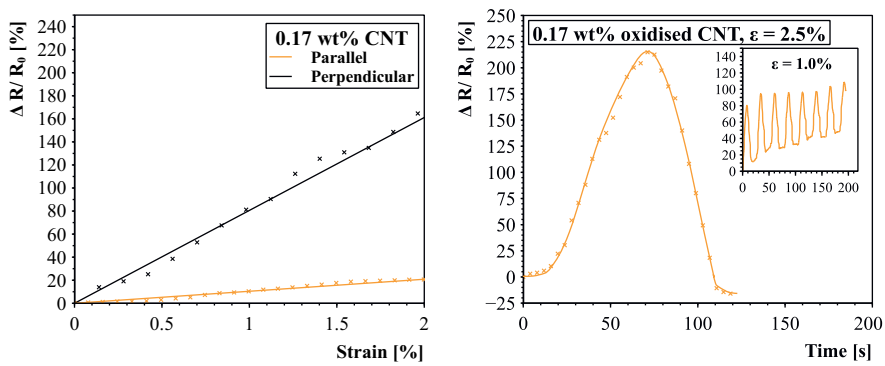

(a) Response in parallel and perpendicular direction. (b) Single and cyclic response.

Figure IV.41: Sensor responses with aligned functionalised nanotubes.

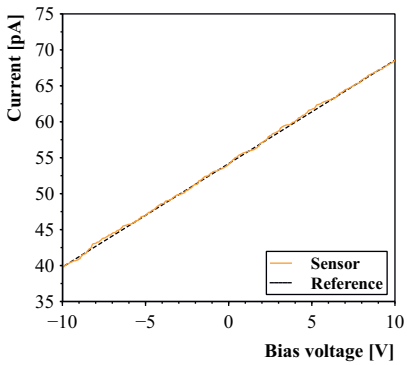

Figure IV.42: Linear voltage-current behaviour for oxidised nanotube-based sensors.

IV.10 Conclusion

This research presents a carbon nanotube based strain sensors that features a preferential direction due to the aligned conductive pathways. The unidirectional property was confirmed by characterising the sensors with two oriented inter-digital electrodes on top of the sensing layers, as well as optical and scanning electron microscope images. The inter-digital structures that were perpendicularly aligned to the alignment direction featured Gauge factors up to k ≈ 4500 (depending on nanotube concentration). The inter-digital electrodes featuring a parallel orientation to the alignment direction were found to have a Gauge factor of around ≈ 22. The sensors featured a two-phase piezoresistive response. Initially, the sensors showed a linear response region, after which the electron tunneling effect becomes more dominant, resulting in a high gauge factor response. This is summarised in Figure IV.43. The sensors show a decrease in sensitivity with increasing carbon nanotube concentration. This effect is similar as with randomly aligned carbon nanotube sensors [10] [11] [14]. The reasoning behind this effect is that increasing the nanotube contents lead to more agglomerations and lowers the sensitivity [10].

The base resistance of the aligned sensors also showed a clear distinction in conductivity between the parallel and perpendicular IDE structures, indicating a change in the CNT-orientation network.

Additionally, the behaviour of the rotating carbon nanotubes and the expected piezoresistive effect was analytically and numerically modelled and confirmed later by experimental results. The analytical model shows an inverse relation between number of nanotube connections and sensitivity, which was proven to be identical for the fabricated sensors in this research. The numerical simulation showed the order of magnitude necessary for rotation of carbon nanotubes due to the presence of an electric field. The reasoning for the effect of turbulent alignment with the direct current alignment method is also shown

in the numerical model and experimental results.

The alignment of carbon nanotubes is greatly influenced by the field strength, frequency and time. An alternating field stops the nanotubes from migrating toward an electrode and longer time creates thicker agglomerated nanotube bundles. However, due to the cross-connections between the conductive pathways, an absolutely unidirectional sensitive sensor is not possible yet. Future research will investigate the possibility to align functionalised carbon nanotubes to enhance the alignment and improve the unidirectional sensor properties.The functional groups at the nanotubes causes a repulsive interaction between the aligning CNTs, increasing the alignment quality and minimising the cross-sensitivity. Another advantage is the fact that the functional groups increase the charge in the carbon nanotubes, increasing their dipole moment [13].

Additionally, first results showed an increase in the sensors sensitive region by decreasing the inter-digital electrode distances. Future research could utilise this property to create CNT-aligned sensors with far greater (linear) sensitive regions.

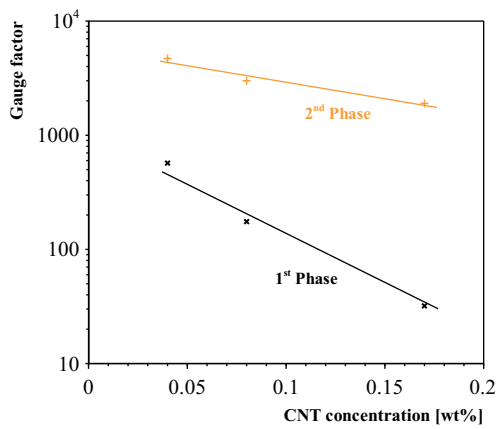

Figure IV.43: Determined Gauge factors divided into the two piezoresistive phases for different carbon nanotube weight percentages (0.04 - 0.17).

References

[1] Hiroshi Ajiki and Tsuneya Ando. "Magnetic properties of carbon nanotubes". In: Journal of the Physical Society of Japan 62.7 (1993), pp. 2470–2480.

[2] Imtisal Akhtar and Seung-Hwan Chang. "Highly aligned carbon nanotubes and their sensor applications". In: Nanoscale 12.41 (2020), pp. 21447–21458.

[3] Alamusi et al. "Piezoresistive strain sensors made from carbon nanotubes based polymer nanocomposites". In: Sensors 11.11 (2011), pp. 10691–10723.

[4] Maxime Arguin, Frédéric Sirois, and Daniel Therriault. "Electric field induced alignment of multiwalled carbon nanotubes in polymers and multiscale composites". In: Advanced Manufacturing: Polymer & Composites Science 1.1 (2015), pp. 16–25.

[5] Francis Aviles et al. "Influence of carbon nanotube on the piezoresistive behavior of multiwall carbon nanotube/polymer composites". In: Journal of Intelligent Material Systems and Structures 27.1 (2016), pp. 92–103.

[6] Marco Cen-Puc et al. "Carbon Nanotubes/Polymer Films for Microsensors Applications". In: 2021 IEEE Sensors. IEEE. 2021, pp. 1–4.

[7] Yuli Chen et al. "Theoretical estimation on the percolation threshold for polymer matrix composites with hybrid fillers". In: Composite structures 124 (2015), pp. 292–299.

[8] Gabriella Faiella. "Process tuning of physical properties of carbon nanotubes polymer composites". PhD thesis. Università degli Studi di Napoli Federico II, 2009.

[9] Dorian Hanaor et al. "Anodic aqueous electrophoretic deposition of titanium dioxide using carboxylic acids as dispersing agents". In: Journal of the European Ceramic Society 31.6 (2011), pp. 1041–1047.

[10] Yin He et al. "Highly stable and flexible pressure sensors with modified multiwalled carbon nanotube/polymer composites for human monitoring". In: Sensors 18.5 (2018), p. 1338.

[11] Ning Hu et al. "Investigation on sensitivity of a polymer/carbon nanotube composite strain sensor". In: Carbon 48.3 (2010), pp. 680–687.

[12] BK Jang and Y Sakka. "Influence of shape and size on the alignment of multiwall carbon nanotubes under magnetic fields". In: Materials Letters 63.29 (2009), pp. 2545–2547.

[13] Prashant V Kamat et al. "Self-assembled linear bundles of single wall carbon nanotubes and their alignment and deposition as a film in a dc field". In: Journal of the American Chemical Society 126.34 (2004), pp. 10757–10762.

[14] Inpil Kang et al. "A carbon nanotube strain sensor for structural health monitoring". In: Smart materials and structures 15.3 (2006), p. 737.

[15] Il Tae Kim, Allen Tannenbaum, and Rina Tannenbaum. "Anisotropic conductivity of magnetic carbon nanotubes embedded in epoxy matrices". In: Carbon 49.1 (2011), pp. 54–61.

[16] Tohru Kimura et al. "Polymer composites of carbon nanotubes aligned by a magnetic field". In: Advanced materials 14.19 (2002), pp. 1380–1383.

[17] Hans J.. Lyklema et al. Fundamentals of Interface and Colloid Science: Solid-liquid Interfaces. Academic Press., 1995, pp. 1–59.

[18] Chen Ma et al. "Alignment and dispersion of functionalized carbon nanotubes in polymer composites induced by an electric field". In: Carbon 46.4 (2008), pp. 706–710.

[19] Dmitry A Markov et al. "Variation in diffusion of gases through PDMS due to plasma surface treatment and storage conditions". In: Biomedical microdevices 16 (2014), pp. 91–96.

[20] CA Martin et al. "Electric field-induced aligned multi-wall carbon nanotube networks in epoxy composites". In: Polymer 46.3 (2005), pp. 877–886.

[21] Laurence W McKeen. Film properties of plastics and elastomers. William Andrew, 2017, p. 163.

[22] AI Oliva-Avilés et al. "Dynamics of carbon nanotube alignment by electric fields". In: Nanotechnology 23.46 (2012), p. 465710.

[23] Jae-Won Seo and Ueon Sang Shin. "Preparation of positively and negatively charged carbon nanotube-collagen hydrogels with pH sensitive characteristic". In: Journal of the Korean Chemical Society 60.3 (2016), pp. 187–193.

[24] Donglu Shi et al. "Magnetic alignment of Ni/Co-coated carbon nanotubes in polystyrene composites". In: Composites Part B: Engineering 42.6 (2011), pp. 1532–1538.

[25] Mostafa Shooshtari, Alireza Salehi, and Sten Vollebregt. "Effect of humidity on gas sensing performance of carbon nanotube gas sensors operated at room temperature". In: IEEE Sensors Journal 21.5 (2020), pp. 5763–5770.

[26] John G Simmons. "Generalized formula for the electric tunnel effect between similar electrodes separated by a thin insulating film". In: Journal of applied physics 34.6 (1963), pp. 1793–1803.

[27] Bill Steele. Cornell physicists cut carbon nanotubes and count single electrons using atomic force microscope. 2001. URL: `https://news.cornell.edu/stories/2001/08/counting-single-electrons-carbon-nanotube` (visited on 08/26/2001).

[28] Chao Sui et al. "Directional sensing based on flexible aligned carbon nanotube film nanocomposites". In: Nanoscale 10.31 (2018), pp. 14938–14946.

[29] Luigi Vertuccio et al. "Piezoresistive properties of resin reinforced with carbon nanotubes for health-monitoring of aircraft primary structures". In: Composites Part B: Engineering 107 (2016), pp. 192–202.

[30] Zhixin Wang, Alex A Volinsky, and Nathan D Gallant. "Crosslinking effect on polydimethylsiloxane elastic modulus measured by custom-built compression instrument". In: Journal of Applied Polymer Science 131.22 (2014).

[31] Takeo Yamada et al. "A stretchable carbon nanotube strain sensor for human-motion detection". In: Nature nanotechnology 6.5 (2011), pp. 296–301.

[32] Gang Yin et al. "A carbon nanotube/polymer strain sensor with linear and anti-symmetric piezoresistivity". In: Journal of composite materials 45.12 (2011), pp. 1315–1323.

[33] Kum-Pyo Yoo et al. "Novel resistive-type humidity sensor based on multiwall carbon nanotube/polyimide composite films". In: Sensors and Actuators B: Chemical 145.1 (2010), pp. 120–125.

[34] Min-Feng Yu et al. "Strength and breaking mechanism of multiwalled carbon nanotubes under tensile load". In: Science 287.5453 (2000), pp. 637–640.

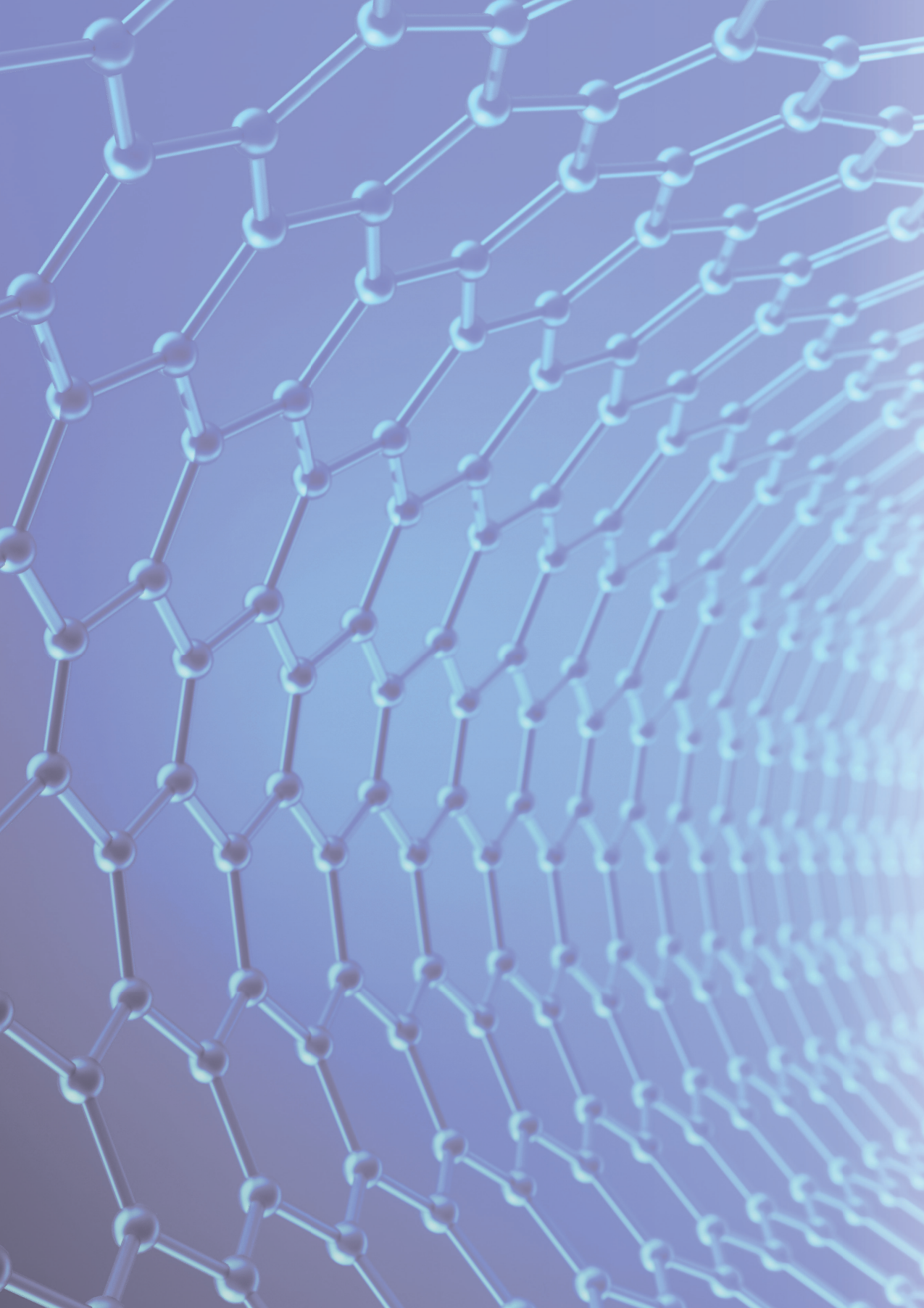

CHAPTER V

Sensor Integration in Rubber Sealings

The contents of this chapter have been submitted to
de Rijk, T. M., Cen-Puc, M., Mirzaei, Y., Schneider, P., Giese, U., & Lang,
W. (2023). Integrated Flexible Polyimide Sensors for Monitoring Compressive Force
in Sealings. In IEEE Sensors Journal Vol 23., No 20., October 2023.

Abstract

This Chapter represents a study on the integration of pressure sensors into rubber sealings. The sensors were used to continuously measure the applied pressure and monitor the sealing's condition. The sensors are made using a single layer of a Polyimide-based piezoresistive material with gold inter-digital electrodes. The working principle is the material conductivity change due to the rearrangement of conductive carbon nanotubes within the polymer caused by the applied pressure. The sensors were integrated into rubber sealings during their vulcanisation process and it was found that higher pressures suggest better integration as the air between the sensors and sealing is reduced. Additionally, the study shows that the relaxation phenomena of the rubber sealing can be measured with the sensor. Overall, the integration of sensors into sealings provides a real-time condition monitoring system that can detect faults and reduce the risk of environmental damage caused by fluid leakage, damage, and corrosion.

V.1 Introduction

Sealings are present in countless machines and are perfect for preventing fluid leakage, fluid damage, corrosion and weathering. Sealings are specifically designed for each task, depending on its application. Typical examples for sealing applications are valves and pumps, piping systems, bearings and mechanical seals. The sealings often have to endure harsh environmental conditions, e.g., temperature, chemical exposure and pressure. However, due to the elastomer-based material, sealings are susceptible to ageing. For example, oxygen penetrates the surface of the rubber material and irreversibly changes the chemical structure of the material. At the same time, the sealing can dry, and under stress, crack. This cracking, can in turn increase the speed of oxidative ageing of the sealing. Currently, sealings are regularly replaced to ensure proper functioning and to prevent any damage caused by faults.

Faulty seals can not only cause mechanical but also potential environmental damages. An example is the explosion of the Deepwater Horizon oil platform in 2010, which was caused by the failure of the blowout preventer's O-ring seal. This allowed for large amounts of hydrocarbons to escape, which then ignited, causing massive amounts of oil to enter the water [5]. In the same year, a seal in an oil pipeline ruptured in Michigan, USA, polluting the environment with millions of liters of oil [14].

The sensors integration enables real-time condition monitoring of the sealing's state. Therefore, sealings can be changed only when they are faulty, and not on a preemptive schedule. This could increase the service intervals and reduce the risk of further damages due to sealing failure. The increased cost of the smart sealings is small in comparison to large environmental spills that may occur due to faulty sealings.

This research shows a flexible polymer-based sensor that is integrated in an HNBR sealing, able to detect and monitor the condition of the sealing by continuously measuring the applied pressure [4].

Flexible pressure sensors are often based on piezoresistive polymers, which changes its conductivity in response to pressure. The non-conductive polymers are filled with electric conductive particles like carbon black, graphene, or carbon nanotubes (CNTs). The advantage of the latter is the percolation threshold (transition from an isolator to conductor material), which is very low due to the CNTs high aspect ratio [15] [3]. For CNTs, the percolation can be below 0.5 vol.-%, which is considerably lower to other materials as shown in Table V.1. This represents an advantage, as the expected influence of the CNTs on the mechanical properties is minimal due to the low CNTs amount required to achieve electrically conduction. This was shown in previous work [17], stating the difference in applied strain for 2% and 4% CNT/polymer composites. Depending on the mixing techniques, type of CNTs and/or the utilisation of solvents, the percolation threshold can drop even to below 0.02 wt% [1].

Ultrasonic dispersion is a common technique for breaking up the strong agglomerated CNTs [1] [11] [13]. However, the effectivity of the ultrasonic treatment decreases with increasing viscosity. For example, when a CNT solution with DI-water and one with a Polydimethylsiloxane (PDMS) polymer are placed inside an ultrasonic bath, the differ-

Table V.1: Aspect ratio versus Percolation threshold [17] [9] [16] [21] [7] [10] [12] [8] [19] [18] [20].

Filler type	Aspect ratio	Dimensions	Percolation threshold wt%
Iron filler	1	d = 1-80μm	10-30
Carbon black	1	d = 1-80nm	5-20
Graphene platelets	1-10	d = 0.5-20 μm, t = 0.8-5nm	1-5
CNTs	100-1000	d = 10-100nm, l = 0.1 - 10μm	0.01-0.5

ences can be noticed immediately. The low viscosity water solution is highly active with the applied ultrasound and de-agglomeration of the CNTs is clearly visible. However, the high viscosity PDMS solution does not visible change.

To circumvent this problem, it is common to add high amounts of (sometimes highly toxic) solvents. [1] [6] [13]. However, complete removal of the added solvents within the polymer is difficult and takes a long time. Additionally, the solvents need to dissolve the polymer and create a low viscosity suspension in which the CNTs also disperse properly.

V.2 Materials and methods

This research is based on a Polyimide film (precursor U-Varnish-S UBE Europe GmbH) with integrated multiwalled carbon nanotubes (Sigma-Aldrich Chemie GmbH with OD = 50-90 nm, aspect ratio >100). Gold interdigital electrodes (IDEs) are sputtered directly on the single layer sensor to provide connections for sensing and measuring.

The sealings are manufactured at the German Kautschuk Institute (DIK in Hannover) and are based of a hydrogenated nitrile rubber (HNBR, type Therban 3407, Arlanxeo). This type of rubber was chosen because of its high oil-, oxidation- and temperature resistance. The recipe and its individual components are shown in Table V.2. The 'phr' quantity indicates parts per hundred rubber, where the measurements are based on a reference unit of 100 parts or rubber. The HNBR compound was prepared with an internal mixer with intermeshing rotors and a chamber volume of 5 liters (Werner & Pfleiderer GK5E) with the following parameters:

- Mixing temperature: 40 °C
- Rotor speed: 50 4pm, 30rpm
- Fill level of mixing chamber: 70%

For homogenisation of the mixture, a post-treatment was carried out on the mill (Type: Berstorff 150 * 350 RR) with a temperature of 50°C at 7.5 RPM.

Table V.2: HNBR Recipe.

Material	phr
HNBR (34% acrylonitrile, fully hydrogentated)	100
Carbon black N550	25
Di-(2-tert-butylperoxy-isopropyl) benzene (DIPP)	4.0
Triallyl isocyanurate 50 (TAIC 50)	2.0

V.2.1 Sensor Fabrication

The CNTs are mixed in the polyimide via the direct mixing method (2.0 wt%), as shown in previous work [2]. The 3D printed 45° angled mixers ensure shear forces and flow of the mixture in the glass beaker, vastly breaking up the CNT agglomerated and ensuring a homogeneous mixture. Afterwards, the mixture is spin-coated onto a single-sided polished 4-inch wafer and cured on a vacuum hotplate with a temperature of 450°C with a total duration of six hours. The gold layer is directly sputtered on top of the polyimide and structured via standard photolithography. The sensors on the wafer are isolated by a final step of dry etching through the polymer layer until the underlying silicon surface has been reached. The finished sensors were manually removed from the wafer using a scalpel and tweezers.

V.2.2 Sensor Principle

The sensor's working principle is based on a piezoresistive material with IDEs. As the sensitive layer is exposed to pressure, the conductive CNTS within the polymer rearrange, changing the material conductivity. The working principle is shown in Figure V.1. The sensors were designed with a step size mark to indicate the insertion limit for the sealing, which ensures the precise placement of the sensor in the middle of the sealing. This can be seen in Figure V.2 (indicated by the orange arrows), showing the point the sensor needs to be inserted in the sealing for perfect alignment.

The sensors are characterised using the bond tester Condor 100 (XYZTEC). This device lets the user specify the pressed distance, speed, iterations, and all with micrometer precision. The samples are placed onto a PDMS cushion, as discussed in Chapter III in more detail.

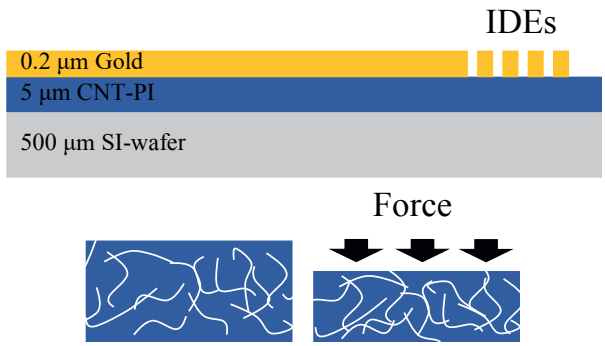

Figure V.1: Schematic side view of single layer pressure sensor (top). Graphical representation of sensor principle (bottom). With applied pressure, more connective paths are built, changing its intrinsic resistance.

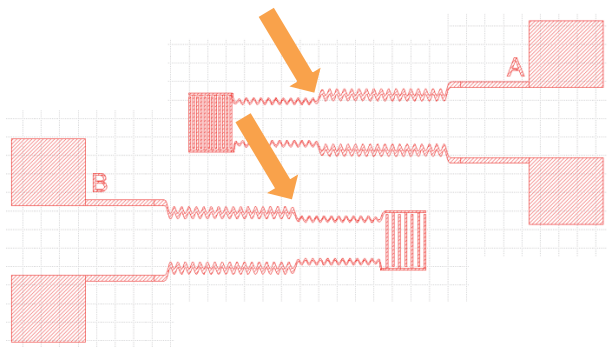

Figure V.2: Schematic layout of two different sensor designs. Blue arrows indicate the insertion depth for integration into the sealings.

V.3 Integration Results

Sensors featuring a 5 μm Polyimide layer with 2 wt% randomly dispersed CNTs were chosen for sensor integration. The fabrication and evaluation of the sensors is stated previously in Chapter III. The HNBR compound is cut in smaller pieces by hand and placed inside the aluminium mold, as shown in Figure V.3. The typical vulcanisation process is carried out at a temperature of 170 °C at 320 bar pressure. The finished sealings have an external diameter of 70 mm and a thickness of 5 mm.

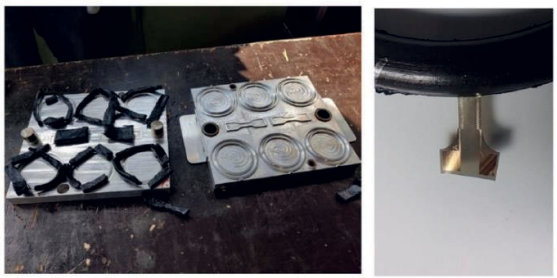

Figure V.3: Preparing the sealings and for integration. (a) HNBR pieces are placed inside the mold, just before the first vulcanisation step. (b) Final integrated sensor inside the sealing.

V.3.1 Integration Process

The rheological behaviour of the HNBR material during its vulcanisation process is shown in Figure V.4. After 5 minutes at 170 °C temperature, the rubber sealing takes the shape of the mold and is mechanically stable enough for the sensor-integration step. The preemptive incision ensures that after sensor insertion, the vulcanisation can be continued and the sensor is merged with the sealing, without any residual sealing incisions and/or damages. The integration steps are depicted graphically in Figure V.5. Additional holes in the sensor structure allow for better contact between the sensor and sealing. In this way, the rubber can flow through the holes and fully engulf the sealing, ensuring the sensor is fixed within the sealing.

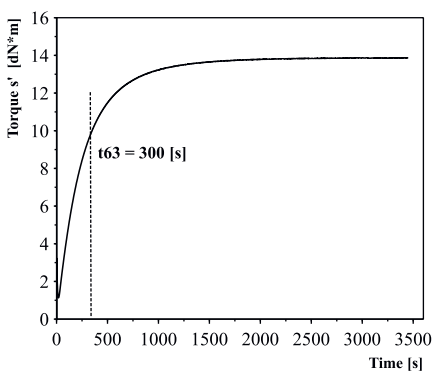

Figure V.4: Rheometer curve of HNBR sealings. The sensors were integrated at the t63 point. Data received from DIK Hannover.

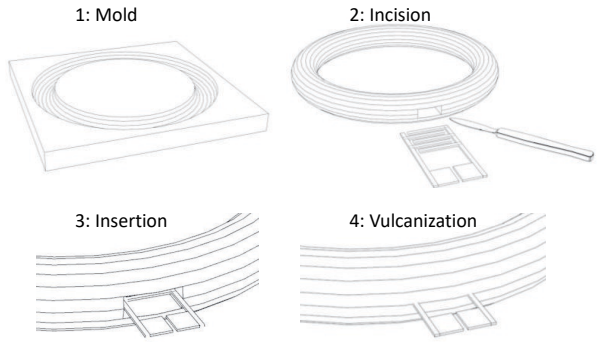

Figure V.5: Representation of the integration process. First, HNBR pieces are placed inside the aluminium mold. The HNBR is vulcanised up until the t63 point (where the sealings were mechanically stable enough for sensor insertion). The sensors were inserted and the sealing was completely vulcanised.

Multiple sealings with integrated pressure sensors were produced and the quality of integration was determined by means of Computed Tomography (CT) images. This way, high resolution 3D images could be taken from the sensors within the sealing. With this method, the precise orientation of the sensors could be visualised to determine whether the sensor was still correctly in place and not crumbled together, shifted, or bend during the second vulcanisation step (Figure V.6). Due to the different density of the sealing (rubber) and the sensor electrodes (gold), the placement of the sensor could be highlighted by filtering the image to only show the sensor. The right side of Figure V.6 shows that the sensor held properly in position at the centre of the sealing during the vulcanisation process.

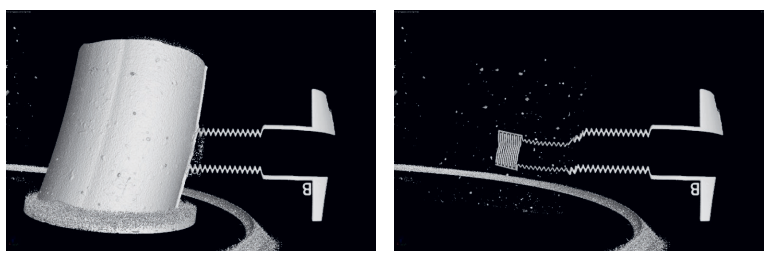

Figure V.6: Left: CT image of the flexible pressure sensor within the sealing. Right: CT image showing the placement of the integrated pressure sensor within a sealing. Due to the gold and rubber density differences, the rubber sealing could be filtered out, showing the exact placement of the sensor (right). The CT images were taken by DIK Hannover.

V.3.2 Vulcanisation Pressure Influence

The vulcanisation pressure was varied between 20 and 320 bar to investigate and ensure the sensors survived the high pressures. Simultaneously, the influence of vulcanisation pressure to sensor placement was determined. The sensors showed no significant changes of electrical resistance after integration, indicating the sensors survive the high vulcanisation pressures.

The CT images showed a possible relationship between the integration quality and the vulcanisation pressure. Samples produced with low pressure vulcanisation showed trapped air between the sensor and the sealing, as can be seen in Figure V.7. Samples with higher vulcanisation (>200bar), did not show visible traces of air next to the sensors, indicating a better integration between the sensor and sealing.

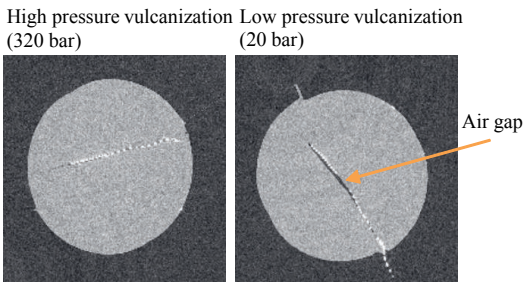

Figure V.7: CT top image. Samples with low vulcanisation pressure show trapped air between the sensor and sealing, indicating an imperfect connection.

V.3.3 Sealing Relaxation Measurement

It is known that sealings that are placed under pressure will show relaxation the first hours due to its polymer nature and network. This relaxation phenomena can also be measured with the proposed pressure sensor. The sealing is pressed a total of 20% and kept in this position for 30 minutes. Due to the relaxation of the rubber sealing, the force applied by the machine decreases over time, which is shown in Figure V.8a. The relaxation force follows an exponential behaviour, and after 30 minutes the measured force applied by the machine is almost constant. The sensor response shows a resistance drop when the pressure is initially applied, after that the electrical signal inversely follows the force curve.

Sensors integrated into the sealing with a low-pressure vulcanisation step (<120 bar) did not show reproducible or reliable responses to pressure, as shown in Figure V.8b. It is thought that the bad interconnect between sealing and sensor, due to the visible air layers in between, does not provide a proper transfer of the applied force for the sealings to the sensors.

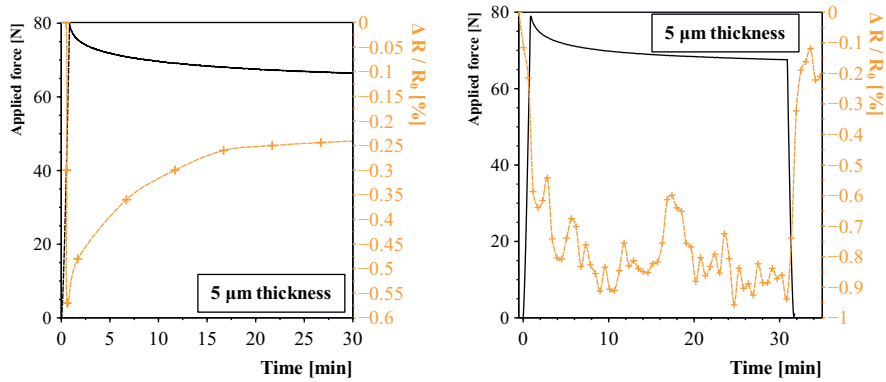

(a) Integrated sensor response with high pressure vulcanisation.

(b) Integrated sensor response with low pressure vulcanisation.

Figure V.8: Integrated sensor results with proper integration (left) and improper integration (right).

The base resistance of the sensors was compared before and after the pressure characterisation (7 cycles per force step, up to 70N). It was found that the thinner sensors (5μm vs. 7μm) showed less irreversible change in base resistance (0.5% vs. 1.7%).

V.4 Conclusion

Flexible single layer piezoresistive pressure sensors were successfully integrated in HNBR sealings. Different sensor designs show an optimal sensor thickness and geometry could increase the sensitivity and/or its pressure region. The placement of the sensor within the sealing was determined by help of CT-guided images and shown to be straightly oriented and not twisted/warped or shifted. Applying high pressure (> 200bar) during the second vulcanisation step seems to minimise the chance of trapped air between the sensors surface and the rubber sealing. Holes at strategic places in the sensing layer enhance the adhesion between both layers even further. Results indicate integrated sensors are able to follow the relaxation behaviour of the sealing.

References

[1] Wolfgang Bauhofer and Josef Z Kovacs. "A review and analysis of electrical percolation in carbon nanotube polymer composites". In: Composites science and technology 69.10 (2009), pp. 1486–1498.

[2] Marco Cen-Puc et al. "Carbon Nanotubes/Polymer Films for Microsensors Applications". In: 2021 IEEE Sensors. IEEE. 2021, pp. 1–4.

[3] H Chougule and U Giese. "Application of Carbon Nano Tubes in specialty Rubbers-Potential and Properties". In: KGK-KAUTSCHUK GUMMI KUNSTSTOFFE 69.6 (2016), pp. 45–52.

[4] Tim De Rijk et al. "Single layer piezoresistive polyimide pressure sensor based on carbon nanotubes". In: 2022 IEEE Sensors. IEEE. 2022, pp. 1–4.

[5] GofInfo. The Gulf Oil Disaster and the Futur of Offshore Drilling. https://www.govinfo.gov/app/details/GPO-OILCOMMISSION. Accessed: 2023-03-02.

[6] Björn Hornbostel et al. "Single-walled carbon nanotubes/polycarbonate composites: Basic electrical and mechanical properties". In: physica status solidi (b) 243.13 (2006), pp. 3445–3451.

[7] Ning Hu et al. "Investigation on sensitivity of a polymer/carbon nanotube composite strain sensor". In: Carbon 48.3 (2010), pp. 680–687.

[8] Jan-Chan Huang. "Carbon black filled conducting polymers and polymer blends". In: Advances in Polymer Technology: Journal of the Polymer Processing Institute 21.4 (2002), pp. 299–313.

[9] Yan Yan Huang and Eugene M Terentjev. "Dispersion of carbon nanotubes: mixing, sonication, stabilization, and composite properties". In: Polymers 4.1 (2012), pp. 275–295.

[10] NASA J. Atkinsen. Langley Research Center, 10 05. https://www.nasa.gov/centers/langley/news/researchernews/rn_Colloquium1012.html. Accessed: 2023-03-02.

[11] Yoon Jin Kim et al. "Electrical conductivity of chemically modified multiwalled carbon nanotube/epoxy composites". In: Carbon 43.1 (2005), pp. 23–30.

[12] Jing Li et al. "Correlations between percolation threshold, dispersion state, and aspect ratio of carbon nanotubes". In: Advanced Functional Materials 17.16 (2007), pp. 3207–3215.

[13] Cynthia A Mitchell and Ramanan Krishnamoorti. "Dispersion of single-walled carbon nanotubes in poly (ε-caprolactone)". In: Macromolecules 40.5 (2007), pp. 1538–1545.

[14] 25 07 2010. NTSB. Hazardous Liquid Pipeline Rupture and Release. https://www.ntsb.gov/investigations/AccidentReports/Reports/PAR1201.pdf. Accessed: 2023-03-02.

[15] MCV Omelan, A Diekmann, and U Giese. "Development of soft electrical conductive PDMS/CNT-composites with extremely low CNT content". In: KGK 73 (2020), pp. 22–30.

[16] Harald Rennhofer and Benjamin Zanghellini. "Dispersion state and damage of carbon nanotubes and carbon nanofibers by ultrasonic dispersion: a review". In: Nanomaterials 11.6 (2021), p. 1469.

[17] Tim Mike de Rijk and Walter Lang. "Low-Cost and Highly Sensitive Pressure Sensor with Mold-Printed Multi-Walled Carbon Nanotubes Dispersed in Polydimethylsiloxane". In: Sensors 21.15 (2021), p. 5069.

[18] Natthakarn Romyen, Supakanok Thongyai, and Piyasan Praserthdam. "Surfactant-dispersed carbon black in polyimide nanocomposites: Spectroscopic monitoring of the dispersion state in the polymer matrix". In: Journal of applied polymer science 115.3 (2010), pp. 1622–1629.

[19] S-P Rwei, F-H Ku, and K-C Cheng. "Dispersion of carbon black in a continuous phase: Electrical, rheological, and morphological studies". In: Colloid and Polymer Science 280 (2002), pp. 1110–1115.

[20] Ge Shi et al. "Graphene platelets and their polymer composites: fabrication, structure, properties, and applications". In: Advanced Functional Materials 28.19 (2018), p. 1706705.

[21] Sónia Simões et al. "Influence of dispersion/mixture time on mechanical properties of Al–CNTs nanocomposites". In: Composite Structures 126 (2015), pp. 114–122.

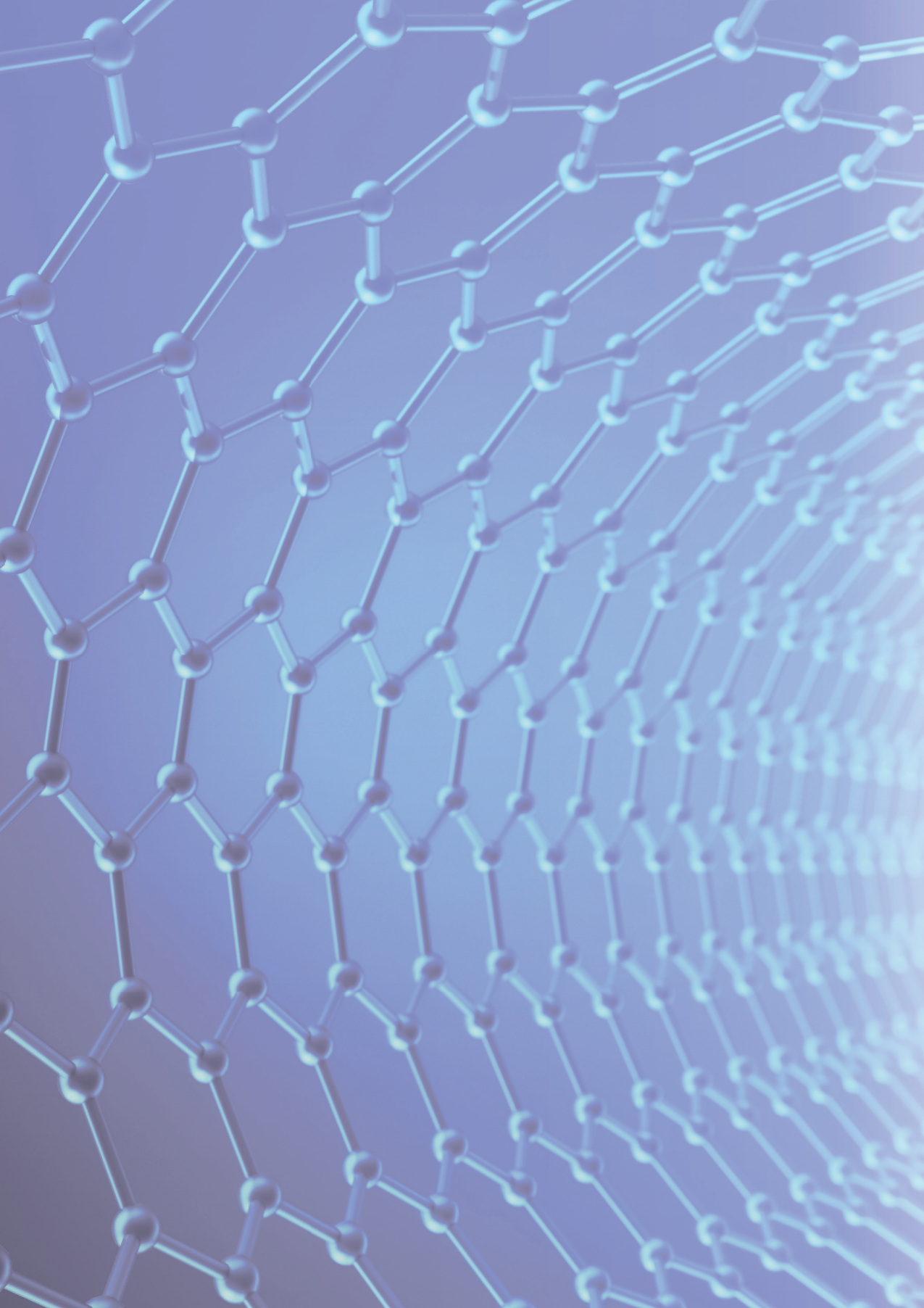

CHAPTER VI

Summery & Conclusion

This Chapter is dedicated to answering the research question stated at the beginning of this dissertation. All questions will be answered and a brief summery of the results is given.

VI.1 Suitable Materials for Flexible Pressure Sensors

Research Question: What are suitable materials for flexible pressure sensors and determine the (dis)advantages of each polymer in terms of manufacturing stability and sensitivity.

Research Answer: Two different polymers with each completely different properties were tested that are both highly common in the IC industry: Polydimethylsiloxane (PDMS) and Polyimide (PI). This study showed several key differences in fabrication, handling, sensitivity and stability. A clear overview of the differences is shown in Table VI.1 and explained in more detail below.

Table VI.1: Colour-coded results for both polymers.

Property	PDMS	PI
Dispersion quality		
High CNT content integration		
Curing Process		
Handling of polymer layers		
Thickness variations		
Sensitivity		
Stability		
Reproducibility		
IC technology compatibility		
Mechanical and temperature stability		

Unfortunately, due to the in-ability to align carbon nanotubes in polyimide, the aligned polymer-based sensors were all fabricated featuring the PDMS polymer. However, the aligned sensors, after properly placed inside the pull-testing device, did show reliable and repeatable sensor data. It is expected, with better metal adhesion to the PDMS, the sensors performance for a long-term basis could be even improved further.

Additionally, the alignment of carbon nanotubes and creating sensors based on this method was performed after the planned integration of sensors into rubber sealings. Therefore, only the stable polyimide non-aligned sensors were integrated into rubber sealings. On top of that is the fact that the aligned sensors fabricated until now, are all strain sensors. This is due to the manufacturing process, which is much easier for aligning the CNTs in the horizontal direction and not vertical (which could be used for pressure sensing).

Dispersion Quality

The ability of dispersing CNTs in both polymers have been extensively tested. Colleague M. Cen-Puc was able to disperse high concentrations of CNTs in polyimide, due to the direct mixing approach. Results in Chapter II indicated improved dispersion and smaller

clusters for CNT-polyimide mixtures (compared to PDMS). Already for low-speed mixing of polyimide, the dispersion quality was superior to that of PDMS. The weighted cluster size averages of PDMS and Polyimide mixing is shown in Table VI.2. Results clearly show better dispersion for Polyimide (smaller cluster sizes) and the effect of prolonged mixing increasing the cluster sizes after a certain time period.

Table VI.2: Weighted average cluster sizes for PI and PMDS mixing. All values are μm^2.

Material	2 min	10 min	30 min
Polyimide 240 RPM	975	129	234
PDMS 240 RPM	2813	2917	1300
PDMS 1200 RPM	1080	450	675

High CNT Percentage Integration

As already mentioned before, the ability of dispersing higher contents of carbon nanotubes in the polymer was possible only for polyimide. A dispersion of greater that 6 wt% was tested (by M. Cen-Puc). These mixtures were thicker in nature but were still able to be spin-coated. This stands in bleak contrast to the maximum found CNT weight percentage of 0.8% for PDMS.

Curing Process

The utilised Polyimide in this research (U-varnish type) must be cured at high temperatures (450°C) inside a vacuum oven to ensure homogeneous and air-bubble free layers. A complete cycle is rather slow and can take up to 6 hours. PDMS in contrary, is simply cured on a hotplate at low temperatures (between room temperature and 150°C) for hours to minutes, respectively.

Handling of the polymer layers

PDMS layers were created with thicknesses varying 20-100 μm. Thinner layers were also fabricated, even up to 5 μm, but handling of those layers became increasingly difficult. The highly thin layers were extremely flexible and possessed some stress in the layer. The layers immediately warped after removal from the layer. Twisted and sticking layers were the result and handling became next to impossible. This gave the clear indication of increasing the thickness slightly to ensure more stable layers.

With Polyimide, this was not the case as all manufactured layers were rigid enough for proper handling.

Thickness variations

This brings the next parameter: the thickness. The polyimide layers, as expected, featured a lower flexibility than its counterpart PDMS. This meant that the thickness could not be increased greatly before the layers became too stiff. It was found that even above 10 μm, the layers were already so inflexible, they became impractical for strain or pressure sensors. This gave us a final tested range of 3-10 μm for PI and 5-100 μm for PDMS.

Sensitivity

Randomly dispersed CNTs in PDMS layers created highly sensitive sensors with a strain range of +-40% with Gauge factors of up to 4%. Aligning the carbon nanotubes by means of an external electric field caused the Gauge factors to increase due to tunneling effects. Experimentally determined Gauge factors for strain went up to the order of 10^3. Sensitivities for the polyimide-based sensors was greatly lower as for the PDMS counterparts (up to 25% resistance change, but unstable). With a maximum of 0.7% resistance change with applying 70N of force. In general, it can be said that the PDMS layers experienced higher sensitivities but lacked the long-term stability (either in case of metal adhesion or reproducible resistance change due to a fixed pressure).

Stability and reproducibility

Both polymer sensors were subjected to cyclic testing. It was found that for non-aligned PDMS sensor, stability of the sensor was rather critical. Results were relatively stable for small pressures or time windows, but overall stability was an issue. This can be partly attributed due to the imperfect adhesion of the gold electrodes to the PDMS samples. Piezoresistive PDMS-based strain sensors clearly showed more stable results. Results were repeatable and cyclic testing showed only minimal drifts. The alignment of CNTs also showed reproducible results for cyclic testing. The main disadvantage of the poor metal-PDMS adhesion only became apparent after repeating the measurement with the same samples multiple times. Placing the samples in the mechanical grippers detached the gold over time, worsening the connection to the substrate. As expected, the polyimide sensors showed a highly linear and repeatable behaviour. The more rigid polymer resulted in a more stable sensor. However, due to the mechanical more robust material, only small changes in pressure or strain were detectable. Whereas the PDMS samples could be strained up to even 100%, the polyimide sensors were only stretched a few percent.

IC compatibility

Polyimide is used extensively in the cleanroom and is a well-known and controlled polymer in the IC technology. PDMS however, is also well-known and often high praised in the literature, but it features multiple downsides. The material's high thermal expansion coefficient and extreme hydrophobic surface make a lot of fabrication steps increasingly

more difficult. On top of that comes the poor metal adhesion to PDMS and difficulty of clean PDMS dry etching. In conclusion, it can be said that polyimide was the much more user-friendly and reliable polymer in the cleanroom for sensor fabrication.

Mechanical and temperature stability

Polyimide is well known for its high temperature stability up to at least 400°C and the ability to resist numerous solvents, as experimentally confirmed. Its counterpart in this research, PDMS, is less resistant for certain chemicals. It was found that trying to clean the wafers with Isopropanol could already cause the layers to swell slightly. Trying to remove the left-over photoresist by the (normally standard) step of placing the wafers in a 50°C AZ100K remover bath resulted in complete detachment of the layer from the surface. Additionally, the PDMS is far more sensitive to temperature due to its very high thermal expansion coefficient (PDMS 310 $\mu m\, m^{-1}{}^{\circ}C^{-1}$ [3], PI 0.3 $\mu m\, m^{-1}{}^{\circ}C^{-1}$ [1])

CNT weight concentration influence on the sensitivity

PDMS: In general it can be seen that with increasing wt%, the PDMS-CNT sensitivities for strain decreased. For 60 μm thick PDMS layers, the Gauge factors are listed in Table VI.3. Decreasing the thickness of the samples, increased the sensitivity (with a Gauge factor up to 4).

Table VI.3: Experimentally determined Gauge Factors for randomly dispersed CNT-PDMS samples.

CNT wt%	Gauge Factor
0.45	3.4
0.60	1.5
0.80	1.42

Polyimide: The influence of sensitivity versus added CNT weight percentages was only briefly tested for the polyimide sensors. It is expected that due to the very thin polyimide layers (5-7μm), most of the CNTs lie flat in the polymer matrix and therefore are perpendicularly aligned to the pressure region. This could explain that when applying pressure from above, after a certain wt% of CNTs, no real jump in sensitivity occurs. CNT-connections get lost due to the expanding geometry, but possible the effect is minimal when a certain threshold of CNTs has been reached.

In this case, the concentrations 1, 1.5 and 2.0 wt% were tested and there were no real sensitivity changes for the pressure sensors. For polyimide strain sensors, it is known that there is a large change in sensitivity depending on the amount of added carbon nanotubes (research from M. Cen-Puc, IMSAS). It was found, similarly to PDMS strain sensors, that thinner layers are less CNTs increase sensitivity.

For aligned carbon nanotube sensors, similar observations were true. Higher CNT concentrations did decrease the sensitivity of the sensors, but increased the linear initial part of the sensor response. It is expected that with higher amount of nanotube connections, the dominant electron tunneling effect takes longer due to the increased CNT-CNT direct connections. There are simply more connecting carbon nanotubes, which takes longer to reach the electron-tunneling stage.

VI.2 Effect of Sensor Geometry on the Sensitivity

Research Question: Does the sensors geometries play a role in the sensitivity or stability of the sensing layer?

Research Answer: The polyimide pressure sensors are based on a flexible piezoresistive sensor layer with gold inter-digital electrodes sputtered directly on top. Two different distances between individual IDEs were manufactured to determine the influence their influence. Results showed wider distances increased the sensitivity (from 0.12‰/N to 0.45‰/N), as shown in Figure VI.1a.

The effect on layer thickness was research intensively and results always showed thinner layers to be more sensitive (to either strain or pressure). The Gauge factors for PDMS samples increased from 1.5 to 3.5 (Section III.3.3). Similar results were found for the polyimide-based pressure sensors, as shown in Figure VI.1b. Here, the sensitivity increased from 0.12‰/N to 0.33‰/N.

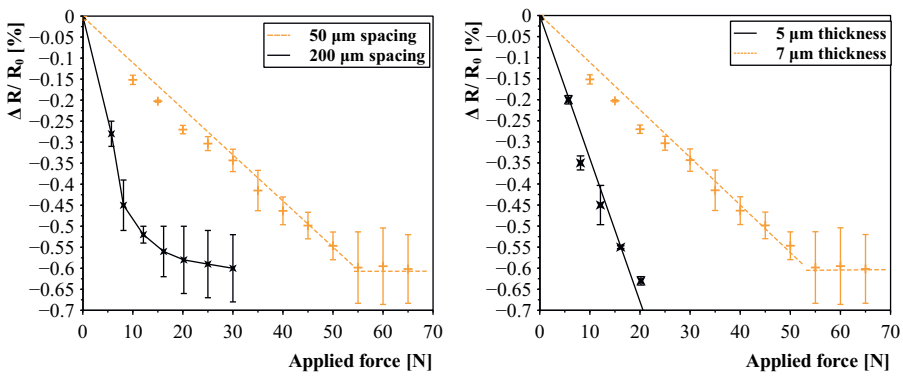

(a) Geometry influence. Larger inter-digital spacing increases the sensitivity but seems to reduce the sensitive regions.

(b) Thickness influence. Thinner layers experience a higher sensitivity to pressure, with a smaller sensitive region.

Figure VI.1: Effect on sensor geometry and thickness changes to its sensitivity.

Similar results were found for the aligned carbon nanotube strain sensors, when looking at Figure VI.2. Increasing the inter-digital electrode spacing, increased the sensor responses (for the linear part the Gauge Factor increased from ≈ 60 ($\epsilon = 1\%$) to 550 ($\epsilon = 0.05\%$). Analytical results did also confirm this when looking at the resistance changes for different number of connecting CNTs, as shown in Chapter IV.6.
After investigating both IDE distances, the results show a smoother sensor response (although lower) for the more tightly packed IDE structures. There appears to be less jumps in the sensor response and a smoother transition from the linear to the exponential

phase. Additionally, the strain range is drastically increased which could be interesting for future research.

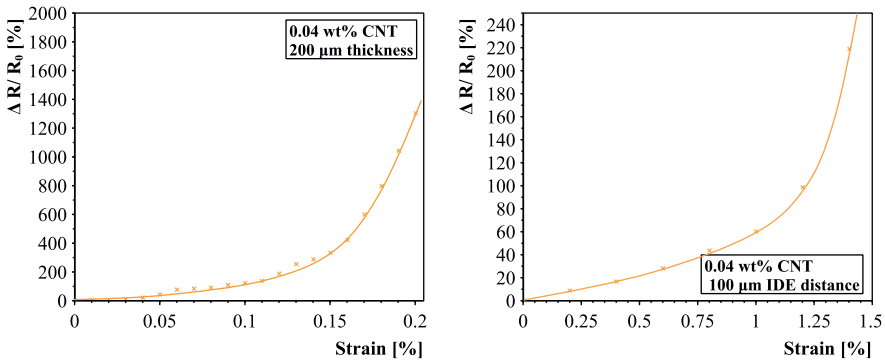

(a) 200 μm IDE distance

(b) 100 μm IDE distance

Figure VI.2: Effect on IDE distances. Please mind the different axis.

VI.3 Creating Uni-directional Sensitive Sensors

Research Question: Is is possible to minimise the cross-sensitivity of sensors by aligning the CNTs in the sensing layer?

Research Answer: Yes, this research showed the possibility to align carbon nanotubes in a viscous polymer, and create sensors with greatly different sensitivities in perpendicular directions. The large differences in sensitivity are shown in Figure VI.3. The sensors show a two-phase response with a first linear region after a sudden exponential increase of sensitivity which is attributed due to electron tunneling. The found Gauge factors are listed in Table VI.4. The concentration 0.33 is not included in the overview as it was hard to qualify the Gauge factors due to the erratic nature of the sensor responses.

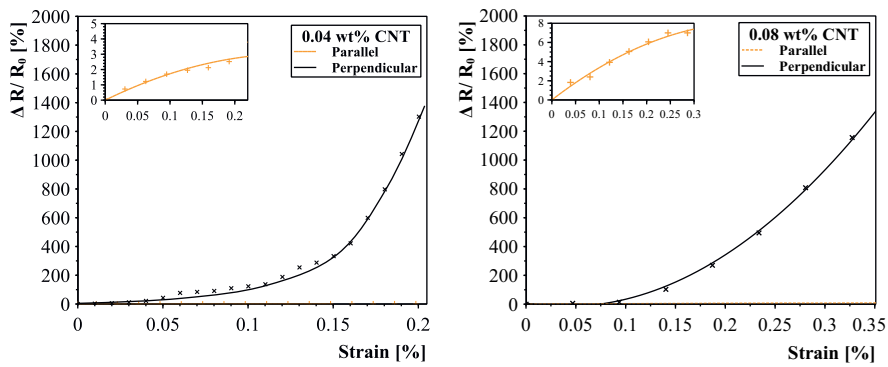

(a) Results for 0.04 CNT wt% sensors.

(b) Results for 0.08 CNT wt% sensors.

Figure VI.3: Strain results for different carbon nanotube concentrations with inter-digital electrode distance of 200μm. A clear distinction in sensitivity is present between the parallel and perpendicular IDE orientation.

Table VI.4: Gauge factors for different concentrations and alignment orientations: Perpendicular (Perp.) and Parallel (Par.).

CNT [wt%]	GF 1^{st} Phase	GF 2^{nd} Phase Perp.	GF 2^{nd} Phase Par.
0.04	570	4700	19
0.08	175	3000	25
0.17	32	1900	18

Several important alignment parameters were characterised that influence the ability to align as well as the time and quality. A brief overview of the parameters and their results is given below.

Electric field strength and alignment Time

The CNTs were aligned by means of an electric field with a maximum of 500kV/m. It was found, for the PDMS polymer, a field strenght above 460kV/m was necessary to show optical movement of CNTs. The maximum of 500kV/m resulted in almost instantaneous alignment of CNTs, which was deemed impractical for this research where the alignment needed to be controllable. Therefore, it was chosen to set the field strength to 480kV/m with a maximum time of 60 minutes.

AC vs. DC alignment

Due to the possible initial charge of carbon nanotubes, it is possible that with an applied DC electric field, the CNTs move to a single direction and the quality of alignment decreases after a certain point. To minimise this effect, a low AC frequency was induced to only rotate the CNTs and not migrate them to a single outer electrode.

Indirect vs. direct alignment

It was found that the direct alignment method featured several difficulties. The CNTs attached to the outer electrodes and changed the electric field, causing highly in-homogeneous rotation of CNTs at the edges. Additionally, the problem of possible and sudden current transfer between both electrodes gave difficulties. After the initial alignment and the first connections were present between both electrodes, a sudden transfer of current caused a short circuit and corresponding 'shock-wave' that thermally cured the polymer.

Frequency influence

The effect of the applied frequency was investigated by determining the point when the carbon nanotubes started moving due to the applied electric field. Frequencies up to 1kHz were tested and results yielded a high dependency between the field frequency and alignment time. Increasing the frequency drastically increased the alignment time (3 minutes for 1Hz, 18 minutes for 10Hz). It was chosen to allow a maximum of 60 minutes for the alignment. It remains a possibility that a longer waiting time could show an alignment also for higher frequencies. However, this was deemed to be outside the area of interest for this research.

Together with all optical results and all acquired electrical results it can be said that the alignment of CNTs to create uni-directional sensitive sensors is possible. However, a certain amount of cross-sensitivity is always present due the fact that complete parallel alignment without any crossing of CNTs in the perpendicular direction is not possible. For clarification, this is graphically shown in Figure VI.4.

The alignment of functionalised carbon nanotubes was greatly different than with regular carbon nanotubes. The additional functional groups created a large dipole moment to enhance the rotational and transnational ability of the nanotubes, as well as

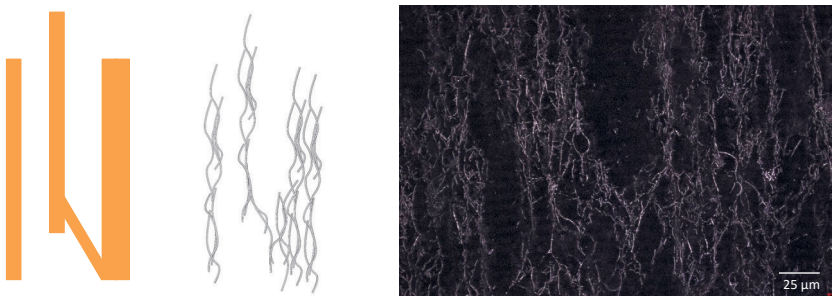

Figure VI.4: No real idealised uni-directional alignment is possible. There are always some cross-overs when utilising pristine multi-walled carbon nanotubes.

increase the repulsion of nanotube interaction which helped in the dispersion. However, some very large clusters remained which formed large beacons on which the nanotube pathways created long and evenly spaced connections. The clear differences between both carbon nanotube types is clearly visible in Figure VI.5.

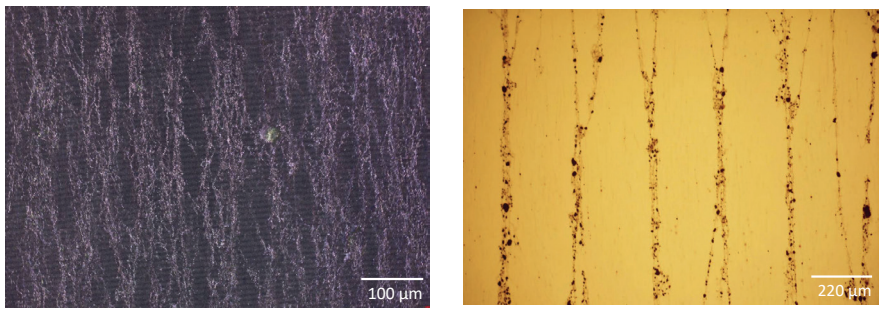

(a) Regular nanotubes

(b) Oxidised nanotubes

Figure VI.5: Comparing alignment of regular and oxidised carbon nanotubes (0.2 wt%). Please mind the different scale-bar.

It appears that the CNT concentration influences the distance between conductive paths. It is theorized that the increased number of carbon nanotubes creates stronger local electric fields when attached in long lines, pulling towards them more and more carbon nanotubes from further away. This would increase the conductive pathway distances with increasing nanotube concentration.

VI.4 Integrating Pressure Sensors Into Rubber Sealings

Research Question: Find a method for integration of sensors into (industrial) sealings.

Research Answer: Hydrogenated nitrile rubber (HNBR) sealings were manufactured at the German Kautschuk Institute (DIK) in Hannover. The Rubber was cut in smaller pieces and placed inside aluminium molds. The sealings were taken out the molds before the vulcanisation was complete. Sensors were integrated and the vulcanisation at 170 ° at 320 bar pressure was continued.

A possible dependency on vulcanisation pressure and sensor quality integration was found when varying the vulcanisation pressure. Trapped air bubbles were found between the sensor and the rubber when the vulcanisation pressure was low <120bar. Increasing the vulcanisation pressure showed that this effect was minimised and the sensors showed proper integration without folding, twisting or damaging the sensor (as was confirmed by CT images, taken by DIK Hannover and presented in Figure VI.6).

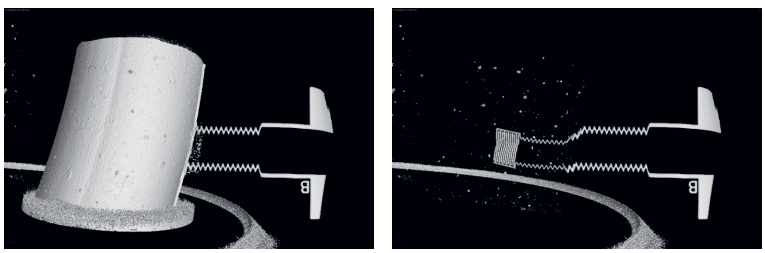

Figure VI.6: Left: CT image of the flexible pressure sensor within the sealing. Right: CT image showing the placement of the integrated pressure sensor within a sealing.

The rubber sealings, when compressed for a longer time, experience a relaxation behaviour. This effect is measurable by a decrease in pressure, which is shown in Figure VI.7. A properly integrated sensor is able to follow the initial relaxation of the rubber. Trapped air worsens the physical force transfer from the sealing to sensor and no monitoring is possible.

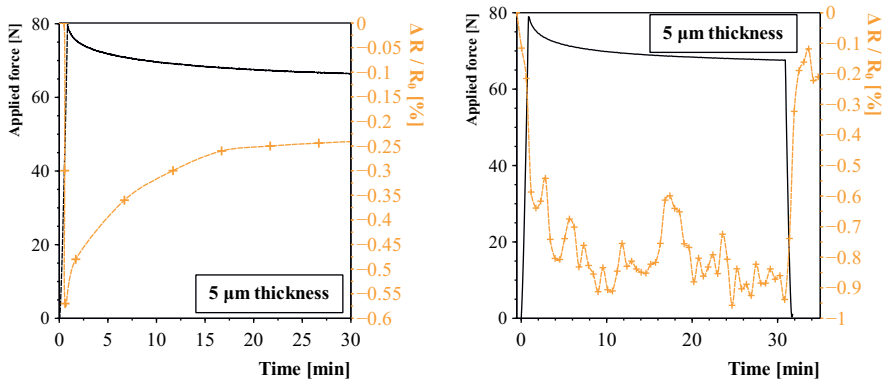

(a) Integrated sensor response with high pressure vulcanisation.

(b) Integrated sensor response with low pressure vulcanisation.

Figure VI.7: Integrated sensor results with proper integration (left) and improper integration (right).

VI.5 Basic Numerical model Confirmations

Research Question: Create an numerical model that features the basic sensor principle and extent it to include the effect of CNT alignment.

Research Answer: Numerical simulations were performed with the program COMSOL Multiphysics to investigate the piezoresistive property of CNTs in polymer layers. Curved CNTs were randomly positioned inside a grid and the effect on CNT geometry and sensor thickness was investigated. Numerical simulations corresponded to experimental data and showed a decrease in sensitivity with increasing layer thickness (Figure VI.8a). Results show that the outer CNT dimensions influence the possible percolation threshold of the compound (as shown by a decrease in CNT-CNT distance in Figure VI.8b.)

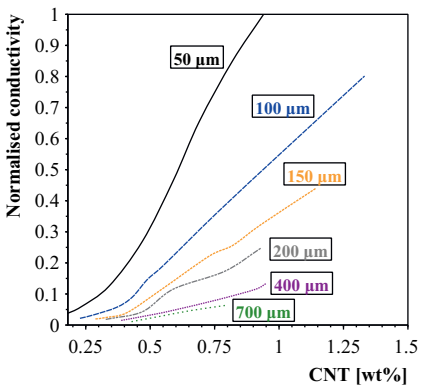

(a) The theoretical conductivity for different sensors thicknesses. The thicker the layer becomes, the less sensitive the sensor.

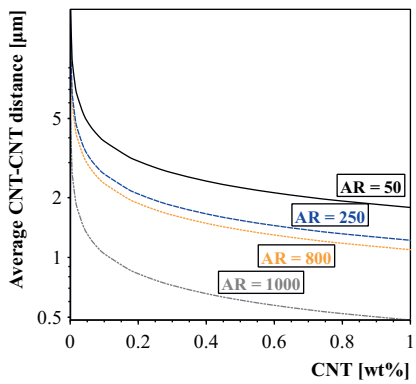

(b) The theoretical CNT inter-particle distance for different CNTs in relation with the wt% in the polymer. Higher AR leads to closer inter-particle distances.

Figure VI.8: Numerical results acquired via a COMSOL Multiphysics model.

The pressure response was investigated by applying a pressure/movement to a single sensor side and monitor the resistance chance. The result is depicted in Figure VI.9. The expected behaviour is observed as the resistance decreases with increasing pressure.

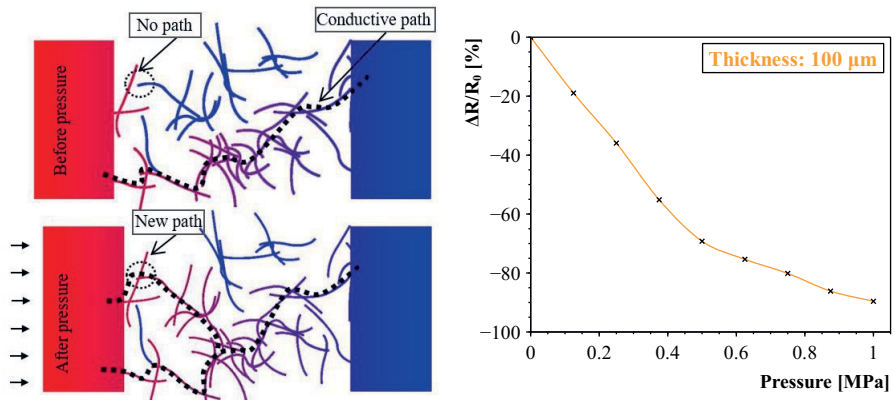

(a) Schematic sensor principle (CNTs not to scale).

(b) Theoretical sensor response

Figure VI.9: Results of theoretical pressure sensor response based on curved carbon nanotubes.

VI.6 Numerical Model of CNT Rotation in Viscous Liquids

Research Question: Create a numerical model that investigates the parameters of CNT-alignment in a viscous liquid.

Research Answer: The concept of rotating CNTs inside a liquid medium was validated by integrating several simulation domains (Electrical, Mechanical and Fluid domain). The model featured a single CNT inside a liquid (water or polymer) after which the influences on several parameters were investigated. Several key parameters and their influences are summarised below and shown in Figure VI.10.

- Electric field strength: As suspected, the stronger the electric field strength, the faster the rotation of CNTs is. However, a too fast rotation could yield in the inability to control the alignment. Hence, increasing the field strength does not necessarily mean a better alignment process.
- Electric field frequency: Numerical results show that rotation of CNTs in PDMS slows down with increasing frequency.
- Effect of direct and indirect alignment methods: Clear results were found of the effect of attaching CNTs to the outer electrodes with the direct current alignment method. The attached CNTs act as local antenna's with high electric field strengths that disrupt the field's homogeneity.

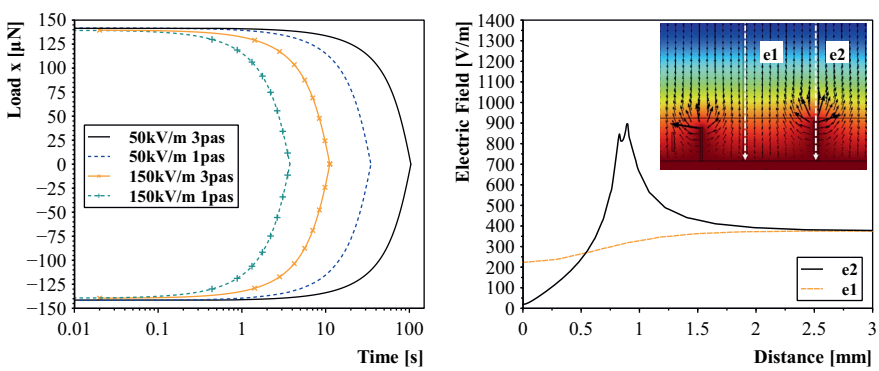

(a) Influence of viscosity and field strength on the alignment of CNTs. Viscosities are chosen to correspond to uncured PDMS.

(b) Effect of connected CNTs to the outer electrodes. The nanotubes cause local high electric fields that disturb the alignment.

Figure VI.10: Numerical simulation results of rotating carbon nanotubes in an electric field.

VI.7 Analytical Determination of Sensors Sensitivity

Research Question: Determine analytically the expected sensor sensitivity when the main piezoresistive effect is electron tunneling.

Research Answer: The analytical method distinguishes between the two main principles of the piezoresistive properties in this research: Loss of conductive networks and the tunneling effect.

The first principle is based on the decreasing interparticle distance with increasing applied stress, as shown in the relation VI.1.

$$s = s_0(1-\epsilon) = s_0(1-\frac{\sigma}{E}) \tag{VI.1}$$

The second principle is based on the fact that at very close distances (<1nm), electrons can jump (a.k.a tunnel) between two conductive materials. With increasing distance, this becomes exponentially more difficult, as shown by Equation VI.2 based on Simmon's theory [2].

$$R_{tunnel} = \frac{V}{AJ} = \frac{h^2 d}{Ae^2\sqrt{2m\lambda}} exp(\frac{4\pi d}{h}\sqrt{2m\lambda}) \tag{VI.2}$$

A more complex analytical model was created to determine the effect of aligned carbon nanotubes and the connections between them via either direct contact or electron tunneling. The behaviour of the networks was similar to the experimentally acquired data: the sensors feature a two-phase response. For the initial small strains, a linear relation is found where it is assumed that most CNT-CNT connections are still properly connected. With increasing strain, the connections widen and electron tunneling becomes more pronounced. The simulation results are shown in Figure VI.11. These results also confirm the experimental results that longer CNT connections feature higher sensitivity.

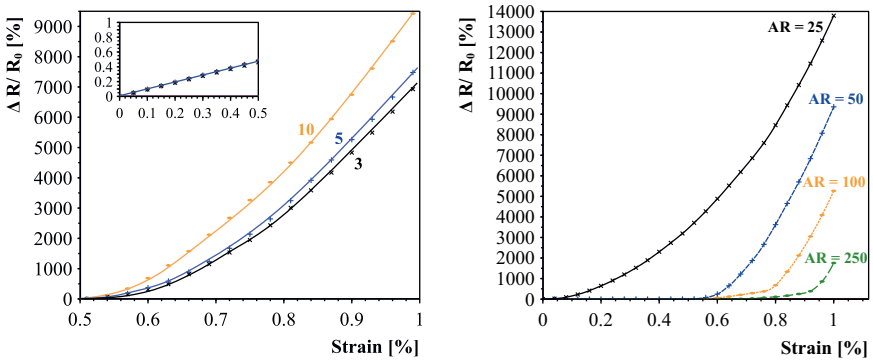

(a) Influence on sensitivity with varying number of CNT-CNT connections (10, 5 and 3). Results show an increase in sensitivity for higher number of connecting nanotubes (similar to wider inter-digital gaps).

(b) Influence on sensitivity by varying the aspect ratio of CNTs. A fixed electrode distance was chosen with varying aspect ratio CNTs. The initial linear low Gauge Factor response seems to lengthen with increasing aspect ratio.

Figure VI.11: Analytical results to model the response of aligned carbon nanotube networks. The inset of (a) shows the linear initial low Gauge Factor response up to 0.5%, after which electron tunneling becomes more dominant and the response drastically increases.

VI.8 Outlook

This research project started in July 2020, in the midst of the Covid19 pandemic. Due to this completely new situation and the long home-office periods, not all research ideas and experiments were performed. Two main topics still have much prospect and will be highlighted below:

- The main difficulty with the randomly oriented or aligned carbon nanotube sensors was the polymer. Unfortunately, the carbon nanotubes were unable to be aligned inside polyimide. This much stabler polymer featured an ideal connection to sputtered metallic electrodes on top (for the randomly oriented nanotube pressure sensors), in large contrast to PDMS. It was possible to align and rotate the carbon nanotubes in PDMS, however, it remained difficult to properly attach electrodes to the polymer to read out the change in the sensor layer due to applied strain or pressure. More research into different polymers or different methods of depositing electrodes onto PDMS could result in great sensor stability and longevity.

- The second item is the continued investigation of implementing functionalised carbon nanotubes. First results show drastic differences in alignment quality and show tendencies of conductive pathway interval distances that can be regulated by alignment time and nanotube concentrations. Furthermore, the proper connection of the gold inter-digital electrodes to the conductive pathways can still be improved.

- At last, the possible dependency on inter-digital electrode distance and sensor strain range could be investigated further. First results show that smaller distances, the range is greatly increased. The sensors sensitivity does decrease, but is still high (Gauge factor >40). Researching this effect in more detail could yield more stable sensors that work for a greater strain range.

Overall it can be concluded that the implementation of unidirectional sensitive sensors is possible, as was shown in this research. Future research could improve the control over the carbon nanotube alignment and the next steps to create fully integrated CNT-aligned sensors.

References

[1] Shun'ichi Numata et al. "Thermal expansion behavior of various aromatic polyimides". In: Journal of applied polymer science 31.1 (1986), pp. 101–110.

[2] John G Simmons. "Generalized formula for the electric tunnel effect between similar electrodes separated by a thin insulating film". In: Journal of applied physics 34.6 (1963), pp. 1793–1803.

[3] Slygard 184 Silicone Elastomer Technical Data Sheet. https://www.dow.com/content/dam/dcc/documents/en-us/productdatasheet/11/11-31/11-3184-sylgard-184-elastomer.pdf. Accessed: 2020-10-10.

A

Interesting Images Acquired during this Project

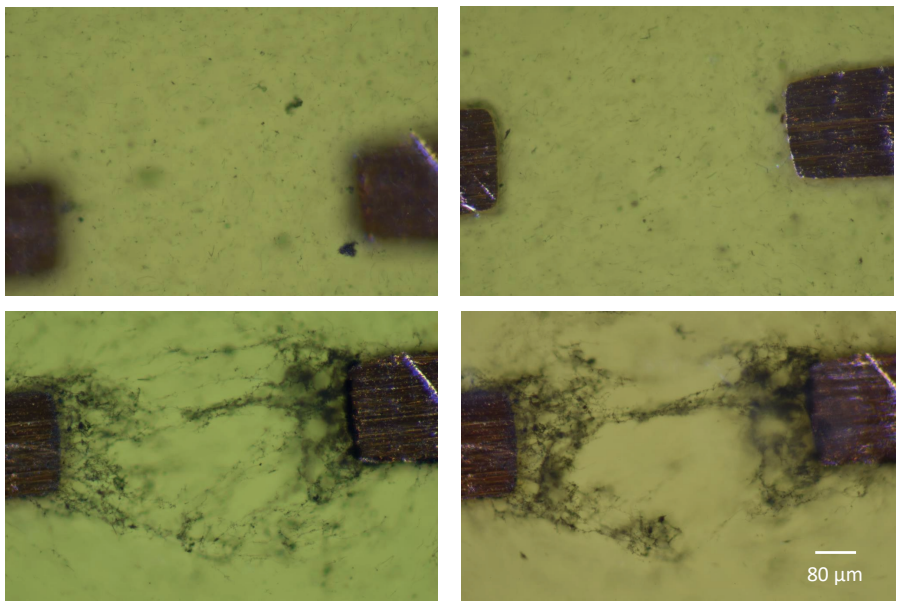

Figure A.1: Alignment of CNTs in PDMS over time. Slowly the CNTs rotate in the direction of the electric field (top right), after which long and thicker connections arise.

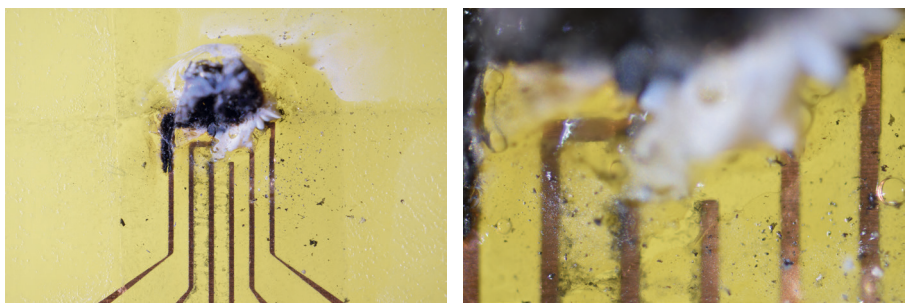

Figure A.2: Result of sudden connection between electrodes with the direct current alignment method.

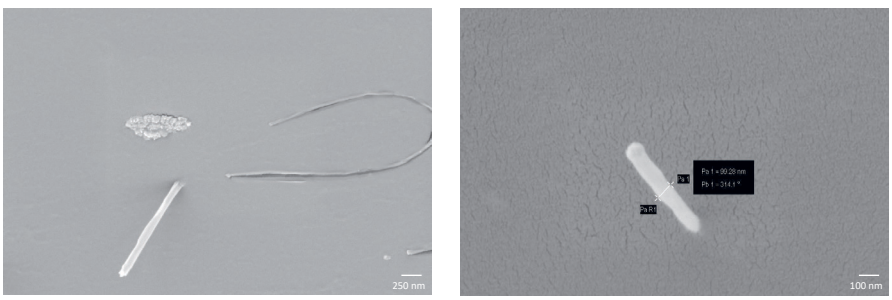

Figure A.3: Individual close-up of carbon nanotubes.

List of Publications

1. de Rijk, T. M., & Lang, W. (2021). Low-cost and highly sensitive pressure sensor with mold-printed multi-walled carbon nanotubes dispersed in polydimethylsiloxane. Sensors, 21(15), 5069.

2. Cen-Puc, M., de Rijk, T.M, Gleason, M. V.,& Lang, W. (2021, October). Carbon Nanotubes/Polymer Films for Microsensors Applications. In 2021 IEEE Sensors (pp. 1-4). IEEE.

3. de Rijk, T.M, Cen-Puc, M., Piening, J. K., & Lang, W. (2022, October). Single layer piezoresistive polyimide pressure sensor based on carbon nanotubes. In 2022 IEEE Sensors (pp. 1-4). IEEE.

4. W. Gehlken, S. Fischer, T.M. de Rijk, M.J. Vellekoop. (2022). A Simple Process to Embed Carbon Nanotubes into DLP Resins for 3D Printing of Conductive Structures. In 2022 MNE 2022.

5. Cen-Puc, M., de Rijk, T.M., Schander, A., Gleason, M. V., & Lang, W. (2023, October). Strain Microsensors Based on Carbon Nanotube/Polyimide Thin Films. In 2023 IEEE Sensors. IEEE.

6. de Rijk, T. M., Cen-Puc, M., Mirzaei, Y., Schneider, P., Giese, U., & Lang, W. (2023). Integrated Flexible Polyimide Sensors for Monitoring Compressive Force in Sealings. In IEEE Sensors Journal Vol. xx, NO. xx, Month x, 2023. Submitted.

7. de Rijk, T. M., Schewzow, A., Schander, A., & Lang, W. (2023). Unidirectional Electron-Tunneling Polymer Strain Sensor Based on aligned Carbon Nanotubes. Sensors Vol. 32, NO. 20, October, 2023.

8. de Rijk, T. M., Mirzaei, Y., Schneider, P., Giese, U., & Lang, W. (28th February 2024). Elastomerforum fpr conference. Invited speaker.

About the Author

Tim was born in Haarlem, the Netherlands in 1993.

In 2011 he started to study Electrical Engineering at the Technical University Delft. In 2015 he received his degree Bachelor of Science.

The first achieved Master of Science involved a combined thesis project with the Delft Technical University and the RWTH Aachen University in Germany. The main topic and newly sparked interest was the fabrication of microelectronics in combination with the biomedical field. The subject was to develop a process to fabricate and bond thinned silicon chips on polyimide films, that could be implemented for epiretinal implants.

At the Delft Technical University he received his second Master of Science in 2020 with the specialisation in Microelectronics, with an Organ-on-Chip thesis project. The research entailed the development of a 3D electrode array suitable for measuring the electrical responses of clustered neurons at different height levels.

At the Institute for Microsensors, - actuators and -systems (IMSAS) University Bremen he started as a PhD candidate working on flexible piezoresistive sensors based on carbon nanotubes.

In his free time he enjoys scuba diving, rock climbing/bouldering and travelling.

Acknowledgement

I would like to use this page to thank all the people around me during my 3.5 years at the university of Bremen. First of all, I would like to sincerely thank Prof. Walter Lang for giving me the opportunity to work at IMSAS university. I enjoyed the freedom and ability to follow my own ideas and experiments but knowing that the expertise of all professors and colleagues was just around the corner. Additionally, I also want show gratitude for the advice and guidance in writing scientific publications and presenting the data in a clear and orderly fashion.

I enjoyed the conversations and working together with all colleagues from the IMSAS institute, but I would like to highlight several that were really closely involved in this project and without their help, this project would not have the results it has now. First of all I would like to thank my direct colleague Marco Cen-Puc who started working at IMSAS some time before me and was already working with carbon nanotubes. His expertise of carbon nanotube dispersion in a polymer saved a great deal of time and improved the sensors fabrication. I had a great time working together and investigating the behaviour of CNT-integrated polymers, and of-course our conference in Dallas Texas! I want to thank Andreas Schander form the technical staff for all the, sometimes long, discussions for planning the fabrication of (aligned) carbon nanotube layers in the cleanroom. Sometimes this took little unorthodox ideas but with his expertise and ideas we figured out methods to successfully manufacture the samples. Similarly, I would like to thank Melanie Kirsch in all technical assistance in and outside the cleanroom. The support in processing the wafers in the cleanroom and finding suitable methods was of valuable help. I would also like to sincerely thank André Bödecker for his help in explaining the chemical part of this thesis and the understanding and ideas of rotating nanotubes in specific media. A great thanks goes to Kai Burdorf for all helpful and interesting discussions and translating the German texts needed for this project.

Additionally, I would like to mention our project partners from the Deutsches Institut für Kautschuktechnologie (DIK Hannover) and thank them for the collaboration these past years.

Last but not least I would like to thank my friends, the Delft pizza group, family, and especially my wife for all the motivation during the years. Coming home to a warm house helped during the long working weeks and writing phases of this project. The holidays and friend visits to the Netherlands were always relaxing and gave new energy.

The end of this project literally brings new life into our lives as we prepare to welcome our firstborn daughter, Annabella Esmée de Rijk, into this world.

Tim Mike de Rijk